UNIVERSITY
OF TRENTO - Italy
Department of Materials Engineering
and Industrial Technologies

Doctoral School in Materials Engineering – XXIII cycle

Geometrical features induced in polymer structures by self-assembly and their exploitation for biomedical use

Giuseppe Alberto Ruffo

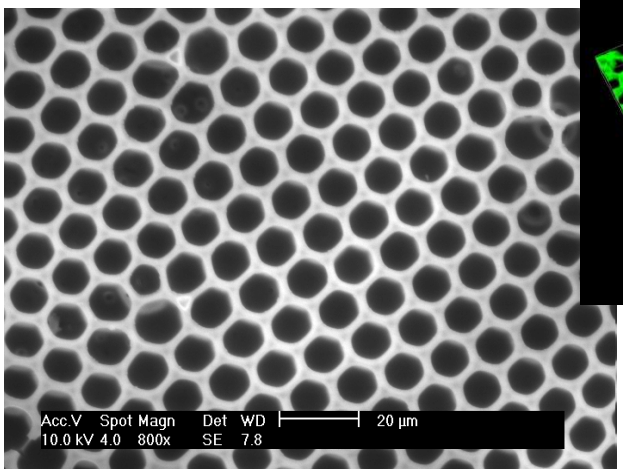

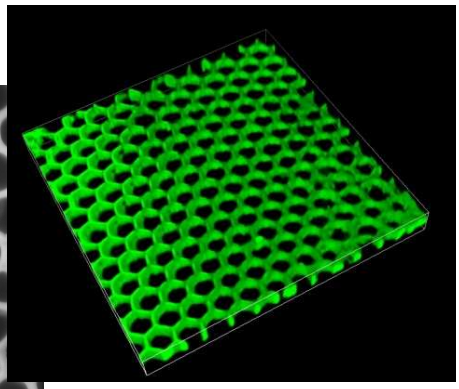

Tutor:

Prof. Claudio Migliaresi

April 2011

Contents

Thesis objective and outline

This thesis work deals with the study of the formation of geometrical features on polymers structure by self-assembling processes. In particular, porous patterns were investigated, resulting from the self-assembling of water droplets on the surface of polymeric solutions (Breath Figures).

The main aim of the thesis is to produce and study customized self-assembled porous polymeric structures and to explore their biomedical applications, in particular in biomolecules encapsulation, chemical patterns formation and drug release.

In the Introduction the techniques used to produce pores patterns are analyzed, with a particular focus on self-assembling mechanisms. The Breath Figures templating method is described in terms of the physical phenomena and process parameters which guide the nucleation, growth and disposition of pores. A literature review is presented on the Breath Figures pattern works.

Chapter 2 presents a study on the interfacial and kinetic factors which influence Breath Figures formation. Porous patterns were produced on cast and spin-cast films using different solvents. A phenomenological model for the development of Breath Figures is proposed, which stresses the relevance of solvent surface tension and of the kinetic parameters. Controlling these factors, films with tailored pores features were produced, obtaining both 2- or 3-dimensional porous structures.

In Chapter 3 the functionalization of pores surface is obtained by a secondary self-assembling process, exploiting the water-solution interface during Breath Figures formation. The chemical functionalization was used to bind a protein to the pores, resulting in films with a controlled topographic and chemical pattern.

Chapter 4 deals with the study of controlled drug release from films or electrospun fibers patterned with the Breath Figures method. Controlled release

of fibrinogen was obtained from porous films and the influence of chemical functionalization of pores on the release was evaluated. Electrospun fibers with a patterned porous surface were produced with the same mechanism used for films. Drug release and its dependence on fibers surface features were studied.

1. Introduction

1.1 Techniques to obtain surface modification

1.1.1 Background

Materials science is a field of science which studies the properties of matter and their relationship with technological applications. The main aim is to understand the deep connection among the micro (and nano)-structure, the properties and the practical applications of materials. For this purpose, materials are studied at different levels, ranging from the atomic and molecular one, involving chemistry and atomistic modeling, passing through the microscopic one to the macroscopic level. For example, electronic devices are based on silicium, which electronic properties strongly depends on the addition of other elements in a concentration measurable in ppm. Metallurgy has developed widely used materials which properties depends on the elemental composition and on the interactions among different phases. It is clear, so, why is interesting the comprehension of the relation between micro- or nano- structure and the macroscopic properties of materials. Depending on the application examined, bulk properties or surface properties can be considered. The study of the latter is the purpose of surface engineering and science, which use chemical and physical surface modifications to obtain proper performances from materials. The possibility of controlling the properties of matters and to tune them to obtain materials suitable for precise aims is the main object of materials science. In this field, the preparation of porous materials has raised a great interest due to their peculiar properties and to

the wide range of applications they can be used for. Catalysis, filtration, chemical analysis, molecular entrapment are all examples of activities where high surface to volume ratio is a key parameter. In optics and electronics materials with a regular porous structure have attracted increasing interest. Several methods have been developed to obtain regular controlled pores pattern, both on the surface (2D) or in the bulk (3D) of materials.

1.1.2 Lithographic techniques

Semiconductor industry has been the main propeller for the development of techniques able to imprint regular pattern on surfaces, such as the group of lithographic methods. The basic concept of traditional lithography is based on a multiple steps mechanism [1]; the first one is to coat the substrate with a coating that is photo-curable, called photoresist. Then, the coating is irradiated with a radiation passing through a mask which reproduces the desired pattern. Part of the resist (a part which mirrors the pattern of the mask) interacts with the photons and changes its physical properties (development), so a selective removal can be performed. Once the coating is selectively removed, the exposed substrate is modified by etching or ion-implanting, while the parts protected by the resist are not affected by the process. In the subtractive patterning process, a positive image of the pattern is created on the deposited film and etching transfers the pattern to the wafer. On the contrary, an additive process can be performed, in which a negative image of the mask is created and, instead of etching, material is deposited into the areas not covered by the resist. The removal of the remaining resist concludes the process of patterning. To build up a complete 3D structure,

this process is repeated several times. Several improvements have been studied to enhance the productivity and the resolution of the technique. Improvement in the design of lens for the projection of the pattern, better photoresists and the use of new types of masks had lead to significant benefits for this industry [2]. The main advantage comes from the use of radiation with very small wavelength; the wavelength used passed to 193 nm [3] and newer technologies involves a radiation at 157 nm. However, several problems rose, connected with the need for materials transparent to that radiation for mask, the environment and the lenses [2]. The use of wavelength of 13.5 nm in EUVL (extreme ultraviolet lithography) leads to similar problems, since all technological materials adsorb this radiation, resulting in limitations in the devices that can be used for the fabrication process [4]. Alternative technologies have been developed, such as Electron-Beam Lithography (EBL) [5] and Ion-Beam Lithography (IBL) [6], which use a high energy beam to develop the photoresist or to directly modify the material by ablation. Other examples are the use of laser ablation, which is a precise technique that can be applied to different material [7], or plasma modification of surfaces after the application of a metallic grid to protect selected area [8]. The precision obtainable with the aforementioned lithographic methods are in the order of sub-100 nm, but there are several problems related to increasing technical difficulties and to the cost of tools, which would make industrial process very expensive [9]. On the other hand, less versatile but cheaper processes have been developed, grouped with the name of soft-lithography, that allow the reproduction of micro- or nano- patterns on the surface of materials. The name derives from the use of elastomeric polymers

(mostly based on poly(dimethylsiloxane) ,abbreviated as PDMS) , used as a mold, stamp, or mask in the process which leads to the pattern formation. The main positive aspect of this group of techniques is the rapid reproduction of the pattern on an high number of copies, with a fast and usually cheap process. Basically, the desired pattern is impressed on an elastomeric surface by means of different techniques, such as molding, ablation or lithography; than that surface is used as a stamp to “print” the pattern on multiple copies. This process was initially used as a contact print with chemical inks which form self-assembled monolayers [10], but then the development of the techniques led to several new applications and to different way of reproducing the desired pattern [11]. Despite the recent improvements, this group of techniques still presents some problems to overcome. In particular, errors occur in the process [12], mainly due to incorrect alignment between the stamp and the substrate, to distortion of PDMS during stamp production and to distortion of stamp during the contact with the substrate. Lithography, in general, allows the reproduction of patterns of desired shape, such as channels, holes, and chosen geometric shapes. Processes involving multiple steps lead to the reproduction of complex patterns, as evident in the production of electronic chips. However, in a wide number of applications the pattern to reproduce is simply a regular array of pores. This kind of pattern is needed for the preparation of anodic aluminum oxide (AAO) patterned surfaces [13,14], for the control of hydrophilic-hydrophobic properties of materials [15,16], for membrane preparation [17], for the porosity control of thin films [18] and other applications, with employment in fields of science such as optoelectronic, biology, chemistry and engineering.

1.1.3 Self-assembling methods

In addition to the aforementioned lithographic methods, there are several techniques based on self-assembling, which allows the formation of regular patterns, both on the surface or in the bulk of materials, forming respectively a 2D or 3D array of pores [19]. Colloidal crystal templating is one of the most diffuse of these techniques. Spherical beads with monodisperse dimension are packed closely together, forming a 3D colloidal crystal matrix. This can be obtained via a variety of crystallization methods, such as sedimentation, centrifugation, filtration, deposition or pressing of the suspension of the particles, usually followed by drying of the suspension [19]. Latex and silica microspheres are the most used beads for this purpose, as they are cheap and the diameter is easily controllable [20]. In this way, the matrix is formed by beads that are regularly packed due to the increase in concentration in the vicinity of a flat surface. The main advantage of this method is the high regularity and the long-range order. The obtained matrix is used as a template to produce the porous material; however, polycrystalline domains are randomly oriented and defects are present, which are transferred to the final material. Thus, the formation of matrix without defects and with oriented domains is a key factor that is still under study. Once the matrix is composed, the voids among beads are filled with a liquid that is then solidified by polymerization, sol-gel transition or precipitation [20]. The final step is the removal of the beads by chemical or physical dissolution, leaving the porous structure, which mimics (in negative) the structure of the original matrix. The need for this step is one of the drawbacks of the process, since it is not simple to remove the material of the beads completely and without damaging the structure

obtained. By the way, pores are regular, with diameters depending on the dimension of the used beads, and present a high interconnectivity, due to the contact points of beads in the closed-pack structure.

A similar method is the emulsion droplets templating. The structure that serves as a template is not formed by solid beads as in the previous cases, but by emulsion droplets. A liquid precursor of the desired material is added to the continuous phase of the emulsion, which is then concentrated, usually by centrifugation, leading to self-assembly of the emulsion droplets. The continuous phase then undergoes a process of gelation by pH modification and, after removal of emulsion components, is dried and sometimes thermally treated [19,21,22]. The process is time-consuming and requires a precise preparation of the emulsion, leading to more defects and less ordered structure compared to other techniques.

Another process which leads to self-assembled nanometric patterns is phase separation of block copolymers. In this class of materials polymeric chains are composed of covalently bonded blocks, each one composed of a long sequence of monomers of the same type. Thus, different parts of the same chain can have different physical and chemical properties. If the blocks are composed of immiscible materials, solidification leads to phase separation, which is the formation of chemically homogeneous areas, with covalent bonds among blocks preventing the separation from extending to large length scale [23-26]. The result is a series of nanometric domains, composed of the smaller blocks, embedded in a matrix composed of the longer blocks. For block copolymers there are mainly three morphologies that the domains can assume: lamellar, cylindrical and

spherical [27]. If a porous structure is needed, the internal nanodomains are removed by chemical dissolution or degradation using UV. Control of the produced patterns depends on the chemistry of the material used, requiring a good characterization of the system, but allows to obtain feature sizes less than 30 nm [19].

A simple, economical and fast templating method based on self-assembly is the breath figures formation. In this case, the template is constituted by an array of water droplets which condensate on the surface of a polymeric solution. The evaporation of a volatile solvent causes the cooling of the surface of the solution, leading to the condensation of the moisture present in the atmosphere. As the droplets grow on the surface, and eventually sink, a series of mechanism prevents the coalescence, thus leading to droplets packing in a low energy arrangement. When the film hardens, the water evaporates, leaving a regular array of monodisperse pores on the surface or in the bulk of the polymeric material [28-30]. Compared to other methods, this is a one-step techniques, meaning it's fast and cheap, and can be used with a wide variety of materials, as it will be discussed in the next chapter.

Beside the templating techniques based on self-assembling here briefly presented, porous structures can be obtained also with other methods: solvent casting, freeze-drying, salt-leaching, fiber bonding and electrospinning are some examples. The structures obtainable, however, are non-ordered and the porosity is irregular, with a wide distribution of pores dimension and, first of all, with a typical pore dimension that is micrometric. A regular porosity is produced with

the group of techniques named solid free-form fabrication, but the typical pores dimension is higher than some microns, often in the range of hundreds of microns. Indeed, these techniques are used in tissue engineering for the fabrication of scaffolds [31], where big pores are required for the penetration of cells.

1.2 Breath Figures templating method

1.2.1 Introduction

Breath Figures (BFs) is a promising way to obtain a regular pattern of pores. The physical phenomenon involved in this process has been studied from different points of view, phenomenological or mathematical [32-36], but still some controversies exist on the full understanding of the mechanisms responsible for the pattern formation. The mechanism was first observed by Lord Rayleigh in 1911, but it has only recently attracted interests from a technological point of view. Breath figures is the name firstly given to the process as it was connected to the drops condensing on a cold glass when someone breathe on it. The term now refers to a wider group of phenomena, involving the arrangement of water droplets formed by the condensation of water vapor on a surface, either solid or liquid. The condensation is caused by the difference in temperature between the atmosphere and the surface, the latter being cooler. In the case of a liquid surface, the cooling is a consequence of the evaporation of the solvent. For this reason the use of volatile solvents is common in the preparation of these structures. The physical properties of solvents are fundamental, such as volatility,

latent heath of evaporation and surface tension, while gravitational effects (linked to solvent density), considered in early works, have been recognized as a minor issue compared to surface tension and kinetic factors[37]. Carbon disulfide, benzene, toluene, chloroform, ethyl acetate, dichloromethane, 1,2-dichloroethane and others solvents have been used, giving the possibility to work with several kinds of polymers and to obtain films with a wide range of porosity features. Three main stages can be observed in BFs formation [32,35]:

- Initial stage. Nucleation of water droplets begins due to condensation of environmental water vapor on the polymeric solution. The surface coverage is small and droplets, once nucleated, growth by diffusion; their average diameter increases according to equation 1.1.

$$D \propto t^{1/3} \qquad [1.1]$$

- Crossover or intermediate stage. The surface coverage reaches its maximum and droplets interact closely together. The entropy of the system decreases drastically due to the rearrangement of droplets in close-packed honeycomb fashion. For the same reason, the number of drops with six other neighboring droplets (typical of honeycomb structures) increases. Droplets are characterized by a monodisperse distribution of diameter and separated by a characteristic inter-droplet distance, due to hard-sphere-like interactions. Depending on the physical

features of the system, drops can arrange on the surface, forming a 2D array, or in the bulk of the solution, leading to a 3D structure.

- Coalescence dominated stage. The surface coverage is high and constant; droplets coalesce, leading to a continuous re-arrangement of their disposition on the surface, leading to a more disordered structure. Droplets diameter increase according to equation 1.2.

$$D \propto t \qquad [1.2]$$

A scheme of the process is shown in Fig.1.1.

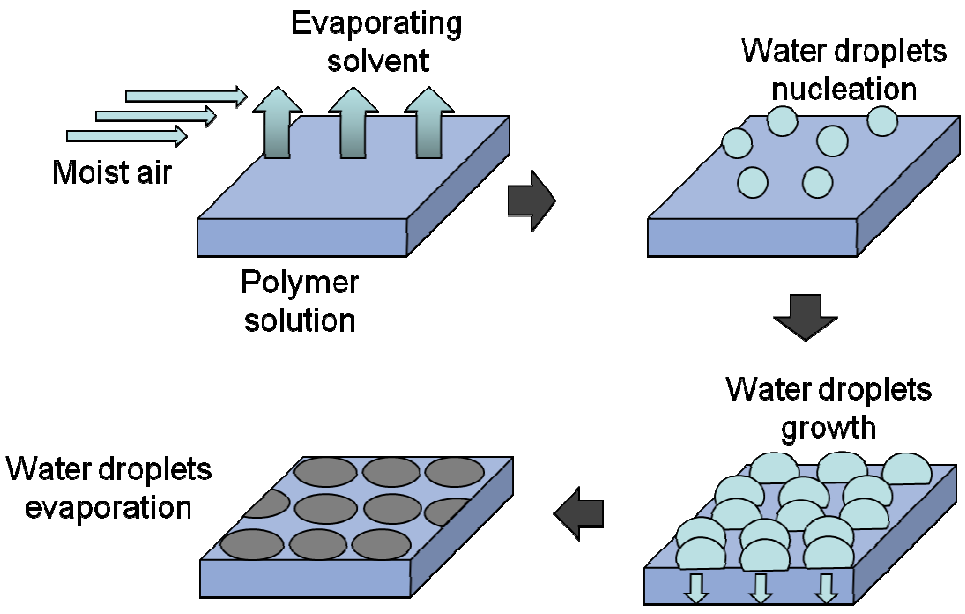

Fig.1.1: process of Breath Figure template method.

1.2.2 Initial stage

Condensation on surfaces occurs preferentially at sites presenting some heterogeneity; on a liquid surface such sites are present in low concentration, so nucleation of droplets occurs at randomly distributed locations. In this initial stage, surface coverage is very low and distance among droplets is big compared to their diameters. The number and location of nucleation sites depends strongly on the temperature difference between the humid atmosphere and the substrate, while nucleation rate has been related to the hydrophilicity of the solution (or better, to the water wettability of the liquid surface) [38]. The temperature of the solution surface was found to be near 0 °C [29] and even less [39], leading to a fast nucleation of water droplets. The growth of a droplet on a liquid substrate locally modifies and deforms the surface, leading to different interactions among the droplets. In fact, drops are on the surface in equilibrium between buoyancy, gravity and capillary forces [40], as shown in Fig.1.2.

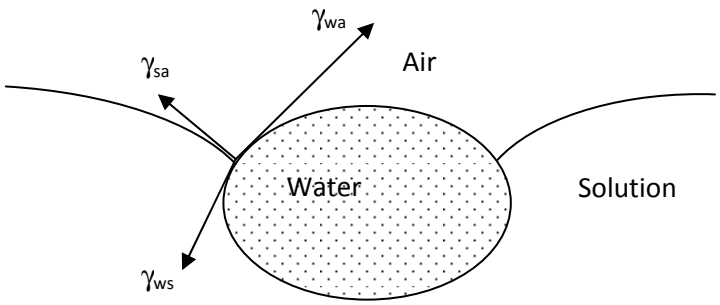

Fig.1.2: droplet on a liquid surface

Hydrodynamic interaction between two water droplets on a liquid surface causes an attractive force [41], calculated by means of equation 1.3.

$$F = \left(\frac{8\pi R^6 \omega^2}{9l\sigma}\right)\left[\frac{1}{\rho_s} - \frac{1}{2} + 0.25(1-p^2)^{3/2} - 0.75(1-p^2)^{1/2}\right]^2 \quad [1.3]$$

where l is the distance between the drops, ρs is the specific gravity of the liquid, ω is the specific weight, γ_{ws} is the solution-air surface tension and p=r/R, where r is the apparent radius of the droplets at the surface and R is the "true" radius of the droplets, measured above the surface. With this definition, p is a parameter accounting for the sinking/buoyancy of the drops respect to the liquid surface. The bending of the liquid substrate leads to long-range elastic interactions among droplets and change the interactions between the forces rising form the surface tensions. This causes the aggregation of the droplets, which form small groups on the liquid surface [40]. In this first stage, disposition of droplets on the surface is guided by the deformation of the substrate and by the convective motion of the drying solution. As discussed by Saunders [38], the nucleation flux, described as the number of droplets forming on a surface at a certain time (number/cm^2 s), depends on the energy required for the formation of the nucleus of drops (ΔΩ), as shown in equation 1.4.

$$J = J_0 \exp\left(-\frac{\Delta\Omega}{kT}\right) \quad [1.4]$$

Where k is Boltzmann's constant, and T is the temperature. This parameter, in turn, depends on the water-air surface tension (γ_{wa}), on a geometrical factor (f) correlated to the shape of the droplets and to the contact angle between water and the solution, and on the difference in water partial pressure in the gas phase and vapor pressure at the liquid interface (ΔP), as described by equation 1.5.

$$\Delta\Omega = \frac{16\pi\gamma_{wa}^3 f}{3(\Delta P)^2} \qquad [1.5]$$

Combining these equations, it is possible to evaluate the influence that the physical parameters of the process have on the nucleation rate, by means of equation 1.6.

$$J \propto exp\left(-\frac{16\pi\gamma_{wa}^3 f}{3(\Delta P)^2 kT}\right) \qquad [1.6]$$

Considering that, it is clear that a decrease in the contact angle of the water droplets on the polymeric solution leads to a faster nucleation, meaning that, at a given time, a higher number of droplets forms on the surface during the nucleation. The variation of the water wettability of the polymeric solution thus allows controlling the rate of nucleation. This parameter is important in the project of the final porous structure; indeed, assuming that a film is completely covered by a regular honeycomb array of monodisperse pores closely packed

together, the surface coverage is approximately the same, independently of the pores size [38]. With this assumption, the pores size depends on the number of pores per unit area, which, in turn, depends on the nucleation rate. This means that, in BFs process with a diffusion limited growth of droplets, the finally pores size is inversely proportional to the nucleation rate in the early stage and, considering the equation shown before, inversely proportional to the water wettability of the polymeric solution. The polymer features (or the presence of surfactants in the solution) affects the value of the solution-water surface tension (γ_{ws}), modifying the nucleation rate; moreover, it affects also the water-air surface tension (γ_{wa}). Due to the high difference in surface tension between the top of the droplet and its base (where it is in contact with the solution), Marangoni convection occurs, driving a thin layer of polymer toward the top of the drop, decreasing the energy due to water-air surface tension. If the polymer (or a surfactant) interacts with the water decreasing γ_{wa}, the contact angle decrease, leading to a faster nucleation. As discussed above, the droplets undergo an attractive force which cause the formation of small groups, or domains, in which droplets interact without coalescing. Actually, their motion is guided not only by hydrodynamic forces among them, but, first of all, by convective flow occurring in the solution. The process usually involves a volatile solvent, which cools down the surface; this causes a large temperature gradient in the solution and, consequently, the rise of convective motions. Moreover, the drying of the solution causes a continuous variation of the process parameters, such as viscosity, temperature and surface tension.

1.2.3 Hydrodynamic phenomena

Convective motion is a phenomenon of mass transfer in liquids, rheids or in granulated materials. The causes of the movement can be various; in the case of BFs formation, convection is a consequence of the temperature gradient. In a liquid layer, the variation of temperature causes a density variation which, as effects of gravity, leads to the formation of convective cells in which cooler (and so denser) parcels of fluids tend to sink, while the hotter parts are less dense and so are subjected to an upward buoyant force. The motion, driven by buoyancy force and called Rayleigh convection, is opposed by viscous drag and by heath diffusion. Viscous drag is a force directed opposite to the direction of the flow and its value is connected to the kinematic viscosity of the solution, which is a measure of the energy required to promote a mass transfer in the fluid, being the ratio of inertial force to the viscous force. Heat diffusion, instead, tends to homogenize the temperature, reducing the temperature gradient and so the cause of motion. This process is more important in liquids with a high thermal diffusivity; in these materials, heat transfer is fast even without fluid motion. On the contrary, if the thermal diffusivity is low (the other parameters being equal) the heat transfer occurs preferentially through a corresponding mass transport. The balance among all these process can be express as a dimensionless number, called the Rayleigh number (R), which can be calculated as the ratio between the buoyant force and the dissipative processes that oppose it (viscous drag and heat diffusion), obtaining equation 1.7.

$$R = \frac{g\alpha\Delta T d^3}{\nu\kappa}$$

[1.7]

where α is the coefficient of thermal expansion, ΔT is the vertical temperature gradient, ν is the kinematic viscosity, k is the thermal diffusivity and d is the thickness of the liquid layer. If buoyancy force is dominant, R has a high value and convective cells form. Contrariwise, if dissipative phenomena are more important, the motion is hindered and no mass transfer occurs. Even though Rayleigh convection should be taken in account, it is not the only kind of mass transport phenomenon occurring in the BFs process. Indeed, the temperature gradient causes also a gradient in surface tension. In fact, surface tension is a function of temperature; usually, it decreases with an increase in temperature, until the liquid-vapor critical point, where surface tension is zero. Generally, differences in surface tension can be caused not only by temperature, but also by local addition of surfactants or by a concentration gradient in the solution. Whatever is the cause of the gradient, fluid tends to move away from regions with a low surface tension toward regions with a high surface tension. The reason for this displacement is that a portion of fluid with higher surface tension pulls more strongly on the surrounding portions or, in other words, energy minimization requires the decrease of the high surface tension areas. Thus, considering a fluid in which the surface tension gradient derives from a temperature difference, fluid tends to move from warmer regions towards cooler areas. In the same way as in Rayleigh convection, this mass transport is opposed by viscous drag and by heat

diffusion. If the gradient overcomes these dissipative processes, a fluid motion occurs, called Marangoni convection. In the case the surface tension gradient is caused by a temperature difference, the phenomenon is called Bénard-Marangoni (or thermo-capillary) convection. To better describe this balance of opposing forces, another dimensionless number is used, called Marangoni number, defined by equation 1.8:

$$M = \frac{\gamma' \Delta T d}{\rho \nu \kappa} \qquad [1.8]$$

where γ'is the temperature derivative of the surface tension, ρ is the density at a reference temperature and other symbols have been defined above. Similarly to Rayleigh convection, Marangoni flow starts if M exceeds a critical value, meaning that the driving force of the process (surface tension differences) is more important than dissipative forces. In the case of a thin layer of fluid, Marangoni convection cause the formation of convective cells, usually hexagonal in shape (provided sufficiently regular boundary conditions), in which fluid flows upward in the centre and downward at the boundaries of cells. One important aspect is that convective motion alters the free-surface of the fluid layer, corrugating it and causing a roughness that increases with the layer thickness. This is due to the fact that regions corresponding to the centers of the cells, which have a high surface tension, tend to reduce the exposed area and so tend to pucker. For this reason, each cell has a centre which is depressed (lower than the level of the unperturbed

free surface). Combining equations RRR and MMM, it is possible to determine the ratio between Rayleigh and Marangoni number, given by equation 1.9.:

$$\frac{R}{M} = \left(\frac{\rho \alpha g}{\gamma'}\right) d^2$$

[1.9]

There are situations in which only one of the mechanism is present (if γ′ is zero or in weightlessness), but usually both types of convection occur, acting synergistically. Equation 1.9 gives an idea of the relative importance of each one in the fluid motion; in particular, the ratio is strongly dependent on the thickness of the fluid layer, such that Marangoni convection is more important in thin films, while for thick films Rayleigh convection is dominant. Convective flow has two main consequences in the process of BFs formation. Firstly, it causes a motion of the condensed droplets on the polymeric surface; droplets move following the liquid flow horizontally on the surface, from the centre towards the boundaries of the cells. This enhances the interaction among droplets, leading to the formation of cluster and domains. If convective fluxes are well developed, droplets can be guided in the bulk of the fluid, following the vertical displacement of fluid. The second consequence is the abovementioned corrugation of the surface, which is deformed also by the condensation of water droplets. Moreover, in BFs method volatile solvents are used, meaning that temperature gradients are important and, so, convective currents are strong. The factor σ/ρ is a measure of the surface resistance to profile modifications due to perturbation. Convective fluxes, for both the effects described above, strongly influence the interactions among droplets.

Limaye [35] argued that convective effects, through perturbations of the surface deformed by droplets condensation, are responsible for the occurrence of coalescence effects since the first stage of the process.

1.2.4 Intermediate stage and non-coalescence

During the intermediate stage, droplets interact closely and surface coverage is at its maximum. Despite some coalescence can occurs during the entire process [35], non-coalescence is the key phenomenon which allows the maintenance of a monodisperse size of droplets and, through hard-sphere-like interactions, their rearrangement in a low-energy compact hexagonal array. Even if the hexagonal arrangement is the one usually observed, sometimes a square disposition occurs, despite its higher energy [42,43]. Several processes have been hypothesized to be the responsible for the non-coalescence. One opinion is that precipitation or adsorption of the polymer at the water-solution interface creates a solid layer around each droplet, which prevents the coalescence but allows the growth by diffusion [44,45]. Encapsulation of water droplets by a thin layer of polymer was described by Bormashenko and coworkers [46]. In this work, water droplets of volume 20-500 µl (much bigger than those involved in BFs formation) were deposited on the surface of a polymeric solution. The radii of the resulting drops were 2-6 mm, allowing a direct observation of the process. Immediately after water was deposited on the surface, the solution got up and tries to cover the droplets to minimize the surface tension. Indeed, water surface tension is much higher than that of the polymer solution, so minimization of drop free surface is highly favorable. Due to fast solvent evaporation, the solution on the droplet

dries, leaving a polymer film encapsulating water. In the case a group a drops is deposited, they are attracted to one other by capillary force, resulting in packing and, eventually, in coalescing. Even though the drops used in this experiment are much bigger than the one observed in BFs (with a different importance of gravity respect to surface tension), the phenomena resulting in water encapsulation can be assumed to occur in both cases. Srinivasarao, instead, proposed that a gaseous layer forms between two drops, keeping them apart and, so, hindering coalescence [29]. This layer can be formed by the solvent vapor escaping from the surface or by the air which is kept between the droplets by thermo-capillary convection. In a work by Dell'Aversana and Neitzel [47], it was demonstrated that two drops of the same liquid can be pressed together without coalescing if a lubricating layer of gas is forced to move between them. In the experiment, the two drops where kept at a different temperature and pressed one against the other. The difference in temperature leads to the formation of thermo-capillary convection in the bulk of the drops and, consequently, the fluid motion drive a flux of air which is forced to pass between the two apparently contacting liquid surface. This thin layer is sufficient to prevent coalescing and to oppose the force pressing the drops, which is a function of the temperature difference. These considerations have been developed for droplets on the surface, but depending on the system, the array can be composed of a monolayer of droplets, leading to a 2D pores structure, or of a multilayer structure, which results in pores formation in the bulk of the material (3D). The formation mechanism for 3D structures is the same as 2D ones, but repeated several times. Sinking of droplets, due to interfacial interactions or to convective fluxes, cause the solution to cover the

droplets, so the process of nucleation and diffusion growth can start again, forming a new layer.

The system, thus, is complex and involves several parameters. Sinking and arrangements of droplets are controlled by surface tension and by capillary and hydrodynamic forces. Marangoni convection causes both convective fluxes in the bulk fluid, deforming the surface, and the motion of the solution toward the top of the droplets, leading to encapsulation. Moreover, fluid motion causes the development of fluxes of the gas of the atmosphere, which form a layer among droplets. On the other hand, droplets are packed together by convective motion, by inter-capillary forces and, where it is present, by the external air flux. The balance among all these processes determines the formation of the final structure, its order and characteristics.

1.2.5 Final stage

In the final stage, droplets can coalesce, leading to a disruption of the ordered array and to a faster but not uniform growth of the mean diameter. To obtain a ordered array of bubbles, this step should be avoided. Once the solvent is completely evaporated, the temperature of the surface rises again to ambient temperature. Then water droplets evaporate, leaving behind an array of pores. Even though the array of water droplets has been always supposed to be the template for the porous structure, only recently this assumption was experimentally demonstrated. Barrow and co-workers [36] observed the formation of droplets with optical microscopy, recording the structure of the

formed array of water beads. Then, they observed with AFM the same region after solidification and water evaporation; they find that the pores disposition is the same as the one of water droplets and the defects are the same in the two arrays, giving a direct demonstration of the templating mechanism.

1.2.6 Parameters influencing BFs formation

Researchers have tried to study the different variables of this pattern formation, focusing their attention on the solvent, on the polymer or on the environmental conditions [28], but the unexplored possibilities are still numerous. The full understanding of the influence of each parameters leads to the possibility of tailoring the surface characteristics, according to the purpose they are used for. The process was studied in early works using polystyrene solutions in carbon disulfide, but several other materials have been investigated. Polymers used for the BFs method include linear homopolymers [29,35,43,48,49], block or statistical copolymers [50], star-like and hyper-branched polymers [45,51] and amphiphilic polymers [44,52].

The polymer used strongly influences the obtained porous structures. It was found that the molecular weight (M_w) have an optimal range (depending on the polymer and on the solution concentration [53]) for regular BFs formation. The use of too low molecular weights results in irregular pores with a wide size distribution while, on the other hand, a too high M_w hinders the process, resulting in films without pores [43]. This is probably due to the change in viscosity, which is proportional to M_w. If the viscosity is low, encapsulation of droplets is not

effective in blocking the coalescence, resulting in a disordered array or in a bimodal distribution of pores size [48]. On the contrary, a high viscosity solution does not allow the droplets to sink and so pores formation is not possible. If molecular weight is in the proper range, a regular structure is obtained and, generally, an increase in M_w leads to an increase in pores diameter and depth [48,53]. Increase in the molecular weight cause an increase also of the average distance between pores and of specific porosity (defined as the pores surface per unit area) [48]. Another parameter often studied is the concentration of polymer in the solution. An increase in concentration determines an increase in viscosity, but also a decrease of the droplets growth rate. The main effect is that average pore size decreases, but changes in concentration also affect the regularity of pores disposition and pore size distribution [53,54].

Pores size is influenced by the growth rate during the initial stage. This parameter is proportional to the temperature difference (ΔT) between the environment in which the process occurs and the solution surface. A solution with a lower polymer concentration presents a higher vapor pressure and so solvent evaporation rate is increased. This cause a more significant cooling of the surface, leading to higher ΔT and so to faster growth, which, finally results in bigger pores [54]. However, since polymer concentration influences also the surface tension and the viscosity of the solution, its influence on pores structures can be different in other systems [53].

Temperature difference, which influences growth rate, depends on solution concentration, but first of all on the solvent used. Moreover, pores size is limited

by the evaporation time of solvent, since film hardening hinders the further droplets growth. Reducing the time required for complete solvent evaporation, with other conditions left unchanged, leads to smaller pores. A solvent with higher vapor tension evaporates faster, reducing process time. The same effect is obtained also casting a smaller quantity of solution [51]. The evaporation rate can be controlled also modifying the air flow of humid air. Evaporation is, indeed, proportional to the air flux, so an increase in the flow causes an increase in evaporation rate and a decrease in the process time, leading to smaller pores [45]. On the other hand, high flow rates of humid air can determine an additional supply of moisture, enhancing droplets growth and so resulting in bigger pores [44].

Also environmental conditions influence the final structure; temperature influences viscosity, the convective flux and the kinetic of the process. Tian and coworkers [53] found that a decrease in temperature leads to a higher order of pores, provided that humidity level is high enough to allow condensation. This is explained by a slow Marangoni convection in the fluid, which causes smoother collisions among droplets, resulting in better order. Disordered structures in process at high temperature have also been observed by Zaho [54]. Moreover, in the range of temperature which maintains the order, an increase in temperature caused the formation of bigger pores. To explain this relation, the authors suggest that higher temperature causes a faster growth of droplets, due to enhanced solvent evaporation and so to a bigger temperature gradient. On the other hand, if evaporation is very fast, the viscosity of the surface rises rapidly; droplets

forming on the solution cannot sink and are not embedded, thus coalescence occurs and the resulting array is not ordered. The other usually studied environmental parameter is humidity. It is, obviously, fundamental for the process, since in dry atmosphere there is no formation of BFs [29]. It was demonstrated that, above a minimum level necessary for BFs formation, increased humidity leads to larger pores, due to the faster growth rate of droplets, driven by the difference in partial pressure of water vapor [43,53,54]. A more complicated problem arises when considering the nature of the solvent and of solvent-polymer interaction. Several solvents have been used and different results obtained. High volatility is usually a requested feature, to promote surface cooling, and low water miscibility is necessary to allow the templating mechanism. However, many other parameters influence the process [29,35,43,53,54]. Enthalpy of evaporation, together with vapor pressure, determines the solution surface cooling and so the nucleation and growth rate of droplets. Thermal conductivity, density, viscosity, surface tension and its temperature derivative, thermal expansion coefficient and specific heat capacity are all parameters which are involved in the development of convective fluxes, which determine droplets motion and aggregation, droplets arrangement and water encapsulation. Since the process is influenced by so many solvent features, a full understanding of the influence of each parameter is very complicated, and results usually do not allow the development of a complete physical model. This is the reason why, despite some common behaviors, each solvent has its particular influence on the porous film produced.

1.2.7 Advantages and evolution of BFs templating method

Despite this, compared to other techniques, BFs formation is quite simple and fast. The template for the final porous structure is easily prepared exploiting water condensation; an ordered array of pores can be obtained exploiting a self-assembling process; the template material is removed simply by evaporation at ambient temperature. The whole process is composed of a single step, that is deposition of the polymeric solution in the humid environment, and it lasts for only tens of seconds. Highly ordered porous structures have been obtained over large areas. In addition to these intrinsic advantages, BFs formation has other interesting aspect, which raised more interest on it. For example, combination of BF and lithography allows the transfer of the pattern to non-polymeric surface [55], while use of micro-contact printing allows the reproduction of the pattern on virtually any surface. Moreover, taking advantage of the interface between the polymeric solution and the water, it is possible to promote the migration of hydrophilic functional groups or particles toward the surface, obtaining a chemically and topographically patterned surface [44,56].

BFs were firstly studied to pattern the surface of polymeric flat films, the aim being the development of 2- or 3-dimensional array of regular mono-dispersed pores. These structures have a lot of potential uses, ranging from photonic crystals [50] to arrays of anamorphic micro-lens [57] and the assembly of nanocrystal [58]. However, different possibilities have been recently considered and exotic structures have been developed, patterning 3-D structures. As the patterning occurs due to solvent evaporation from a polymer solution, it was

observed also in other process involving polymer solution, such as electrospinning. This technique allows the formation of fibers ranging from micrometric to nanometric size and has been used for the production of nets, composed of either randomly or aligned fibers [59]. These structures are interesting in the biomedical field due to their morphological analogy with the extra cellular matrix (ECM), composed of biological nanofibers, and are so promising scaffold for cell growth [60]. The presence of pores on electrospun fibers was observed using high vapor tension solvent, such as chloroform or dichloromethane. Researchers have attributed the cause of that to different physical process, mainly BFs formation or phase separation [61-63]; as far as we know, a decisive study on the true causes of the pattern formation is still not present in literature. Patterned electrospun nets posses some interesting features: very high surface to volume ratio, hierarchical structure, nanoroughness and superhydrophbicity [16,64], which can be useful in filtration, chemical analysis and biomedical applications. Moreover, electrospinning can leads to fibers with interesting features, both related to the geometry of fibers and to surface characteristics [65,66], and even to the formation of beads, or microparticles [67].

1.3 Bibliography

[1] C. Mack, *Fundamental principles of optical lithography: the science of microfabrication*, Wiley-Interscience, 2007.

[2] K. Ronse, "Optical lithography—a historical perspective," *Comptes Rendus Physique*, vol. 7, Oct. 2006, pp. 844-857.

[3] B. Lin, "Optical lithography—present and future challenges," *Comptes Rendus Physique*, vol. 7, Oct. 2006, pp. 858-874.

[4] K. Kemp and S. Wurm, "EUV lithography," *Comptes Rendus Physique*, vol. 7, Oct. 2006, pp. 875-886.

[5] T.H.P. Chang, M. Mankos, K.Y. Lee, and L.P. Muray, "Multiple electron-beam lithography," *Microelectronic Engineering*, vol. 57-58, Sep. 2001, pp. 117-135.

[6] B.R. Appleton, S. Tongay, M. Lemaitre, B. Gila, J. Fridmann, P. Mazarov, J.E. Sanabia, S. Bauerdick, L. Bruchhaus, and R. Mimura, "Materials modifications using a multi-ion beam processing and lithography system," *Nuclear Instruments and Methods in Physics Research Section B: Beam Interactions with Materials and Atoms*, Feb. 2011, pp. 1-5.

[7] B.H. Luo, P.W. Shum, Z.F. Zhou, and K.Y. Li, "Preparation of hydrophobic surface on steel by patterning using laser ablation process," *Surface and Coatings Technology*, vol. 204, Jan. 2010, pp. 1180-1185.

[8] S. Hsieh, Y. Cheng, C. Hsieh, and Y. Liu, "Plasma induced patterning of polydimethylsiloxane surfaces," *Materials Science and Engineering: B*, vol. 156, Jan. 2009, pp. 18-23.

[9] B. LIN, “The ending of optical lithography and the prospects of its successors,” *Microelectronic Engineering*, vol. 83, Apr. 2006, pp. 604-613.

[10] D. Choi, “2D nano/micro hybrid patterning using soft/block copolymer lithography,” *Materials Science and Engineering: C*, vol. 24, Jan. 2004, pp. 213-216.

[11] V.N. Truskett and M.P.C. Watts, “Trends in imprint lithography for biological applications.,” *Trends in biotechnology*, vol. 24, Jul. 2006, pp. 312-7.

[12] Q. He, “Angular evaluation to quantify planar distortions of PDMS stamps in soft lithography,” *Materials Chemistry and Physics*, vol. 83, Jan. 2004, pp. 60-65.

[13] a Bai, C. Hu, Y. Yang, and C. Lin, “Pore diameter control of anodic aluminum oxide with ordered array of nanopores,” *Electrochimica Acta*, vol. 53, Jan. 2008, pp. 2258-2264.

[14] R. Bertholdo, M.C. Assis, P. Hammer, S.H. Pulcinelli, and C.V. Santilli, “Controlled growth of anodic aluminium oxide films with hexagonal array of nanometer-sized pores filled with textured copper nanowires,” *Journal of the European Ceramic Society*, vol. 30, Jan. 2010, pp. 181-186.

[15] Y. Li, G. Duan, and W. Cai, “Controllable superhydrophobic and lipophobic properties of ordered pore indium oxide array films.,” *Journal of colloid and interface science*, vol. 314, Oct. 2007, pp. 615-20.

[16] A. Tuteja, W. Choi, J.M. Mabry, G.H. McKinley, and R.E. Cohen, “Robust omniphobic surfaces.,” *Proceedings of the National Academy of Sciences of the United States of America*, vol. 105, Nov. 2008, pp. 18200-5.

[17] E. Egidi, G. Gasparini, R. Holdich, G. Vladisavljevic, and S. Kosvintsev, “Membrane emulsification using membranes of regular pore spacing: Droplet size and uniformity in the presence of surface shear,” *Journal of Membrane Science*, vol. 323, Oct. 2008, pp. 414-420.

[18] C. Zhou and D. Gall, “Surface patterning by nanosphere lithography for layer growth with ordered pores,” *Thin Solid Films*, vol. 516, Dec. 2007, pp. 433-437.

[19] M.L.K. Hoa, M. Lu, and Y. Zhang, “Preparation of porous materials with ordered hole structure.,” *Advances in colloid and interface science*, vol. 121, Sep. 2006, pp. 9-23.

[20] O. Velev and a Lenhoff, “Colloidal crystals as templates for porous materials,” *Current Opinion in Colloid & Interface Science*, vol. 5, Mar. 2000, pp. 56-63.

[21] A. Towata, M. Sivakumar, K. Yasui, T. Tuziuti, T. Kozuka, and Y. Iida, “Ultrasound induced formation of paraffin emulsion droplets as template for the preparation of porous zirconia.,” *Ultrasonics sonochemistry*, vol. 14, Sep. 2007, pp. 705-10.

[22] Y.-S. Cho, S.-H. Kim, G.-R. Yi, and S.-M. Yang, “Self-organization of colloidal nanospheres inside emulsion droplets: Higher-order clusters, supraparticles, and supraballs,” *Colloids and Surfaces A: Physicochemical and Engineering Aspects*, vol. 345, Aug. 2009, pp. 237-245.

[23] a Rasmont, P. Leclère, C. Doneux, G. Lambin, J. Tong, R. Jérôme, J. Brédas, and R. Lazzaroni, “Microphase separation at the surface of block copolymers, as studied with atomic force microscopy.,” *Colloids and surfaces. B, Biointerfaces*, vol. 19, Dec. 2000, pp. 381-395.

[24] B. Lowenhaupt and G. Hellmann, “Microphase and macrophase separation in blends with a two-block copolymer,” *Polymer*, vol. 32, 1991, pp. 1065-1076.

[25] R. Phillips and S. Cooper, “Phase separation in crystallizable multiblock poly(ether-ester) copolymers with poly(tetramethylene isophthalate) hard segments,” *Polymer*, vol. 35, Sep. 1994, pp. 4146-4155.

[26] Y. Feng, “Phase separation in a commercial block propylene-ethylene copolymer,” *Polymer*, vol. 39, Oct. 1998, pp. 5277-5280.

[27] S. Darling, “Directing the self-assembly of block copolymers,” *Progress in Polymer Science*, vol. 32, Oct. 2007, pp. 1152-1204.

[28] U.H.F. Bunz, “Breath Figures as a Dynamic Templating Method for Polymers and Nanomaterials,” *Advanced Materials*, vol. 18, Apr. 2006, pp. 973-989.

[29] M. Srinivasarao, D. Collings, a Philips, and S. Patel, “Three-dimensionally ordered array of air bubbles in a polymer film.,” *Science (New York, N.Y.)*, vol. 292, Apr. 2001, pp. 79-83.

[30] D. Fritter, C. Knobler, and D. Beysens, “Experiments and simulation of the growth of droplets on a surface (breath figures),” *Physical Review A*, vol. 43, Mar. 1991, pp. 2858-2869.

[31] D.W. Hutmacher, M. Sittinger, and M.V. Risbud, “Scaffold-based tissue engineering: rationale for computer-aided design and solid free-form fabrication systems.,” *Trends in biotechnology*, vol. 22, Jul. 2004, pp. 354-62.

[32] A. Steyer, P. Guenoun, D. Beysens, and C. Knobler, “Two-dimensional ordering during droplet growth on a liquid surface,” *Physical Review B*, vol. 42, 1990, pp. 1086-1089.

[33] A. Steyer, P. Guenoun, D. Beysens, and C. Knobler, “Growth of droplets on a substrate by diffusion and coalescence,” *Physical Review A*, vol. 44, 1991, pp. 8271-8277.

[34] D. NOEVER, “Order and Statistical Crystallography of Patterned Breath Figures,” *Journal of Colloid and Interface Science*, vol. 174, 1995, pp. 92-96.

[35] A. Limaye, R. Narhe, A. Dhote, and S. Ogale, “Evidence for Convective Effects in Breath Figure Formation on Volatile Fluid Surfaces,” *Physical Review Letters*, vol. 76, May. 1996, pp. 3762-3765.

[36] M.S. Barrow, R.L. Jones, J.O. Park, C.J. Wright, P.R. Williams, and M. Srinivasarao, “Studies of the Formation of Microporous Polymer Films in "Breath Figure" Condensation Processes,” *Modern Physics Letters B*, vol. 22, 2008, p. 1989.

[37] E. Servoli, G.A. Ruffo, and C. Migliaresi, “Interplay of kinetics and interfacial interactions in breath figure templating – A phenomenological interpretation,” *Polymer*, vol. 51, May. 2010, pp. 2337-2344.

[38] A. Saunders, J. Dickson, P. Shah, M. Lee, K. Lim, K. Johnston, and B. Korgel, “Breath figure templated self-assembly of porous diblock copolymer films,” *Physical Review E*, vol. 73, Mar. 2006, pp. 1-7.

[39] B.D. Boer, U. Stalmach, H. Nijland, and G. Hadziioannou, “Microporous Honeycomb-Structured Films of Semiconducting Block Copolymers and Their Use as Patterned Templates,” *Advanced Materials*, vol. 12, Nov. 2000, pp. 1581-1583.

[40] A. Steyer, P. Guenoun, and D. Beysens, “Hexatic and fat-fractal structures for water droplets condensing on oil,” *Physical Review E*, vol. 48, 1993, pp. 428-431.

[41] D. Chan, “The interaction of colloidal particles collected at fluid interfaces,” *Journal of Colloid and Interface Science*, vol. 79, Feb. 1981, pp. 410-418.

[42] O. Karthaus, “Mesoscopic 2-D ordering of inorganic/organic hybrid materials,” *Materials Science and Engineering: C*, vol. 10, Dec. 1999, pp. 103-106.

[43] J. Peng, “The influencing factors on the macroporous formation in polymer films by water droplet templating,” *Polymer*, vol. 45, Jan. 2004, pp. 447-452.

[44] K.H. Wong, T.P. Davis, C. Barner-Kowollik, and M.H. Stenzel, “Honeycomb structured porous films from amphiphilic block copolymers prepared via RAFT polymerization,” *Polymer*, vol. 48, 2007, pp. 4950-4965.

[45] M.H. Stenzel, C. Barner-Kowollik, and T.P. Davis, “Formation of honeycomb-structured, porous films via breath figures with different polymer architectures,” *Journal of Polymer Science Part A: Polymer Chemistry*, vol. 44, 2006, pp. 2363-2375.

[46] E. Bormashenko, A. Musin, Y. Bormashenko, G. Whyman, R. Pogreb, and O. Gendelman, “Formation of Films on Water Droplets Floating on a Polymer Solution Surface,” *Macromolecular Chemistry and Physics*, vol. 208, 2007, pp. 702-709.

[47] P. Dell’Aversana and G.P. Neitzel, “When Liquids Stay Dry,” *Physics Today*, vol. 51, 1998, p. 38.

[48] E. Bormashenko, R. Pogreb, O. Stanevsky, Y. Bormashenko, and O. Gendelman, “Formation of honeycomb patterns in evaporated polymer solutions: Influence of the molecular weight,” *Materials Letters*, vol. 59, Dec. 2005, pp. 3553-3557.

[49] Y. Fukuhira, E. Kitazono, T. Hayashi, H. Kaneko, M. Tanaka, M. Shimomura, and Y. Sumi, “Biodegradable honeycomb-patterned film composed of poly(lactic acid) and dioleoylphosphatidylethanolamine.,” *Biomaterials*, vol. 27, 2006, pp. 1797-802.

[50] M. Haupt, S. Miller, R. Sauer, K. Thonke, a Mourran, and M. Moeller, “Breath figures: Self-organizing masks for the fabrication of photonic crystals and dichroic filters,” *Journal of Applied Physics*, vol. 96, 2004, p. 3065.

[51] W. Dong, Y. Zhou, D. Yan, Y. Mai, L. He, and C. Jin, “Honeycomb-structured microporous films made from hyperbranched polymers by the breath figure method.,” *Langmuir : the ACS journal of surfaces and colloids*, vol. 25, 2009, pp. 173-8.

[52] P. Tung, C. Huang, S. Chen, C. Hsu, and F. Chang, “Regular honeycomb porous polymer films based on amphiphilic block copolymer,” *Desalination*, vol. 200, Nov. 2006, pp. 55-57.

[53] Y. Tian, Q. Jiao, H. Ding, Y. Shi, and B. Liu, “The formation of honeycomb structure in polyphenylene oxide films,” *Polymer*, vol. 47, May. 2006, pp. 3866-3873.

[54] B. Zhao, J. Zhang, H. Wu, X. Wang, and C. Li, “Fabrication of honeycomb ordered polycarbonate films using water droplets as template,” *Thin Solid Films*, vol. 515, Feb. 2007, pp. 3629-3634.

[55] L. Li, Y. Zhong, J. Li, J. Gong, Y. Ben, J. Xu, X. Chen, and Z. Ma, “Breath figure lithography: A facile and versatile method for micropatterning.,” *Journal of colloid and interface science*, vol. 342, 2010, pp. 192-7.

[56] H. Sun, H. Li, and L. Wu, “Micro-patterned polystyrene surfaces directed by surfactant-encapsulated polyoxometalate complex via breath figures,” *Polymer*, vol. 50, 2009, pp. 2113-2122.

[57] K. Chari, C.W. Lander, and R.J. Sudol, “Anamorphic microlens arrays based on breath-figure template with adaptive surface reconstruction,” *Applied Physics Letters*, vol. 92, 2008, p. 111916.

[58] X. Xu and X. Wang, “Combinatorial two-dimensional architectures from nanocrystal building blocks: controlled assembly and their applications,” *Journal of Materials Chemistry*, vol. 19, 2009, p. 3572.

[59] Z.-ming Huang, “A review on polymer nanofibers by electrospinning and their applications in nanocomposites,” *Composites Science and Technology*, vol. 63, 2003, pp. 2223-2253.

[60] J.J. Norman and T.A. Desai, “Methods for fabrication of nanoscale topography for tissue engineering scaffolds.,” *Annals of biomedical engineering*, vol. 34, 2006, pp. 89-101.

[61] M. Bognitzki, W. Czado, T. Frese, A. Schaper, M. Hellwig, M. Steinhart, A. Greiner, and J.H. Wendorff, “Nanostructured Fibers via Electrospinning,” *Advanced Materials*, vol. 13, 2001, pp. 70-72.

[62] S. Megelski, J.S. Stephens, D.B. Chase, and J.F. Rabolt, “Micro- and Nanostructured Surface Morphology on Electrospun Polymer Fibers,” *Macromolecules*, vol. 35, Oct. 2002, pp. 8456-8466.

[63] M. Galvin, K. Kiick, D. Pochan, J. Sun, and N. Wagner, “Enhancing the Properties of Nanoscale Electrospun Polymer Fibers Through Chemical Architecture, Surface Texturing and Optimization of Processing Protocols,” *Macromolecules*, 2003, pp. 16-18.

[64] M. Ma, M. Gupta, Z. Li, L. Zhai, K.K. Gleason, R.E. Cohen, M.F. Rubner, and G.C. Rutledge, “Decorated Electrospun Fibers

Exhibiting Superhydrophobicity," *Advanced Materials*, vol. 19, 2007, pp. 255-259.

[65] L. Wang, C.-L. Pai, M.C. Boyce, and G.C. Rutledge, "Wrinkled surface topographies of electrospun polymer fibers," *Applied Physics Letters*, vol. 94, 2009, p. 151916.

[66] K. Kim, M. Kang, I.-joo Chin, and H.-joon Jin, "Unique Surface Morphology of Electrospun Polystyrene Fibers from a N,N-Dimethylformamide Solution," *Macromol. Res.*, vol. 13, 2005, pp. 533-537.

[67] Y. Wu and R.L. Clark, "Controllable porous polymer particles generated by electrospraying.," *Journal of colloid and interface science*, vol. 310, 2007, pp. 529-35.

2. Influence of interfacial and kinetic factors on BFs process

2.1 Introduction

Polymer films with controlled porosity are attractive for a variety of applications, from photonics to biomedical devices [1]. Many different techniques are currently employed in the production of porous substrates, but self-organization of matter is arising as the most convenient approach. Among them, Breath Figure templating is regarded as a simple and cost effective technology since François and coworkers first observed the phenomenon [2].

Breath Figures are patterns originated by water drops that condense as isolated objects from moist air upon contacting a cold solid or liquid surface. When the pattern is formed on a solution casting film, the droplets print pores on the surface. This physical phenomenon has been studied all across the XX century [3-6] and is currently exploited for BF templating as it follows: (i) polymers are dissolved in solvents with high vapor pressure and low miscibility with water; (ii) the solution is allowed to dry in a humid environment, generally under flow conditions, in order to induce water condensation and nucleation of water droplets at the air/liquid interface; (iii) during the first stages of solvent evaporation water droplets slowly grow by uptake of moisture from the surrounding water vapor, without merging; (iv) after a few seconds droplets start to experience coalescence and their radius R increases with time according to $R \sim$

$t^{1/3}$ [7]; (v) water droplets self-organize into regular patterns while growing, thus creating a template for the subsequent arrangement of polymer chains: as film hardening occurs and the evaporation of water is completed, a regular porous structure is obtained.

Pore size can range from a few hundreds of nanometers to several micrometers depending on the experimental conditions, as relative humidity, the rate of moist airflow, surface temperature, polymer concentration, polymer architecture, interfacial tension between solvent and water [8-10]. The same parameters are also believed to regulate the arrangement of water drops into honeycomb patterns, preventing or reducing coalescence: soon upon condensation, water drops have high mobility on the surface and attractive interfacial forces induce the aggregation of few drops into small ordered areas; later on, a force proportional to the sixth power of area radii attracts other ordered islands, thus extending the regular pattern [11]. Although the mechanism has not fully clarified, many experimental results indicate that airflow and thermocapillary flow drive the hexagonal packing of water drops: solvent evaporative-cooling causes a temperature gradient within the solution and a subsequent surface tension gradient is produced, with colder areas corresponding to regions at higher surface tension. At this point Marangoni convection produces a thermocapillary flow that directs the solution with water drops to colder areas in order to minimize surface energy, until the surface is completely covered by water drops [8,12]. As long as a temperature gradient is maintained, thermocapillary convection also prevents water drops from coalescence, inducing convective motion inside the drops and

between them, where the presence of a lubricating air film has been demonstrated [13,14]. Alternatively, it has been suggested that non-coalescence is related to solvent vapor, which creates a separating layer between droplets [12]. Along with superficial patterns, multilayer structures with a regular arrangement of pores can be obtained via BF templating. However, despite the growing interest for the phenomenon itself and its technological implications, controversial models have been proposed to explain the formation of monolayer vs multilayer arrays: some reports relate the presence of pore multilayer to solvent density [12,15], others attribute pore stacking to interfacial tension [16,17]. This point will be discussed thoroughly in the subsequent sections.

In pioneering works only star polystyrene SPS and rod-coil block PS were believed to generate BF templating [2,7,18,19], nowadays a variety of polymers are currently employed, as reported in the reviews by Bunz [1] and Stenzel [10]: linear conjugated polymers, polyimides, light emitting polymers, liquid-crystalline polymers, organometallic polymers and degradable polymers. More recently, BF templating on biocompatible, biodegradable polymers has become very attractive for many biomedical applications, from tissue engineering to drug delivery [20-22]. The present work is intended as a phenomenological discussion about the mechanisms of BF templating on polylactic acid PDLLA, a biocompatible aliphatic polyester that is particularly attractive for its biodegradability. We report the formation of a variety of porous structures via BF templating on PDLLA solutions, by varying polymer concentration, solvent type, and experimental setup; then the BF phenomenology on PDLLA has been related to processing conditions, in order

to investigate the role of physical and chemical interactions, together with kinetics, in regulating the process.

2.2 Materials and Methods

2.2.1 Films production

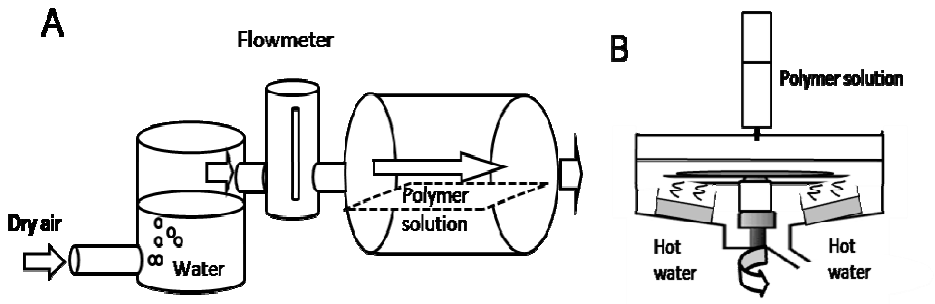

Fig.2.1: Experimental set-up for the production of BF films: humid flow system (A) and spin casting approach (B). In A compressed air is bubbled into water to generate moist air, the airflow is controlled by a flowmeter and inlet into the glass chamber, where polymer solutions are allowed to dry; in B polymer solutions are injected into the spin coater chamber, where a water bath ensures the desired values of relative humidity.

Linear Poly(D,L)Lactic Acid (PDLLA) Resomer R207 (MW=200 kDa) was purchased from Boeringher Ingelheim (Germany). PDLLA was dissolved at room temperature

in Chloroform (CHL) and Ethyl Acetate (EA) at 3%, 6%, 11% w/v concentration and used within 18 hours to produce porous PDLLA films. Porous films were obtained via BFs templating according to two different experimental set-ups, in which the timescale of film hardening could be varied from seconds (spin coating system) to minutes (humid flow system).

The former set of samples was produced by casting the polymer solution under controlled humid flow (Fig. 2.1 A): 600 µl of PDLLA solution were spread on glass slides and placed in a cylindrical chamber (3 cm diameter, 18 cm length), connected at one end to an air bubbler. Blowing compressed air into distilled water at room temperature generated moist air; the other end of the casting chamber was let open. Complete solvent evaporation required up to 15 minutes; the typical sample thickness was within 40 µm. Flow rate was adjusted between 0.8 and 1.4 L min^{-1} according to polymer concentration, in order to avoid waving effects on the film surface and favor the regular arrangement of water droplets during water condensation.

The second set of PDLLA films was produced via spin coating (Spin150 – SPS-Europe) under controlled humidity, generated by heating at different temperature a water bath inside the spin chamber (Fig. 2.1 B); relative humidity RH of (78 ± 3)% or (87 ± 3)% were used for this study. Experiments were carried out as follows:

(i) 100 µl of polymer solution were loaded on a square cover glass (25 x 25 mm) while rotating at 6000 rpm; after few seconds the spin rate was reduced to 1000 rpm;

(ii) 300 µl of polymer solution were dropped on a square cover glass (25 x 25 mm) and spin coated at 4000 rpm for few seconds before reducing the spin rate to 1000 rpm.

Total spin time of 30 seconds was required for complete solvent evaporation; typical sample thickness was less than 5 µm. All glass substrates were used as received. Assuming that fast film hardening can freeze BF templating in its early stage, the analysis of porous films obtained on different timescales can thus indirectly describe subsequent steps of the process itself.

2.2.2 Films and process observation

The formation of BF patterns on PDLLA-CHL 6% (w/v) and PDLLA-EA 11% (w/v) casted films has been observed in real time by optical microscopy (Axiotech, Zeiss) and videos have been recorded via a microscopy camera (Infinity, Lumenera);for this purpose the cylindrical chamber has been substituted with parallel-plate chamber in order to improve focusing. Average drop radius has been measured on individual video frames via the free software Gwyddion and plotted versus time; curve fitting has been carried out via Origin - Advanced fitting tool.

Film structure was characterized by light microscopy (Zeiss Axiotech 100 Hal) and Scanning Electron Microscopy (SEM), both in High Vacuum (Cambridge Stereoscan

200) and in Low Vacuum mode (Philips TMP ESEM), operating between 10 kV and 16 kV accelerating voltage. Cross sections of the porous films were obtained by cryofracture in liquid nitrogen and analyzed by SEM as previously explained. All samples were gold sputtered before SEM analysis. The image analysis software ImageJ was used to measure the average pore size of each sample and to calculate two-dimensional Fast Fourier Transform (2D-FFT) in order to characterize surface structures and identify the presence of regular patterns [23].

2.3 Results and Discussion

2.3.1 Structure of BF Films via Humid Flow System

Among organic solvents, Chloroform and Ethyl Acetate were selected for this study because of their volatility and good solubility for PDLLA; moreover, the differences of their physical and chemical properties (Table 2.1) can give new insights into the contribution of solvent type to the entire process. CHL is a customary solvent for BF templating while EA is quite unusual for this application, possibly because of its higher solubility in water; however the low toxicity of EA makes this solvent an attractive choice.

Solvent	Surface tension [mN m^{-1}]	Interfacial tension with H_2O [mN m^{-1}]	Density g cm^{-3}	Solubility in H_20 [g/l]	Vapour Pressure (@20°C) [kPa]	Enthalpy of Vaporization (@25°C) [kJ mol^{-1}]
CHL	27.5	28.3	1.48	8	21.1	31.68
EA	23.9	25.9	0.89	83	12.4	35.66

Table 2.1: Some relevant physical and chemical properties of solvents used in this study [25-26].

Porous films with different structures were obtained in the humid flow chamber (Fig. 2.1A) by varying the solvent type and concentration. The flow rate F was adjusted according to polymer concentration in order to optimize the regularity of the pore patterns and, under certain conditions, to control pore size (Fig. 2.2).

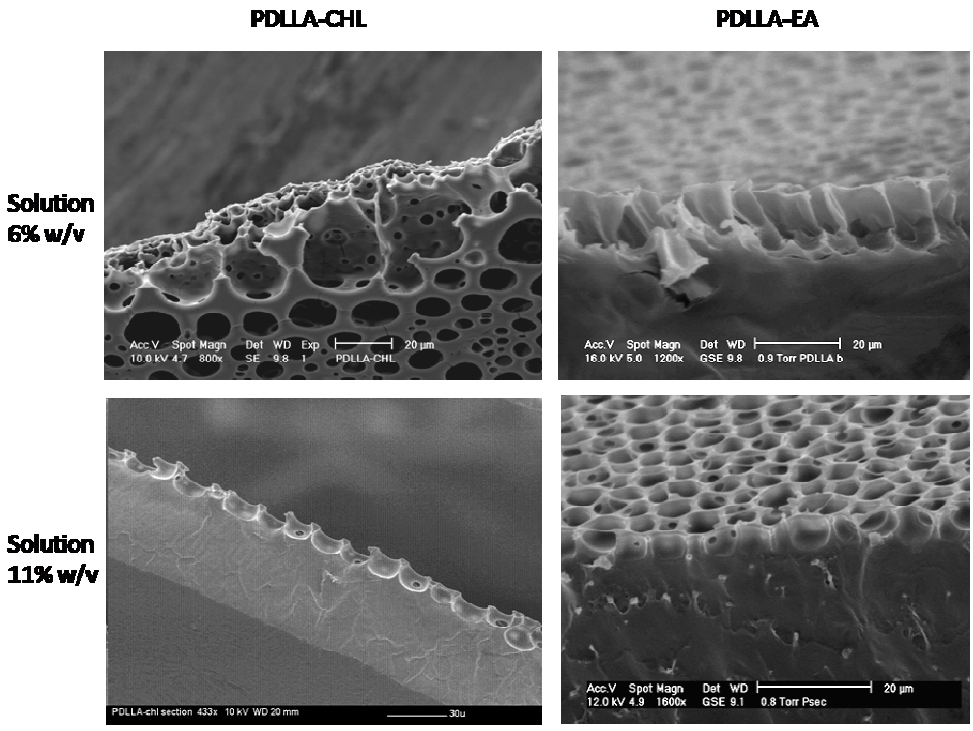

Fig.2.2: Cross sections of BF films produced in the humid flow chamber. The effects of solvent type (columns) and polymer concentration (rows) on pore structure have been evaluated by SEM analysis.

When PDLLA was dissolved in CHL, either multilayer pore structures or single layers of pores were produced depending on polymer concentration: 6% w/v solution created tridimensional porosity with at least three porous layers stacked up, where pore size increased from the bottom to the upper surface; conversely pore monolayer was produced by 11% solution. Irrespective of concentration, pores of films obtained in the humid flow system were interconnected, even if a

reduced degree of interconnection was observed with higher polymer concentration.

Pore dimension was affected by the flow rate F, with larger pores produced by lower F values: the apparent diameter (i.e., pore lateral dimension measured on the film surface) was d=(11.1 ± 2.8) µm for F=0.8 L min^{-1} while it was reduced to d=(5.1 ± 0.7) µm for F=1.2 L min^{-1}. Polymer concentration had no significant effects on pore size when PDLLA was dissolved in CHL and spherical-like pores with a typical aspect ratio R = 0.8 were observed.

PDLLA-EA solutions produced a single layer of interconnected pores. Films obtained under flow rate F=1.2 L min^{-1} with 6% w/v solution exhibited columnar pores with spherical basis of diameter d=(7.2 ± 1.6) µm and lateral walls of (15.7 ± 0.8) µm (aspect ratio R = 0.5); interconnections were generally observed at the junction between pore walls and pore basis. Higher solubility of water in EA, with respect to other solvents commonly employed for BF templating, might be responsible for columnar pores.

In contrast to PDLLA-CHL system, PDLLA-EA produced smaller pores of d=(5.5 ± 0.3) µm by increasing polymer concentration to 11% w/v; pores exhibited a square-like shape (R = 0.9) and lower degree of interconnection.

Although honeycomb structures could not be obtained by these experimental setups, 2D-FTT analysis of pore patterns [23] revealed that the higher level of order and regularity was achieved by dissolving PDLLA in chloroform (Fig. 2.3). The power spectrum of PDLLA-CHL films showed a six-fold modulation superimposed

to a ring of weaker intensity, which indicates the presence of a characteristic interpore distance with preferred hexagonal order. PDLLA-EA produced a sharp ring, suggesting a random distribution of monodispersed pores.

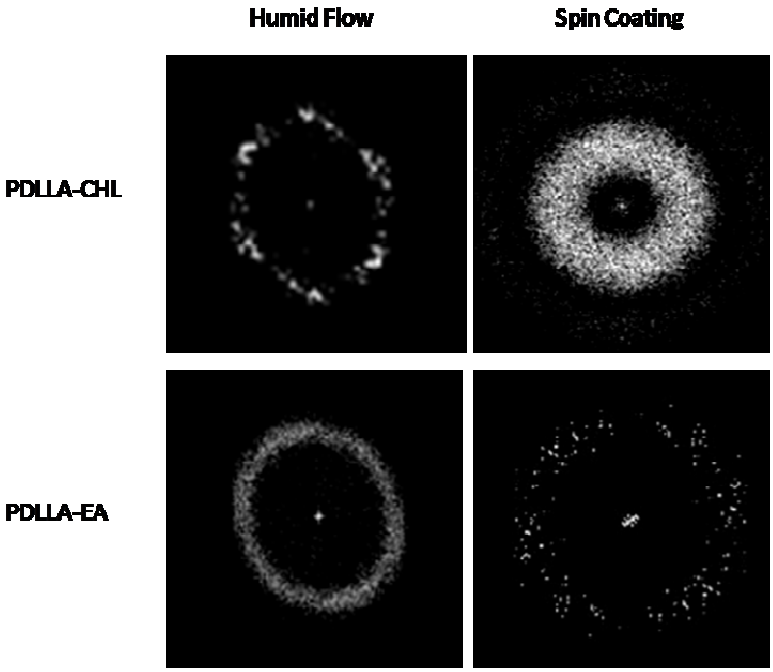

Fig.2.3: 2D-FFT characterization of surface patterns of BF films. Power spectra show the effects of processing conditions (columns) and solvent type (rows) on the regularity of pore patterns and pore monodispersity.

2.3.2 Structure of BF Films via Spin Casting Procedure

In the spin casting procedure, PDLLA films were made under controlled humidity, by adjusting the spin rate to polymer concentration (Fig. 2.1B). Humidity values were varied in order to optimize the regular arrangement of water droplets and the subsequent regularity of porous films (Fig. 2.4).

BFs films with PDLLA solution 6% w/v in CHL were characterized by a single layer of individual pores, with tunable size according to the volume of solution loaded in the spin coater: 100 µl of solution produced pores of diameter (2.0 ± 0.3) µm and depth (1.0 ± 0.1) µm (aspect ratio R=2), while 300 µl gave diameter of (2.2 ± 0.4) µm and depth of (1.7 ± 0.2) µm (aspect ratio R=1.3).

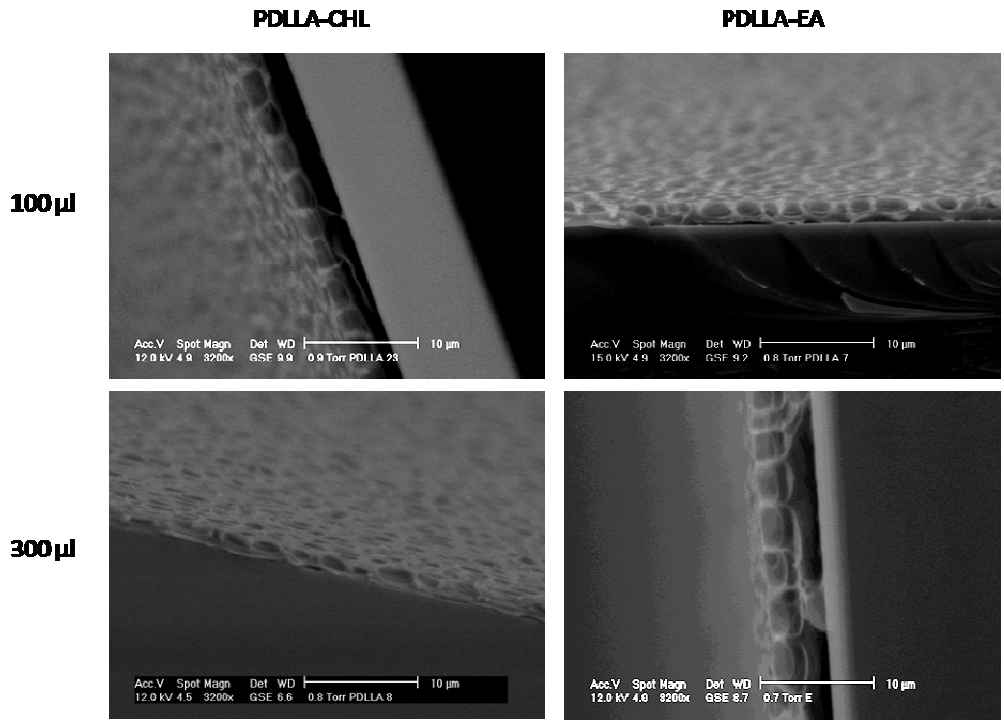

Fig.2.4: Cross sections of BF films produced via spin coating. The effects of solvent type (columns) and volume of solution (rows) have been evaluated by SEM analysis.

When PDLLA was dissolved in EA (6% w/v), the volume of polymer solution had a different effect on the process: films with a single layer of pores were obtained from 100 µl, while two layers were stacked up after loading 300 µl. In the latter case, two layers of pores with constant diameter (3.7 ± 0.8) µm were piled up and interconnections were generally observed in-plane rather than out-of-plane; the bottom layer was (1.2 ± 0.1) µm depth, the top layer (1.5 ± 0.1) µm.

The value of relative humidity affected single layer films mostly: individual pores of depth (1.1 ± 0.2) μm were obtained at 78% RH, while deeper interconnected pores of depth (3.1 ± 0.1) μm were produced at 87% RH. Pore diameter was measured as (2.5 ± 0.4) μm in both cases, meaning that the aspect ratio of pores can be modified by changing the humidity parameters in the spin chamber: pore aspect ratio could be varied from R=2.3 for 78% RH to R=0.8 for 87% RH. In addition, lower humidity favored the formation of individual pores while interconnected pores were typically observed at higher RH values.

The 2D-FFT analysis of surface patterns (Fig. 2.3) showed an inverse trend of spin coated films with respect to the humid flow system: the power spectrum of PDLLA-EA exhibited diffuse spots in preferred directions, while a large, blurred ring in PDLLA-CHL films.

Table 2.2 summarizes the typical values of pores size and pores aspect ratio (diameter/depth) when PDLLA was dissolved either in CHL (top) or EA (bottom). Experimental data clearly demonstrate that pore size is affected by both solvent type and processing conditions, suggesting that the final structure of BF films is determined by both thermodynamic and kinetic contributions.

PDLLA-CHL	Pores Depth (µm)	Pores Diameter (µm)	Pores Aspect Ratio, R
Humid flow (F=0.8 L min $^{-1}$)	12.9 ± 2.7	10.4 ± 0.4	0.8 (± 21%)
Spin coating – 300 µl	1.7 ± 0.2	2.2 ± 0.4	1.3 (± 18%)
Spin coating - 100 µl	1.0 ± 0.1	2.0 ± 0.3	2.0 (± 15%)

PDLLA-EA	Pores Depth (µm)	Pores Diameter (µm)	Pores Aspect Ratio, R
Humid flow (F=1.2 L min $^{-1}$)	15.7 ±0.8	7.2 ± 1.6	0.5 (± 22%)
Spin coating - 300 µl	2.7 ± 0.1	3.7 ± 0.8	1.4 (± 22%)
Spin coating - 100 µl	1.1 ± 0.2	1.5 ± 0.1 top 1.2 ± 0.1 bottom	1.4 (± 18%) 1.1 (± 18%)

Table 2.2: Effects of processing conditions and solvent type on BF films obtained from PDLLA-CHL (top) and PDLLA-EA (bottom) solutions at 6% w/v.

2.3.3 Contribution of Interfacial Interactions

In order to relate the structure of porous films to physical and chemical interactions occurring at the interface polymer/solvent/water, we referred to the

work by Bolognesi et al. [16]: they linked the relative pore penetration z_0 in BF films obtained in a humid flow system to interfacial interactions, namely water surface tension γ_w, solvent surface tension γ_s, and water/solvent interfacial tension $\gamma_{w/s}$, as follows (Eq. 2.1):

$$z_0 = (\gamma_w - \gamma_{w/s}) / \gamma_s \qquad [2.1]$$

According to this model, water drops penetrated the solution and produced multilayer for z_0 higher than 1, while for z_0 between -1 and 1 the drops float at the interface air/solution, resulting in pore monolayer.

Assuming γ_w = 72.8 mN m^{-1}, $\gamma_{w/s}$ = 28.3 mN m^{-1}, γ_s = 27.5 mN m^{-1} for CHL and $\gamma_{w/s}$ = 25.9 mN m^{-1}, γ_s = 23.9 mN m^{-1} for EA (Table 1), the relative penetration was calculated as z_0 = 1.6 for PDLLA-CHL and z_0 = 1.9 for PDLLA-EA. Since these values are higher than 1, the penetration of water drops into PDLLA solutions is thermodynamically favorite either for CHL or EA, with deeper penetration allowed for EA.

The predictions of the model have been compared to the experimental data in Table 2, especially for films produced according to similar processing conditions (i.e., humid flow chamber); the term of comparison was the reciprocal of z_0, $1/z_0$, which can be associated to the experimental R value, the pore aspect ratio. When polymer solution of concentration 6% w/v were subjected to controlled humid flow, a good match was observed: PDLLA-CHL produced multilayer structures as a result of the penetration of water drops and their arrangement in multilayer and $1/z_0$ = 1/1.6 = 0.6 was compatible to the experimental value R=0.8; for PDLLA-EA

films the theoretical value $1/z_0$ = 1/1.9 = 0.5 fully corresponded to the experimental R value but multilayer was not obtained, while columnar pores were observed instead. Nevertheless, PDLLA-EA created multilayer when 300 µl of solution were spin coated under controlled humidity. Columnar pores could be related to the higher solubility of water in EA with respect to CHL, that can produce coagulation; alternatively, pore depth can be explained via the low vapour pressure of EA, since during solvent evaporation $\gamma_{w/s}$ decreases and longer time is left to water droplets to continuously penetrate the polymer solution.[16]

2.3.4 Contribution of Kinetic Factors

Despite the good match observed with Bolognesi model, our experimental data suggest that interfacial interactions alone cannot explain the complexity of BF templating, especially when different porous structures have been obtained from the same polymer/solvent system by varying concentration and processing conditions.

Since comparable pore size can be obtained with the same processing system regardless of the type of solvent used, we have hypothesized that kinetics of film drying has an active role in determining BF templating. In order to support this hypothesis and better clarify the dynamics of the process, it has been recorded in the humid flow system in real time via a microscope camera.

The videos demonstrated that BF templating follows different dynamics depending on the solvent used: in PDLLA-CHL coalescence took place over the entire time domain, even if increasing in the apparent diameter of water droplets

was observed just in the last stages of the process and was not detected in the first ones (Fig. 2.5). Conversely, in PDLLA-EA single droplet growth dominated the first events of BF formation while a burst of coalescence was observed when film hardening became visible.

These findings suggest that in PDLLA-CHL system water drops can be surrounded and eventually covered by a polymer layer, thus allowing (i) in the first stages of the process (diluted solution) the formation of new water droplets and (ii) in the last stages, when the increased concentration of polymer reduces the molecular mobility of the system, the redistribution of existing drops on the top surface and the subsequent increase in pore diameter due to coalescence. This mechanism can account for the formation of multilayers observed in Fig. 2.2, where pore size increases from the bottom to the top surface.

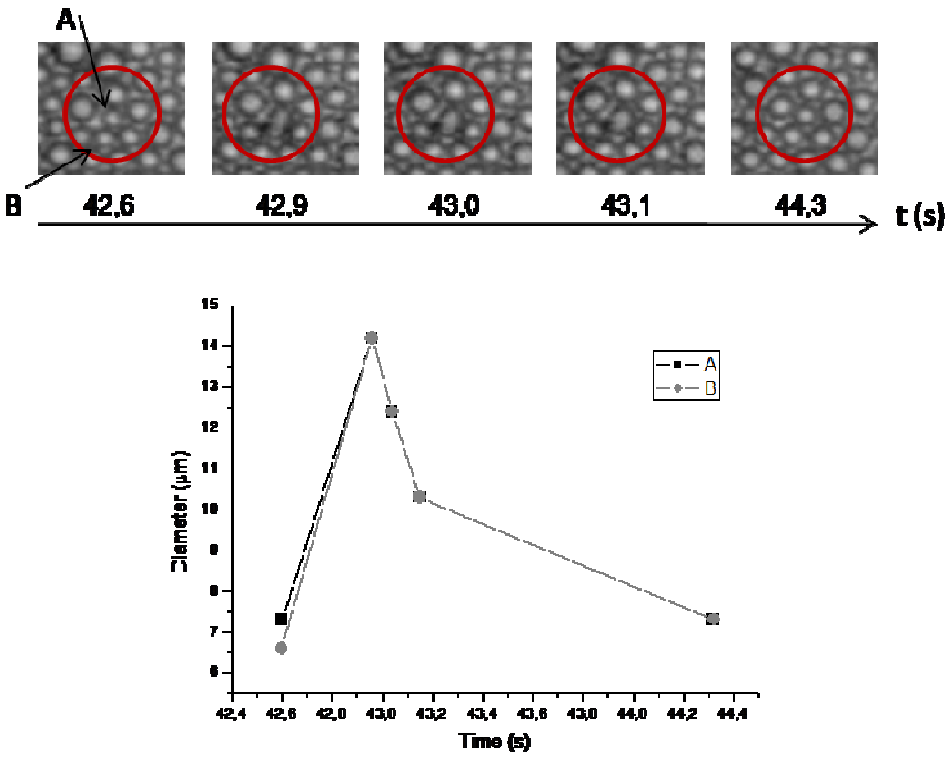

Fig.2.5: Diameter of drop A and B before, during and after coalescence in the first stages of BF templating in PDLLA-CHL solution.

According to the literature [7], experimental data points have been fitted by $R \sim t^{\alpha}$, resulting in $\alpha = 0.49 \pm 0.02$ for PDLLA-CHL and $\alpha = 0.33 \pm 0.02$ for PDLLA-EA (Fig. 2.6); these α values reflect the dynamics of droplet growth observed in the

videos and confirm the findings of Lymaye et al. [24], where α ~ 0.3 is related to single droplet growth and α ~ 0.5 to coalescence-dominated growth.

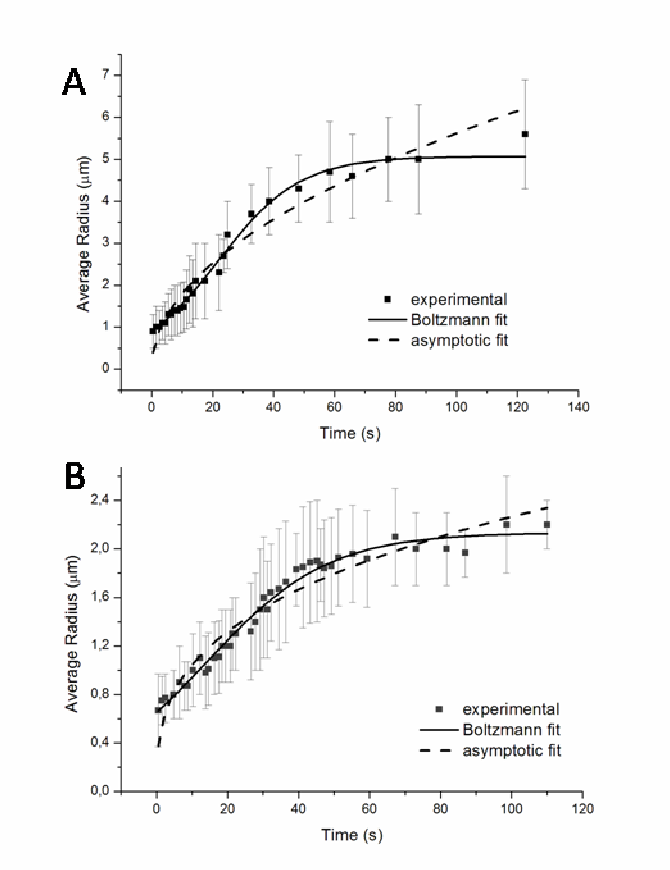

Fig.2.6: Data fitting of experimental data points reporting the average radius of water droplets as a function of drying time in PDLLA-CHL (A) and PDLLA-EA (B).

Despite the good agreement of asymptotic fit with the literature, the experimental data in Fig. 6 were best fitted by a Boltzmann sigmoid (Eq. 2.2):

$$R = \frac{R_f}{1 + e^{-\frac{(t-t_0)}{k}}} \qquad [2.2]$$

where R_f is the final average radius of water drops, t_0 is by definition the time at which $R=R_f/2$, k is related to the slope m of the linear part of the curve by

$$m = \frac{R_f}{4k} \qquad [2.3]$$

The starting radius R_0 have been imposed $R_0 = 0$.

Fitting parameters for PDLLA-CHL and PDLLA-EA are reported in Table 2.3.

Solvent	R_f	t_0	k	Reduced chi^2
CHL	5.14 ± 0.09	21.8 ± 0.9	14.2 ± 0.8	0.03
EA	2.14 ± 0.03	14.1 ± 0.7	17.2 ± 0.8	0.004

Fig.2.3: Fitting parameters for PDLLA-CHL and PDLLA-EA obtained by Boltzmann sigmoid fit.

The sigmoid fit is in agreement with the cooperative nature of droplet growth by coalescence, clearly shown in the PDLLA-EA video; moreover a kinetic interpretation of t_0 and k can be provided if the time evolution of BF patterning is coupled to the kinetics of the evaporation flux approximated to a sigmoid curve. This approximation is justified by the two successive regimes characterizing the drying kinetics of polymer/solvent solutions: in the first stage (diluted solution)

the process is fast and mainly controlled by solvent evaporation in air (i.e., heat and mass transfers between the moving interface and the air). In the second stage, as the solvent concentration is decreasing in the upper layer near the interface, the reduction of the partial pressure vapour produces slow diffusion and evaporation. [25]

By expressing the time evolution of the evaporation flux J according to Eq. 2.4

$$J = \frac{1+e^{-\frac{(t-1-t_0)}{k}}}{1+e^{-\frac{(t-t_0)}{k}}} - 1 \qquad [2.4]$$

and considering that

$$J_{t_0} = \frac{Js}{2} = \frac{1+e^{-\frac{(t_0-1-t_0)}{k}}}{1+e^{-\frac{(t_0-t_0)}{k}}} - 1 = e^{\left(\frac{1}{k}\right)} - 1 \qquad [2.5]$$

where Js is the value of evaporation flux at the starting time of water drop nucleation, which is mainly determined by the solvent vapor pressure and the flux of humid air.

The parameter k can now be written as

$$k = \frac{1}{\ln(Js+1)} \qquad [2.6]$$

thus demonstrating a relationship between the slope of the curve representing the time evolution of droplet growth and the evaporation flux produced on the polymer solution during the initial stages of BFs templating.

This interpretation accounts for the experimental observation that starting from the same polymer-solvent solution larger pores can be produced by decreasing the rate of the humid flux.

The physical meaning of t_0 is related to the transition from the fast, evaporation-limited stage of the drying kinetics to the slow, diffusion limited one [27]; t_0 can be determined by both polymer concentration and evaporation flux. The videos clearly showed that at t_0 PDLLA-EA experienced a burst of coalescence, while in PDLLA-CHL the apparent diameter of water droplets started to increase. Both the phenomena can be related to the reduced mobility of the system caused by the strong solvent/polymer interactions produced in concentrated solutions [28].

2.3.5 Phenomenological model

Starting from our experimental observations the following model for BFs templating is hereby proposed (Fig. 2.7): upon the exposure of evaporating polymer solution to a flow of humid air, the cooling of polymer surface favors the condensation of water vapor and water droplets undergo a burst of nucleation at the interface; the flow can be directly introduced in a chamber or indirectly produced upon spin coating the polymer solution in environments with high values of relative humidity. According to specific water/solvent interfacial interactions water drops start to grow via diffusion limited (e.g., PDLLA-EA) or

coalescence-driven growth (e.g., PDLLA-CHL), thus producing a population of monodisperse drops. If proper interfacial conditions are satisfied, the polymer solution can surround them all around until film hardening occurs (Fig. 2.7).

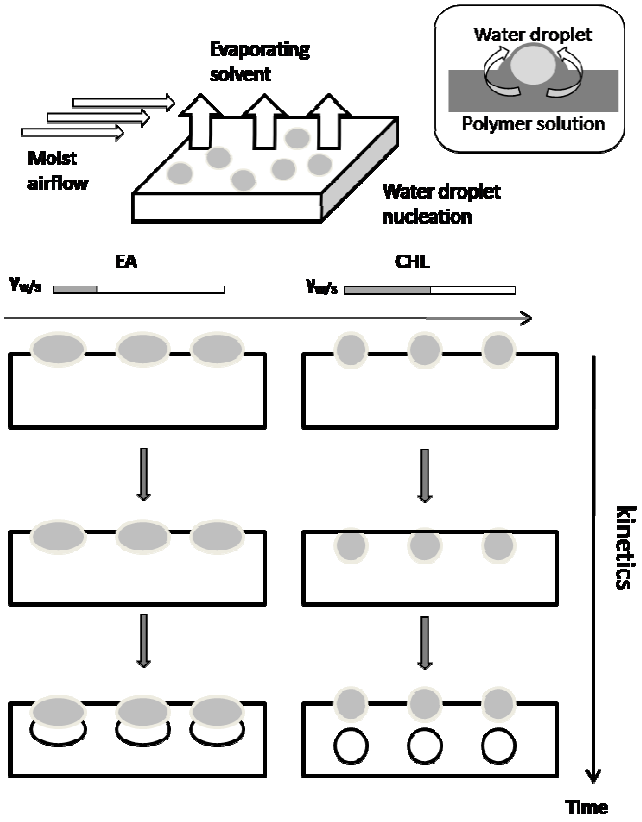

Fig.2.7: Mechanism proposed for Breath Figure templating on PDLLA-EA, and PDLLA-CHL. The interplay of kinetics of film hardening and water-solvent interfacial interactions determines the structure of BF films.

When solvents with proper interfacial properties are subjected to slow evaporation (represented by high t_0 and k values in the Boltzmann sigmoid), a new layer of polymer solution is produced at the interface with air; new water drops can nucleate and grow via coalescence, resulting in BF films with pore multilayers. Conversely, just a monolayer is observed for fast film hardening despite favorable water/solvent interfacial tension, as appears by comparing PDLLA-CHL films produced in the humid flow chamber with the ones obtained via spin coating.

These findings exclude that solvent density has a key role in the determination of pore monolayer/multilayer, as proposed by earlier works: controversial opinions have been advanced, with some authors reporting the formation of monolayer from solvents denser than water [2,19], while other papers showed opposite results [12]. Two main considerations have suggested the non influential role of solvent density: (i) interfacial forces overcome gravitational forces for water drops whose size is compatible with pores observed in our BF films and (ii) either pore monolayer or multilayers have been produced by the same polymer solution (e.g., PDLLA-EA), just acting on the processing conditions.

2.4 Conclusion

Porous PDLLA substrates with a variety of structures were obtained via Breath Figure templating, by varying the physical and chemical properties of polymer solution and processing conditions; this approach was pursued to evaluate the contribution of interfacial interactions and kinetic factors to BF phenomenon. Starting from phenomenological observations, our study has indicated that the entire process is governed by the interplay of kinetic factors and interfacial interactions (Fig. 2.7). In particular, interfacial tension between the evaporating solvent and condensing water mainly accounts for pore diameter and regulates the ability of polymer solution to surround water droplets, leading to pore multilayer films for suitable drying time. On the other side the rate of film hardening can define the actual structure of BF films: our modellization based on Boltzmann sigmoid could explain the time evolution of pore size in terms of solvent vapor pressure, humid flow rate, and polymer concentration. Moreover, the kinetics of film drying overcomes the contribution of interfacial interactions, hindering the formation of pore multilayers despite thermodynamics allows the process. The careful evaluation of the kinetics of film hardening and interfacial forces developed between evaporating polymer solution and condensing water represent a powerful tool for tuning the structure and pore size of BF films, making them suitable for several applications.

2.5 Bibliography

[1] Bunz UHF. Adv Mater 2006; 18: 973-89.

[2] Widawski G, Rawiso M, François B. Nature 1994; 369: 387-9.

[3] Lord Rayleigh Nature, 1911; 86: 416-7.

[4] Beysens D, Knobler CM. Phys Rev Lett 1986; 57: 1433-6.

[5] Briscoe BJ, Galvin KP. J Phys D 1990 ; 23 : 422-8.

[6] Limaye AV, Narhe RD, Dhote AM, Ogale SB. Phys Rev Lett 1996; 76: 3762-5.

[7] Pitois O, Francois B. Colloid Polym Sci 1999; 277: 574-8.

[8] Peng J, Han Y, Yang Y, Li B. Polymer 2004; 45: 447-52.

[9] Zhao B, Li C, Lu Y, Wang X, Liu Z, Zhang J. Polymer 2005; 46: 9508-13.

[10] Stenzel MH, Barner-Kowollik C, Davis TP. J Polym Sci part A: Polym Chem 2006; 44: 2363-75.

[11] Chan DYC, Henry JD, White LR. J Colloid Interface Sci 1981; 79: 410-8.

[12] Srinivasarao M, Collings D, Philips A, Patel S. Science 2001; 292: 79-83.

[13] Dell'Aversana P, Banavar JR, Koplik J. Phys Fluids 1996; 8: 15-28.

[14] Dell'Aversana P, Tontodonato V, Carotenuto L. Phys Fluids 1997; 9: 2475-85.

[15] Karthaus O, Maruyama N, Cieren X, Shimomura M, Hasegawa H, Hashimoto T. Langmuir 2000; 16: 6071-6.

[16] Bolognesi A, Mercogliano C, Yunus S, Civardi M, Comoretto D, Turturro A. Langmuir 2005; 21: 3480-5.

[17] Park MS, Joo W, Kim JK. Langmuir 2006; 22: 4594-8.

[18] Pitois O, Francois B. Eur Phys J B 1999; 8: 225-31.

[19] Jenekhe SA, Chen XL. Science 1999; 283: 372-5.

[20] Nishikawa T, Nonomura M, Arai K, Hayashi J, Sawadaishi T, Nishiura Y, Hara M, Shimomura M. Langmuir 2003; 19: 6193-201.

[21] Zhao B, Zhang J, Wang X, Li C. J Mater Chem 2006; 16: 509-16.

[22] Chaudhuri JB, Davidson MG, Ellis MJ, Jones MD, Wu XJ Macromol Symp 2008; 272: 52-57.

[23] Steyer A, Guenoun P, Beysens D, Knobler CM. Phys Rev B, 1990; 42: 1086-9.

[24] Limaye AV, Narhe RD, Dhote AM, Ogale SB. Phys Rev Lett 1996; 76: 3762-65.

[25] Guerrier B, Bouchard C, Allain C, Benard C. AIChE J. 1998; 44: 791-98.

[26] Zielinski JM, Duda JL. AIChE J.1992; 38:405-.

[27] Lide DR. *CRC* Handbook of Chemistry and Physics, 82nd ed., 2001.

[28] Yaws CL. In: *Thermophysical Properties of Chemicals and Hydrocarbons*, ed.. Yaws CL, Andrew W, Norwich, NY, 2008.

3. Functionalization of Breath Figures

3.1 Introduction

3.1.1 Chemical functionalization by self-assembling

Breath Figures template method was firstly studied for the production of ordered array of pores, as explained in the previous chapters. The possibility of controlling dynamically the process, obtaining different pores size, order and interconnectivity, has since the beginning attracts the interest of scientists. BFs templating allows the production of 2D or 3D porous structures with controlled features. However, this method allows the modification not only of the topographical characteristics of the sample, but also of the chemical properties. In particular, it is possible to functionalize selectively the inner surface of pores, leading to a chemically patterned porous material. This is possible simply by exploiting the interface between the condensing water droplets and the polymeric solution. Indeed, the presence of such a interface between two phases with very different hydrophilicity allows the promotion of the migration of molecules. Hydrophilic chemical groups (part of the polymeric chains or linked to nanoparticles) present in the polymeric solution, which is more hydrophobic, tend to migrate toward the water-solution interface. A chemical gradient is thus formed in the material, depending on the hydrodynamic conditions (such as viscosity, drying time, mobility of the molecules). These groups deposited on the interface and, after polymeric film has hardened and water has evaporated, the

surface of pores results enriched with them. Interestingly, disposition of chemical groups on the pores surface is a self-assembling process, as well as the BFs formation. The combination of this two self-assembling mechanisms, acting at different length scales, leads to a regular array of pores with functionalized surfaces. When amphiphilic block copolymers are used, hydrophilic blocks precipitate at the interface with water, while the polymeric film upper surface remains mainly hydrophobic, resulting in a nano-scale suborder development [1].

The same mechanism has been observed when nanoparticles with hydrophilic groups are added to the solution. Bocker and coworkers [2] observed a hierarchical self-assembly structure when they add CdSe nanoparticles (1 wt%, 4 nm core size, trioctylphosphine oxide (TOPO) stabilized) to a polystyrene solution cast in humid environment. Breath Figures form on the polymeric film, both with and without the addition of the nanoparticles. In the former case, however, a phase-separation on a nano-scale was observed, as the TOPO-stabilized CdSe nanoparticles are concentrated at the inner surface of pores. Segregation of the nanoparticles was demonstrated by the observation of a nano-layer covering the pores, while in the bulk material or on the top of the film few nanoparticles were detected.

Functionalization of pores has been obtained also using amphiphilic polymers, composed of a long hydrophobic chain with a hydrophilic end group. Zhang and Wang [3]added a small amount of amino-terminated polystyrene (PS) to a PS solution. Using the BFs method, they observed that amino-groups migrated toward the surface of pores. Using glutaraldehyde as a crosslinker, they bound a

fluorescent die (FITC) to the amine groups to demonstrate through confocal microscopy the presence of hydrophilic groups preferentially on the pores surface.

3.1.2 Protein patterns: production and applications

The possibility of producing a hierarchical self-assembly structure can be of great scientific interest, in the field of tissue engineering, biomolecule- or cell-based biosensors and in the understanding of the interactions between proteins, biomolecules and cells. One interesting opportunity given by patterned surface is the study of fundamental biological processes, in particular cells adhesion and spreading [4]. In a natural tissue, cells interact in a continuous and dynamic way with the extra-cellular matrix (ECM) and with other cells. Mimicking the physical and chemical complexity of the ECM is a challenging task, which while receiving numerous contributions in the literature, is still elusive to the biomedical community. However, significant results have been obtained in this field of research and combining topographical and chemical modification to create multi-functional surfaces has raised increasing interest. A study by Chen and coworkers has described geometric control over cells apoptosis [5]. They used substrates containing extracellular matrix-coated adhesive islands of various sizes. Depending on the dimension of the islands, cells modify their shape and their activity, switching from growth to death. Keeping constant the total contact area, cell spreading was observed to depend on the spacing between multiple focal adhesion-sized islands. The spacing among adhesion receptors was found to influence also the strength of cells adhesion to the substrate [6]. Moreover, cell

differentiation, proliferation, migration and commitment to a specific lineage (in the case of stem cells), are guided and determined by the topographical and chemical features of the surfaces they are in contact with, such as type, density, conformation and distribution of cells-binding ligands [7]. In addition, also nanotopography of the substrates influences cells adhesion and activity [8]. Cell cultures performed on nano-scale gratings evidenced that topographical features guided conformation, integrin clustering and focal adhesion of mesenchymal stem cells, changing their cytoskeletal organization and mechanical properties [9]. A different application based on the same principles is anti-fouling [4,10]. Surfaces with specific topographic and chemical features can hinder the adhesion of micro-organisms. Development of hierarchical structured patterns allows the extension of anti-fouling properties to a wide range of scale lengths, obtaining surfaces that block the adhesion of a variety of entities, from proteins and micro-organism to macro-organism. This is of special interest in marine and environmental applications, where adhesion and settlement of natural organisms leads to the necessity of periodical removal and cleaning. However, non-adhesion is a relevant problem also in biomedical applications [4]. Unwanted inter-adhesion of biological tissues sometimes occurs after surgery, resulting in patient health problems and in the necessity for further surgical operations. Considering the importance of physical and chemical cues that cells are in contact with, it is evident the necessity of creating multi-functional substrates. Topographical and chemical features ranging from the mm to nm are intended to mimic characteristic length scales of tissues, from cells to proteins and other biomolecules [11].

Biologically active patterns are fundamental also in the development of bioanalytical devices, such as biochips and biosensors. Detection and quantification of chemical compounds in biological samples is gaining increasing relevance in the development of biomedical techniques for diagnosis and treatment of diseases, as well as in the understanding of biological fundamental principles [4]. Detection of biomarkers is usually performed through the interaction of a biological sample with a set of bio-recognition elements immobilized on a surface, which results in analyte binding and, as a consequence of the chemical interactions, in a detectable signal. To perform high quality parallel detections of multiple analytes, a patterned surface is required, which allows specific interactions in defined and well addressed positions [4,12]. Patterning techniques are, so, required to develop analytical surfaces with such features, focusing on the production of substrates consisting of precisely distributed areas composed of specific bio-recognition elements and separated by a inert background.

To produce surfaces with desired and specific features, several techniques have been developed. Lithography, micro-contact printing, soft-lithography, laser guided patterning, ink-jet patterning, micro-fluidic and photoimmobilization are methods used to produce patterns on flat surfaces [7]. However, self-assembling methods present several advantages; a very regular structure can be obtained with nanometric precision. The Breath Figures templating method allows to obtain a regular array of pores on the surface of polymers. Water droplets condensing on the surface of a polymeric solution constitute a template for the

formation of pores. Non-coalescence phenomena lead to the formation of droplets with a monodisperse distribution of diameters and allow their arrangement in a hexagonal, honeycomb close-packed array. However, the main advantage is the self-assembling mechanism which guides the disposition of hydrophilic chemical groups at the water-solution interface, as discussed before.

3.2 Materials and Methods

3.*2.1 Breath Figures formation*

Linear Poly(D,L)Lactic Acid (PDLLA) Resomer R207 (MW=200 kDa) was purchased from Boeringher Ingelheim (Germany). Linear poly-ε-caprolactone (PCL), M_w= 80 kDa, was kindly provided by the Hebrew University of Jerusalem. Polymers were dissolved at room temperature in Chloroform (CHL)or Ethyl Acetate (EA) at 6% of concentration. To functionalize the surface of pores, an amphiphilic polymer was added. Jeffamine ED2300 is a poly(propylene glycol)-block-poly(ethylene glycol)-block- poly(propylene glycol) bis(2-aminopropyl ether), purchased from Sigma Aldrich. Typical M_w is 2000 Da and its structure is shown in figure 3.1. The two amino groups at the ends of the polymeric chain are more hydrophilic than the backbone, resulting in an amphiphilic behavior.

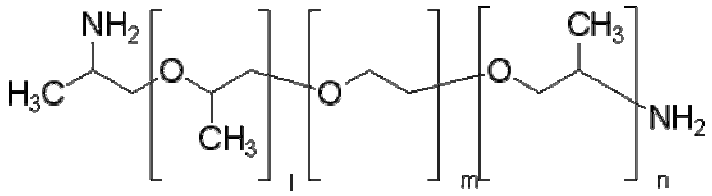

Fig.3.1: structure of Jeffamine ED2300. Approximate composition is m=39, l+n=6

Jeffamine was added to the polymeric solution in a concentration of 0%, 4% or 8% respect to PDLLA or in a concentration of 0%, 8% or 12% respect to PCL.

Breath Figures (BF) pattern was obtained depositing the polymeric solution on a glass slide through tape casting, with an initial thickness of the solution of 200µm. The glass slide was inserted in a chamber, described in chapter 2, where humid air flows. Moist air flux was regulated to obtain monodisperse size droplets and to avoid strong air fluxes which could induce disorder in pores arrangement.

3.2.2 Contact angle measurements

Sessile drop measurements were performed using a self-developed goniometer. A 3µL drop of MilliQ grade water was gently deposited on the sample and immediately acquired by a digital camera, to avoid absorption and evaporation. The drop deposited is in a local minimum of energy, but irregularity of the surface can hinder the achievement of the global energy minimum, giving non-equilibrium contact angle measurements. For this reason, the film laid on a substrate that can vibrate, with a vertical small displacement. Vibrations allow the drop to achieve its equilibrium configuration, as explained by Della Volpe and coworkers [13,14]. A vibration at 215 Hz was applied to samples for 10 seconds; measures was

performed before and after the vibration was applied. The obtained image was successively analyzed using a free-available software (ImageJ) and the contact angle was calculated applying spherical approximation. Each value was achieved as the mean of 10 measures carried out on each film.

3.2.3 Order and structure of pore array

Produced films were analyzed by Scanning Electron Microscopy (SEM), using a Field Emission SEM, Supra40 Zeiss with a Gemini column. The surfaces and the cross sections of films were observed, to obtain information on pores structure and arrangement. Cross sections of the porous films were obtained by cryofracture in liquid nitrogen. Images were analyzed using the software ImageJ, to obtain both the measure of pores size and information about pores structure. The same software was used to calculate and visualize the Fast Fourier Transform (FFT) of the images. This technique was used to determine the order of pores arrangement. Monodisperse but disordered pores results in the image of rings, while honeycomb structures leads to images with spots disposed in a regular hexagonal array.

3.2.4 X-ray Photoelectron Spectroscopy

The experiments were carried out in ultra-high-vacuum (UHV) at a base pressure of 10^{-9} mbar. X-ray photoemission data were recorded with a double pass Perkin Elmer PHI 15-255G cylindrical-mirror electron analyzer (CMA) operated at constant pass energy. X-ray photoemission was carried out with non-monochromatic Mg K_α photons (hv = 1253.6 eV) from a Vacuum Generators XR3

dual anode source operated at 15 kV, 18 mA. Carbon 1s (C_{1s}), Oxigen 1s (O_{1s}), Nitrogen 1s (N_{1s}) core level scans were recorded with a resolution of 0.2 eV, using a pass energy of 100 eV. Overview scans were recorded with a resolution of 1 eV using a pass energy of 100 eV. The spectra were angle integrated and they are reported in binding energy, referenced to the C_{1s} signal (fixed at 284.8 eV of binding energy). Quantitative analysis of surface composition was made through the evaluation of the photoemission peak areas, *I*, of C_{1s}, O_{1s}, N_{1s} and using appropriate empirical atomic sensitivity factors (ASF). The relative atomic concentration of *i* element can be obtained through the relation

$$C_i = \frac{I_i / ASF_i}{\sum_j \left(I_j / ASF_j \right)}$$

3.2.5 Protein encapsulation

The porous structure obtained on film surface was exploited to trap fibrinogen (FNG), M_w=340 KDa, purchased from Sigma Aldrich. Three sets of samples were produced, depending on the mechanism of protein entrapment. Films composed of PDLLA or PCL were hydrated in PBS for 1 hour and then incubated in a solution of FNG in PBS, 100µg/ml, for 2 hours at room temperature. A second set of films containing Jeffamine at different concentration underwent the same procedure. In this way, fibrinogen can interact, through carboxylic groups, with Jeffamine, forming peptide bonds. The third set, composed of films with Jeffamine, was hydrated in MES 0.1M. A solution was prepared, composed of (i) 1 ml of FNG 100µg/ml in MES-SDS, (ii) 30 µl of EDAC 10 µg/ml in water, than diluted 10X in

MES, (iii) 70 µl of sulfo-NHS 10µg/ml in water, than diluted 10X in MES. This solution was incubated for 15 minutes at room temperature. Films were immersed in the solution for 2 hours at room temperature. The solution containing EDAC and sulfo-NHS enhance the formation of peptide bonds between fibrinogen and amino groups of Jeffamine, as shown in figure 3.2.

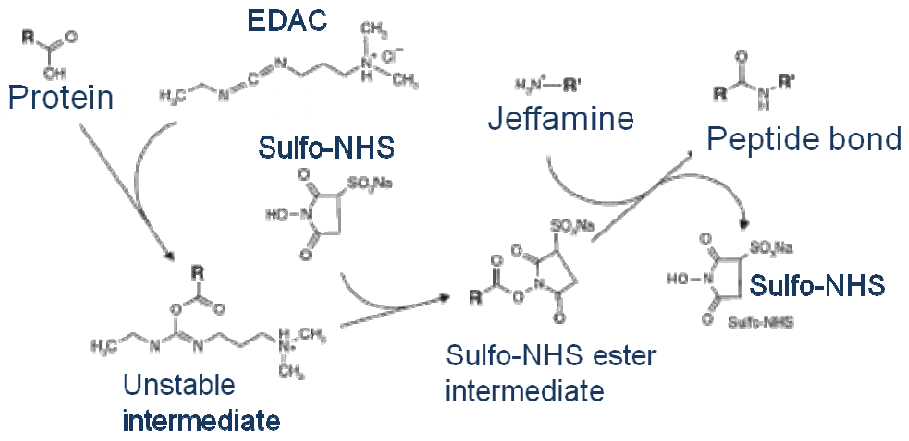

Fig.3.2: sketch of chemical reactions that lead to binding between a protein and Jeffamine

The three sets of films have fibrinogen linked or adsorbed to their surfaces. Samples were than washed with PBS, 3 times, incubate in a blocking solution of Bovine Serum Albumin (BSA) 5% in PBS for 30 minutes at room temperature and finally washed twice, again in PBS.

To observe the distribution of fibrinogen in the pores, a confocal microscope was used (Nikon eclipse, TI-E). Samples were immersed in a solution of FITC-

conjugated concanavalin A (FITC-conA), 100µg/ml in PBS, for 18 hours at 4°C; then they were washed again in PBS, 3 times. ConA is a lectin which binds alpha-mannose and alpha-glucose. Fibrinogen has four oligosaccharide chains, which contains 3 mannose residues. So, ConA can form specific bonds with the mannose groups of fibrinogen, connecting the fluorescent dye to the protein. Samples were observed with the confocal microscope, acquiring the signal at a wavelength of 488nm.

3.3 Results and Discussion

3.3.1 Breath Figures formation: pore size

Films of poly-d,l-lactic acid (PDLLA) and poly-caprolactone (PCL) presenting BFs on their surfaces have been produced, obtaining an array of monodisperse pores. The addiction of an amphiphilic polymer (Jeffamine) was considered, evaluating its influence on pores size, films wettability and pore regularity. Jeffamine was added in three different concentrations and the influence of its concentration on the films properties was also measured.

The first observation is that its presence strongly influences pores structure formation. In PDLLA (dissolved in chloroform) films, pores size was generally found to decrease with the addition of Jeffamine (figure 3.3).

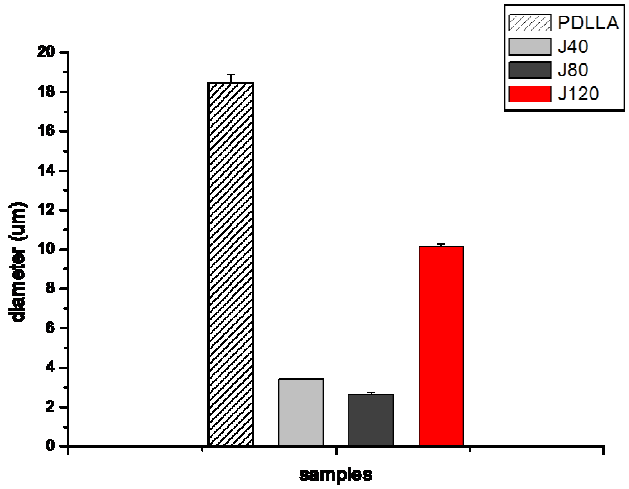

Fig.3.3: pore size related to the Jeffamine concentration in PDLLA films

This is probably due to the increase in hydrophilicity of the solution, which strongly enhances droplets nucleation. As discussed in chapter 1, pore size is inversely proportional to the solution wettability. The addition of Jeffamine in a concentration of 4%, respect to PDLLA content, causes a drastic decrease in pore size in the films. A further increase in its concentration (8%) leads to even smaller pores. To obtain a monodisperse distribution of size, flow rate was decreased from 1.4 l/min for 0% and 4% of Jeffamine to 0.8 l/min for samples with 8%. Despite the decrease of humid air flow rate generally would cause an increase in pores size, nucleation rate is high enough to counterbalance and even overcome this effects, with the result that smaller pores are obtained. However, films with

8% of Jeffamine prepared in these conditions have a particular structure, with pores highly interconnected, as shown in figure 3.4. The reason for that can be better understood analyzing films produced with 12% of Jeffamine and even lower humid air flow rate.

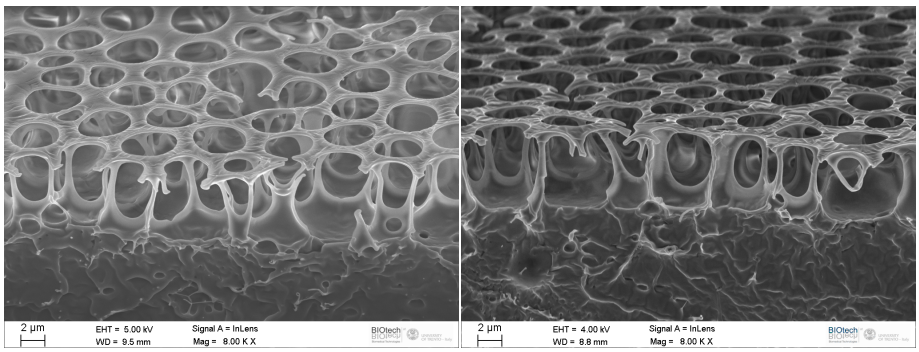

Fig.3.4: two images of PDLLA-8% Jeffamine film. Initial solution PDLLA 6% in chloroform, air flow 0.8l/min

Samples prepared with 12% of Jeffamine need a flow rate of 0.3 l/min. This value is very low if compared to other samples; in this situation, evaporation is slow down and droplets have time enough to growth. In addition to that, another effect should be taken in account when amphiphilic polymers are added to the solution. Due to this addition, water vapor condenses rapidly on the surface, and nucleation is enhanced by the presence of amino groups, resulting in a high number of nucleation sites. A high number of droplets per unit area form, thus limiting the space each droplet has to growth; as a consequence, smaller pores result. On the other hand, the surface is rapidly covered by droplets, which get in touch very early, when the solution has still a low viscosity since solvent

evaporation has just begun. This effect, in combination with a longer process time due to the decreased air flow, leads to the fact that droplets interact while immersed in a solution that is still rich in solvent; the polymer layer forming among water beads cannot separate them effectively and, thus, coalescence occurs. As coalescence causes a faster growth than diffusion, pores are bigger, but also less regular. Moreover, droplets are pressed one against each other in a early stage, separated only by a very thin polymer solution layer. The arrangement, thus, tends to the honeycomb one, but coalescence locally destroys this order. After solution drying, droplets, as a consequence of their heating to room temperature, break the thin layer separating them, leading to an highly interconnected porous structure, shown in figure 3.5.

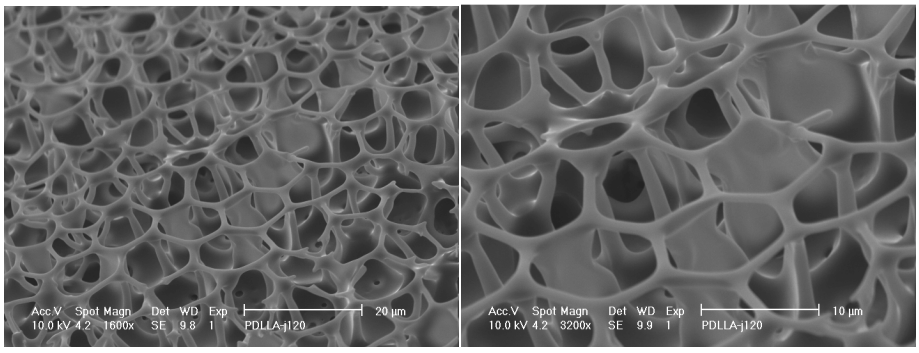

Fig.3.5: PDLLA-12%Jeffamine film at two magnifications. Initial solution PDLLA 6% in chloroform, air flow 0.3l/min

The films prepared with 8% of Jeffamine are in a intermediate situations. Droplets are pressed together and separated by a thin layer of polymer, leading to the

interconnectivity, but still coalescence is hindered and the high nucleation rate leads to monodisperse and small pores.

Similar experiments were performed also using PCL; pores size distribution has a broader distribution compared to PDLLA films. In addition, very small pores (with diameter less than one micrometer) formed among bigger pores. For this reason, the entire distribution of pores size, and not only the mean value, has been considered. The results of measurements are presented in figure 3.6.

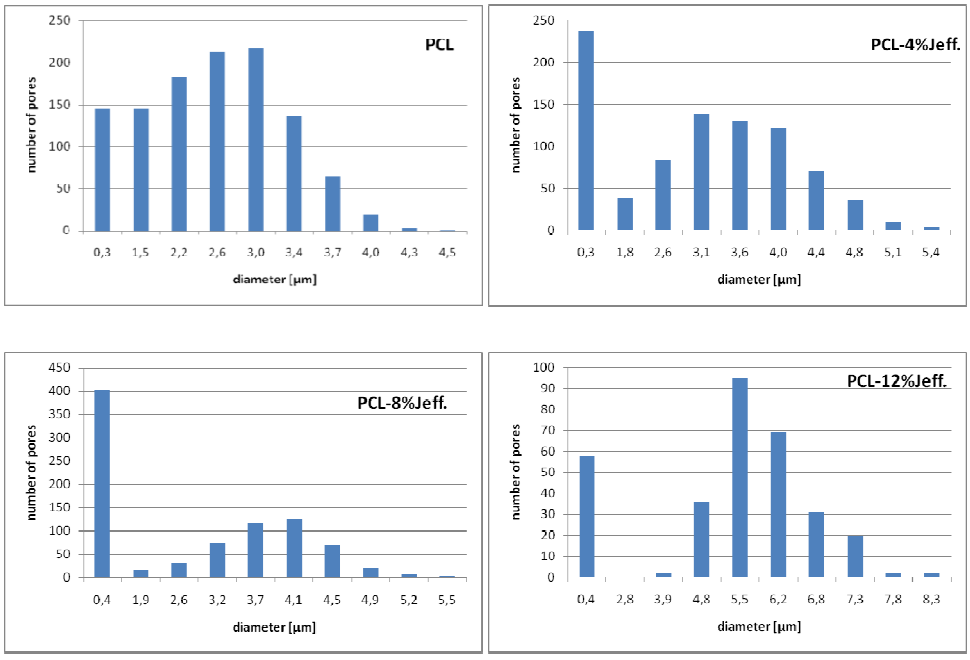

Fig.3.6: pores size distribution in PCL films at different Jeffamine content

As evidenced by the results, addition of Jeffamine in PCL leads to an increase in the mean pores size, but also results in a high number of sub-micrometric pores. A high concentration of hydrophilic groups causes the droplets to interact very early during the process, so coalescence occurs. The sub-micrometric pores population can be composed of small droplets that don't coalesce, tough the most probably explanations is that they nucleate later at the surface among early-formed big drops. Due to the better results obtained with PDLLA films, PCL was not used extensively in further experiments.

3.3.2 Contact angle measurement

As discussed above, the addition of an amphiphilic polymer changes the diameter of pores. This involves also another feature of porous films, which is wettability. The addition of hydrophilic groups in the solution increases nucleation rate, but also increases the interaction of water molecules with the surfaces of dried film. To measure wettability, the contact angle of a sessile water drop deposited on the surface was measured. The measure was performed in two different situations for each sample: a traditional static measurement and a measure after the surface, with the drop on it, underwent a vibrational vertical motion at high frequency. Vibrations of the system allow reaching an equilibrium state, avoiding measures performed when the drop is in a local minimum of energy, but not at the lowest energy. First of all, cast flat films without Breath Figures were tested, to evaluate the influence of Jeffamine on the wettability of materials (see figure 3.7).

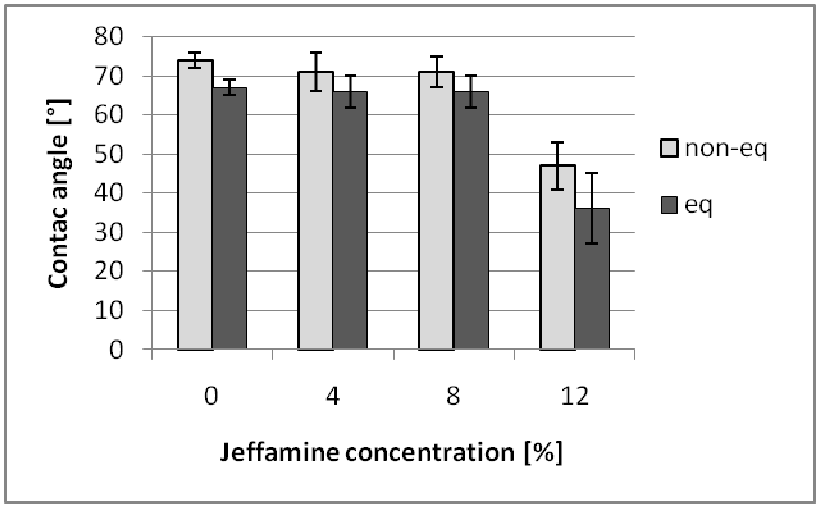

Fig.3.7: contact angle measurements on cast flat films of PDLLA with different Jeffamine concentration, with traditional method and in the equilibrium state

Addition of Jeffamine decreases the contact angle significantly in films with 12% of concentration. In other films, variations are not relievable, probably because of their low value. The abrupt changes observed in films with the highest content of Jeffamine can explain the particular structures of BFs formed using this solution composition.

Secondly, contact angle was measured on films with BFs. The interaction of a liquid drop with a surface depends strongly on the chemistry of the two materials, but is strongly influenced also by micro-geometrical features of the solid surface. Topographical patterns on a surface modify its contact angle [15-18]; indeed, films patterned with the BFs templating method show an increase in contact angle respect to flat films, as shown in figure 3.8.

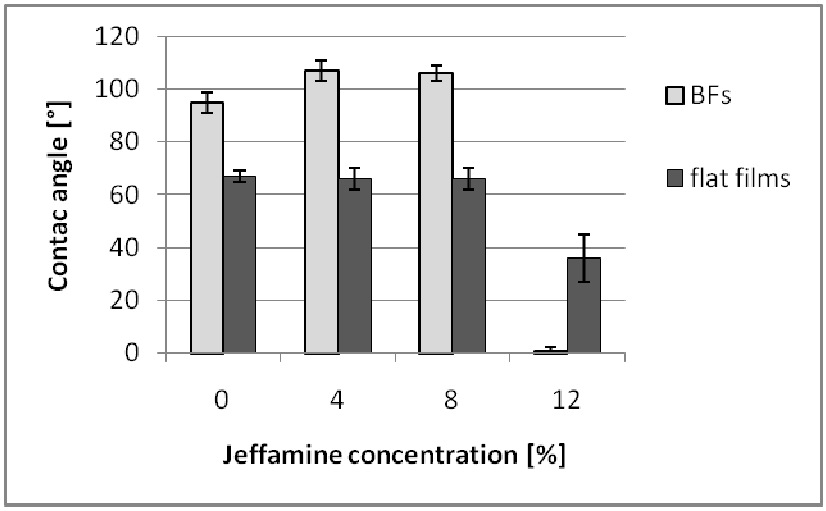

Fig.3.8: contact angle measurements, at the equilibrium state, on films of PDLLA with different Jeffamine concentration and patterned with BFs

In this case topography is the main parameter influencing wettability; cast flat films composed of PDLLA has a contact angle (with water) of 74±2°, while the presence of pores of 18µm on the surface increases this value to 107±3°. The increase due to pores is even bigger if 4 or 8 % of Jeffamine is present. Pores are smaller, in the range of 2-3µm, and contact angle rise up to 109±4° and 110±2°, respectively, even though the material is slightly more hydrophilic. As seen before, 12% of Jeffamine leads to a structure with highly interconnected pores. When water droplets were put on these films, a complete wetting was observed. Capillary forces guided water into the pores and through the pores array, so droplets were completely spread on the films.

3.3.3 Order and structure of pore array

As the amphiphilic polymer precipitate at the water-solution interface, the addition of Jeffamine, in a certain range of concentration, stabilize water droplets. This process can hinder coalescence and thus leads to more regular structures.

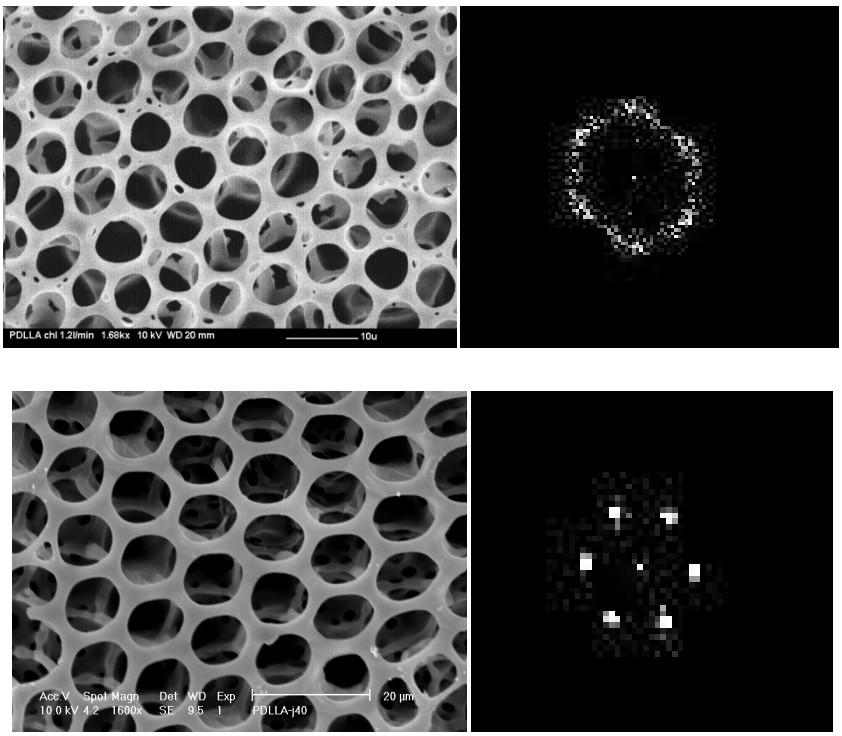

Fig.3.9: SEM images (left) and FFT (right) of PDLLA (top) and PDLLA-4%Jeffamine (bottom) films

FFT analysis of the pictures obtained by SEM (figure 3.9) reveals that PDLLA films have a narrow distribution of pores size, such that FFT result in the image of a

ring. Disposition of pores is not honeycomb-like, but an hexagonal order is present, highlighted by the presence of six blurred points in the FFT image. In the film with 4% Jeffamine, the pores array is very regular, honeycomb-like. The resulting FFT image, thus, is composed of six defined points, disposed as the vertexes of a hexagon.

Experiments with the addition of the same amphiphilic molecule were performed also dissolving PDDLA in Ethyl Acetate (EA), instead of Chloroform. Changing the solvent causes relevant differences in the features of the final films, as discussed in chapter 2. The presence of Jeffamine in PDLLA-Ethyl Acetate solutions leads to further noticeable characteristics. Columnar pores were observed when casting PDLLA-EA films (Figure 3.10).

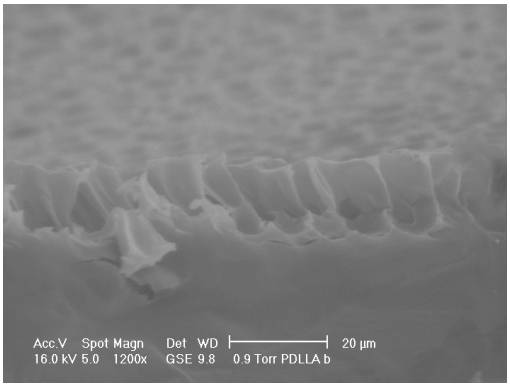

Fig.3.10: Film of PDLLA-EA 6%

The presence of Jeffamine determines a decrease in superficial pores diameter, from 7.2 ± 1.6 to a mean diameter of 3±2.1 µm, as expected. However, the analysis of a section of films shows an interesting structure. Pores are still

columnar, but below the surface some pores coalesce, forming big cavities in the bulk material. The inner surface of these cavities is patterned by smaller pores, as shown in figure 3.11.

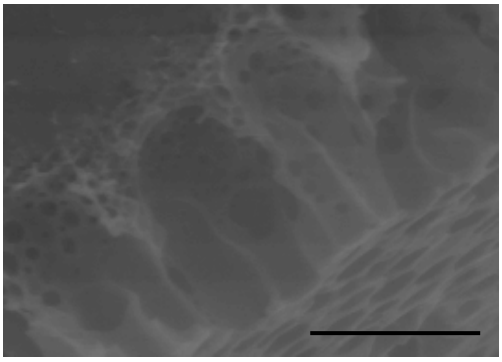

Fig.3.11: particular of the section of a PDLLA-4%Jeffamine film. Scale bar is 20 µm

Hydrophilic groups tend to migrate towards the water-solution interface, as in all other experiments performed. On the other hand, EA has higher water solubility, compared to chloroform (83 and 8 g/l, respectively). This means that part of the water enters in the polymeric solution, where amphiphilic groups are. This could leads to a rearrangement of Jeffamine molecules to encapsulate micro-droplets at the interface of bigger pores. The result is a sub-micro-structure superimposed to the micro-structure of BFs. The development of a nano-structure superimposed to the honeycomb array of pores was observed by Stenzel and coworkers when producing BFs on amphiphilic block-copolymers [1]. They observed that nanopores formed on the top surface of the film and on the inner surface of BFs micropores. Water droplets arrange following the BFs template process, while

excess water is encapsulated within the pores, leading to the formation of nanopores.

3.3.4 X-ray Photoelectron Spectroscopy

The amphiphilic polymer added to the solution strongly influences the templating mechanism, modifying pores size and arrangement through its migration toward the water-solution interface. The presence of amine groups on the inner surface of pores was detected through the use of XPS. This technique allows an elemental analysis, with a resolution of 1% in atomic composition, of the surface of samples. The electrons analyzed escape only from a very thin layer of the surface of the material, resulting in a depth of analysis of 1-10 nm. The measure was focused on the detection of nitrogen atoms, which are present in the amine groups. Films of PDLLA containing 12% of Jeffamine were used, meaning that the calculated mean atomic concentration in the material is 0.1%, which is a value below the detection limit of the used apparatus. Cast flat films, where no concentration gradients are expected, were tested, giving no detectable signals. On the contrary, films patterned with the BFs method present a signal corresponding to the presence of nitrogen on the surface (Figure 3.12).

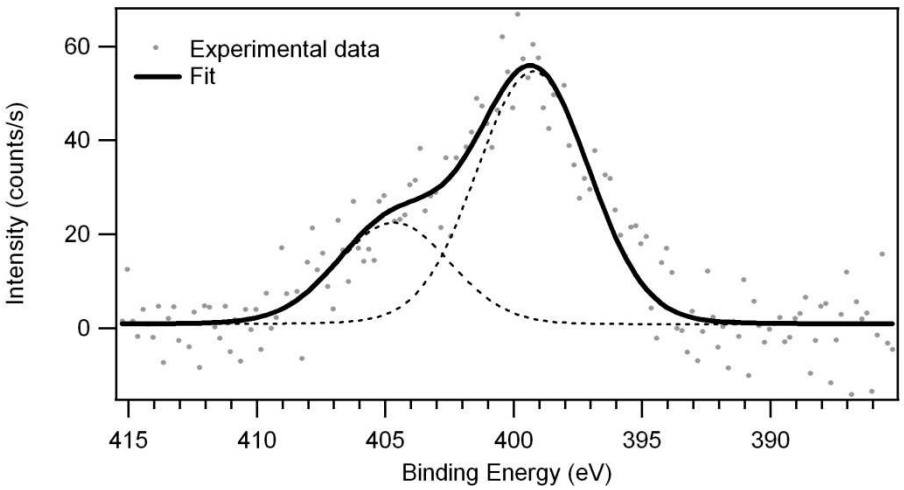

Fig.3.12: XPS spectrum of films of PDLLA-12%Jeffamine with BFs

The spectrum obtained displays a main peak at 400 eV, due to nitrogen, and a second peak at higher binding energy (405 eV). This smaller peak can be related to the presence of nitrogen with a different oxidation state. Oxidation probably occurs due to the contact between amine groups and water, leading to a shift of the binding energy measured. This component of spectra is not present in samples where BFs formation is not fully developed. In fact, to monitor the evolution of the process of migration, films were tested in which the BFs patterning process was not completed, flowing humid air only for a short time in order to "freeze" the process at an intermediate step. Areas where BFs are fully developed show two peaks, while areas where droplets growth and sinking was blocked show only one peak, with a smaller intensity (figure 3.13).

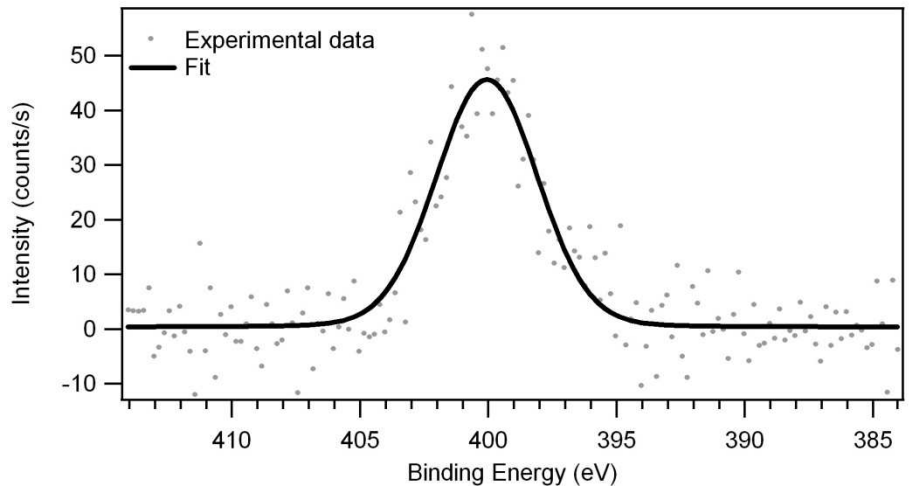

Fig.3.13: XPS spectrum of films of PDLLA-12%Jeffamine with incomplete BFs formation

As a control, pure Jeffamine was tested and the obtained spectrum (figure 3.14) shows an intense peak similar to the one observed in the films tested. The analysis of the XPS spectra shows that in films with no BFs there is no detectable signal related to nitrogen, in films with a partial pattern formation only traces of nitrogen are detected, while in films with a complete development of the BFs pattern nitrogen concentration is around 1% (see table 3.1). Even though this value is close to the detection limit of the apparatus, these results give an indication of the effective migration of Jeffamine towards the surface.

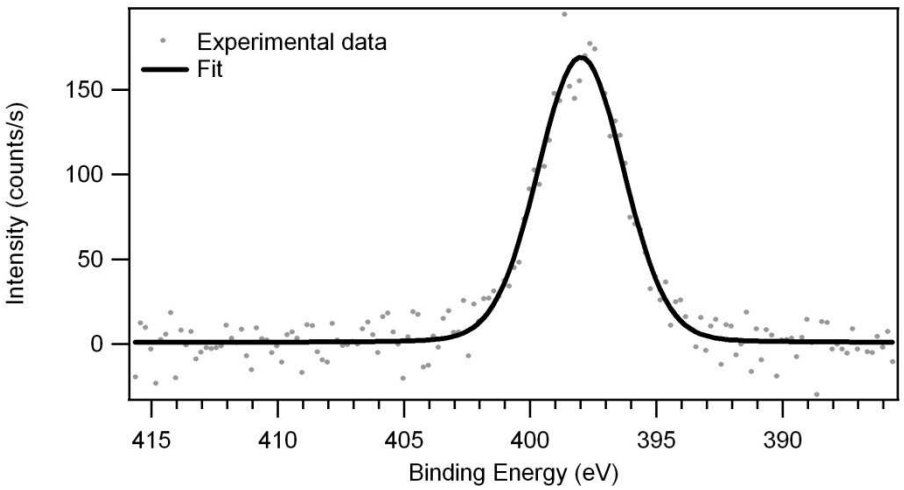

Fig.3.14: XPS spectrum of pure Jeffamine

	%C	%O	%N
BFs	80.7	18.6	1.0
Incomplete BFs	74.9	24.8	traces
Jeffamine	73.7	25.1	1.2
No BFs	65.7	34.3	0

Table 3.1: XPS result: elemental composition

3.3.5 Protein encapsulation

Chemical functionalization, consequence of self-assembled organization of amine groups, gives the possibility to bind proteins to the surface of pores. Fibrinogen was used as a model protein to be encapsulated in pores. BFs patterned films were incubated in a protein solution and the distribution of fibrinogen was observed. Concanavalin A, FITC conjugated (conA-FITC), was used to detect the proteins via confocal microscopy. Concanavalin A attaches to the mannose groups of proteins, constituting a good link between them and the fluorescent dye. This technique allows the analysis of a 3D volume of samples, localizing the fluorescent molecules also below the surface, resulting in a 3D reconstruction of the distribution of dyes (and so of the proteins) on the surface and in the pores.

A first test was performed on patterned films without the addiction of Jeffamine. An example of the results obtained starting from a solution of PDLLA and EA is shown in figure 3.15. The protein enters bigger pores and deposits on the bottom, as visible in images taken below the top surface of samples, but it is unevenly distributed in small pores. A similar result is observed in films produced with PDLLA dissolved in chloroform (figure 3.16). The distribution of fibrinogen is not uniform in both cases. The protein solution enters the pores, can reach their bottom and diffuses also to small inner pores, below the surface. Moreover, washing cycles with PBS probably remove part of the fibrinogen that was adsorbed on the polymeric surface, resulting in areas with small quantities of protein; the same effect is the cause of lack of fluorescent signal in correspondence of some big pores (about 40μm).

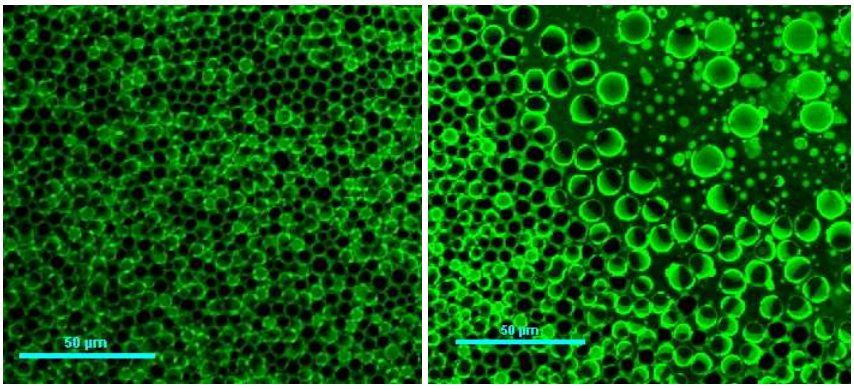

Fig.3.15: confocal microscopy images of fibrinogen on PDLLA films made from EA solution. Protein distribution on surface (left) and below the surface (right). Scale bar is 50µm

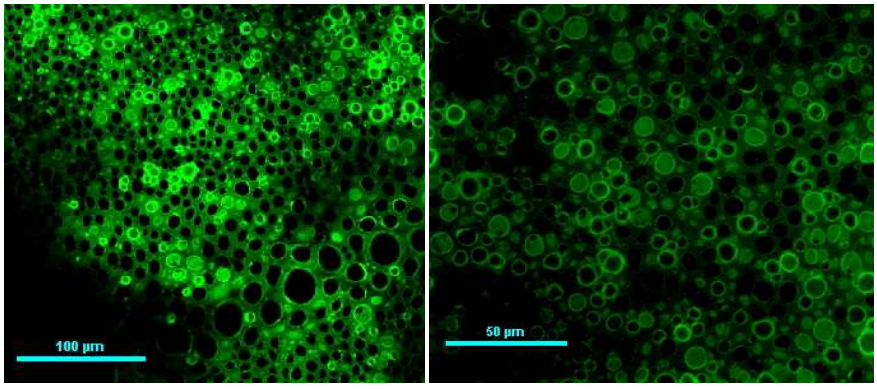

Fig.3.16: confocal microscopy images of fibrinogen on PDLLA films made from chloroform solution. Protein distribution on surface (left) and below the surface (right). Scale bar is 100µm(left) and 50µm(right)

The presence of Jeffamine, instead, leads to a stronger bounding between the surface and fibrinogen. Amine groups favor the adsorption of the protein, resulting in a more homogeneous distribution, as shown in figure 3.17. Moreover, analysis of vertical sections of samples shows that protein is adsorbed evenly also on pore walls.

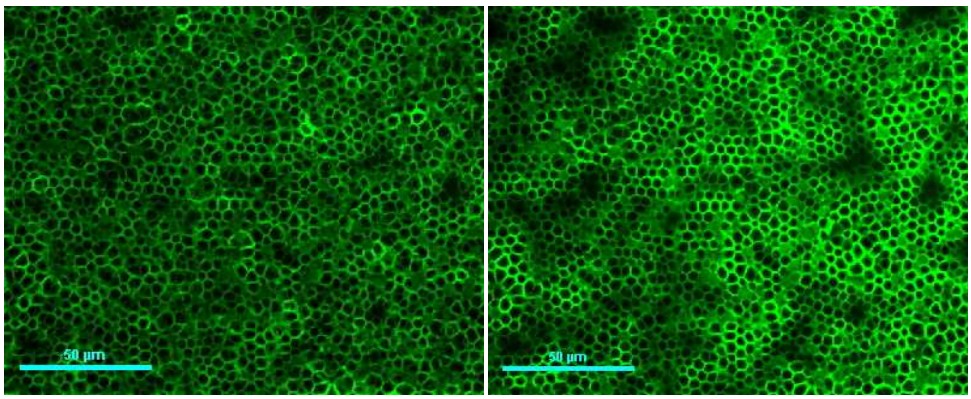

Fig.3.17: confocal microscopy images of fibrinogen on PDLLA films made from chloroform solution. Protein distribution on surface (left) and below the surface (right). Scale bar is 50µm

This demonstrates that fibrinogen interacts with the amino groups that are present at the pores surface. In the case the film is composed of PDLLA, the protein adsorbs on the surface by means of weak bonds, but if Jeffamine is present the interaction is stronger and chemical bounding occurs between carboxylic groups of proteins and amino groups of Jeffamine. To further enhance the chemical interactions between these two components, a cross-linker can be added during the protein encapsulation. In these experiments EDAC was used as a

zero-length cross-linker, resulting in a more efficient formation of peptide bonds, as shown in figure 3.18. Fibrinogen appears regularly distributed on the films; furthermore, observing the intensity of the dye fluorescence, a higher encapsulation efficiency results.

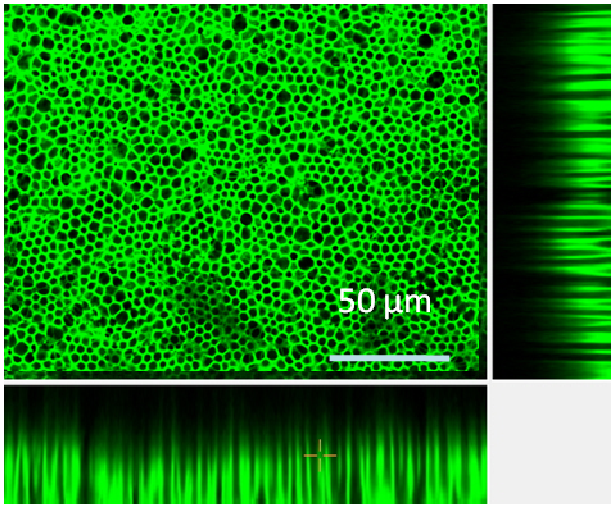

Fig.3.18: confocal microscopy images of fibrinogen on PDLLA films made from chloroform solution. Top view and sections. Scale bar for top view is 50µm, sections are zoomed along z-axis

Fibrinogen is disposed on pores walls, forming a functionalized coating. Lateral views of the films evidence this, showing a homogeneous disposition of the protein inside the films, as sketched in figure 3.19.

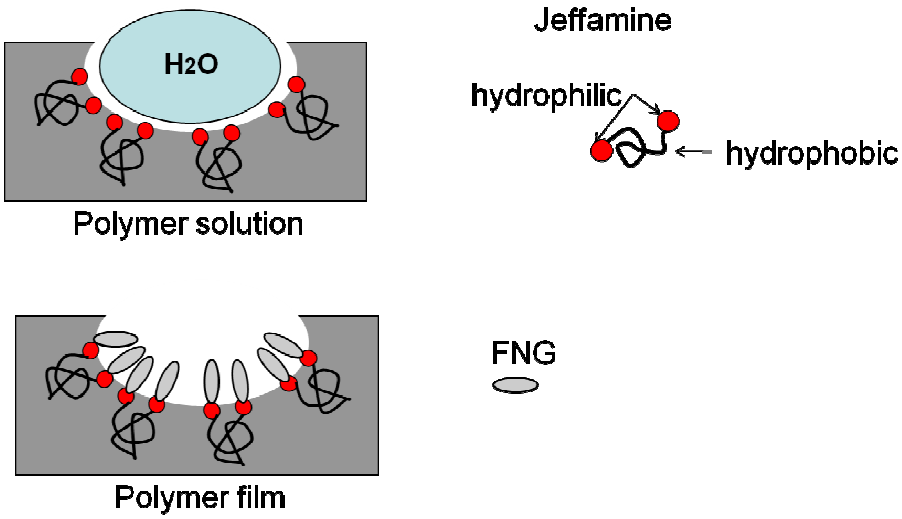

Fig.3.19: functionalization process; Jeffamine self-assembling (top) during BFs patterning and final result after fibrinogen (FNG) binding (bottom)

3.4 Conclusion

The concomitance of two self-assembling processes has been observed in BFs patterning when an amphiphilic polymer was added to the polymeric solution casted in humid environment. The disposition of water droplets on the surface in a regular arrangement is a self assembling process which is basilar for the templating mechanism which leads to pores array formation. The second self-assembling process is the migration of the hydrophilic parts of amphiphilic molecules toward the water-solution interface. This superimposes a chemical functionalization to the controlled topography of the surface of polymeric films. Addition of Jeffamine to polymeric solution which undergoes the BFs formation process was demonstrated to modify the final porous structures in terms of pore size and better regularity. The wettability of the resulting films were measured and related to pore structure, finding a general increase in contact angle compared to flat non-patterned films, even though also a super-hydrophilic behavior was observed in particular pore structures. The final result of the experiment performed is the creation of an array of pores which internal surface is chemically functionalized with amino groups, while the top surface of the films is composed of hydrophobic polymer. Amino groups were used to chemical bind fibrinogen, obtaining a controlled arrangement of the protein in a 3D disposition. This result was demonstrated by means of XPS analysis and with a direct observation using confocal microscopy. The generation of a controlled 3D arrangement of fibrinogen or, in general, of other proteins can be used in studies

dealing with fundamental biological process, in biomedical devices and in drug release.

3.5 Bibliography

[1] K.H. Wong, T.P. Davis, C. Barner-Kowollik, and M.H. Stenzel, “Honeycomb structured porous films from amphiphilic block copolymers prepared via RAFT polymerization,” *Polymer*, vol. 48, 2007, pp. 4950-4965.

[2] A. Böker, Y. Lin, K. Chiapperini, R. Horowitz, M. Thompson, V. Carreon, T. Xu, C. Abetz, H. Skaff, a D. Dinsmore, T. Emrick, and T.P. Russell, “Hierarchical nanoparticle assemblies formed by decorating breath figures.,” *Nature materials*, vol. 3, May. 2004, pp. 302-6.

[3] Y. Zhang and C. Wang, “Micropatterning of Proteins on 3D Porous Polymer Film Fabricated by Using the Breath-Figure Method,” *Advanced Materials*, vol. 19, Apr. 2007, pp. 913-916.

[4] T. Ekblad and B. Liedberg, “Protein adsorption and surface patterning,” *Current Opinion in Colloid & Interface Science*, vol. 15, Dec. 2010, pp. 499-509.

[5] C.S. Chen, “Geometric Control of Cell Life and Death,” *Science*, vol. 276, May. 1997, pp. 1425-1428.

[6] C. Selhuber-Unkel, T. Erdmann, M. López-García, H. Kessler, U.S. Schwarz, and J.P. Spatz, “Cell adhesion strength is controlled by intermolecular spacing of adhesion receptors.,” *Biophysical journal*, vol. 98, Feb. 2010, pp. 543-51.

[7] D. Falconnet, G. Csucs, H.M. Grandin, and M. Textor, “Surface engineering approaches to micropattern surfaces for cell-based assays.,” *Biomaterials*, vol. 27, Jun. 2006, pp. 3044-63.

[8] E.K.F. Yim and K.W. Leong, “Significance of synthetic nanostructures in dictating cellular response.,” *Nanomedicine : nanotechnology, biology, and medicine*, vol. 1, Mar. 2005, pp. 10-21.

[9] E.K.F. Yim, E.M. Darling, K. Kulangara, F. Guilak, and K.W. Leong, "Nanotopography-induced changes in focal adhesions, cytoskeletal organization, and mechanical properties of human mesenchymal stem cells.," *Biomaterials*, vol. 31, Feb. 2010, pp. 1299-306.

[10] D. Falconnet, G. Csucs, H.M. Grandin, and M. Textor, "Surface engineering approaches to micropattern surfaces for cell-based assays," *Biomaterials*, vol. 27, 2006, pp. 3044-3063.

[11] R. Ogaki, M. Alexander, and P. Kingshott, "Chemical patterning in biointerface science," *Materials Today*, vol. 13, Apr. 2010, pp. 22-35.

[12] R. Ogaki, M. Alexander, and P. Kingshott, "Chemical patterning in biointerface science," *Materials Today*, vol. 13, Apr. 2010, pp. 22-35.

[13] C. Della Volpe, D. Maniglio, S. Siboni, and M. Morra, "An Experimental Procedure to Obtain the Equilibrium Contact Angle from the Wilhelmy Method," *Oil & Gas Science and Technology*, vol. 56, Jan. 2001, pp. 9-22.

[14] C. Della Volpe, "The determination of a 'stable-equilibrium' contact angle on heterogeneous and rough surfaces," *Colloids and Surfaces A: Physicochemical and Engineering Aspects*, vol. 206, Jul. 2002, pp. 47-67.

[15] Y. Li, G. Duan, and W. Cai, "Controllable superhydrophobic and lipophobic properties of ordered pore indium oxide array films.," *Journal of colloid and interface science*, vol. 314, Oct. 2007, pp. 615-20.

[16] B.H. Luo, P.W. Shum, Z.F. Zhou, and K.Y. Li, "Preparation of hydrophobic surface on steel by patterning using laser ablation process," *Surface and Coatings Technology*, vol. 204, Jan. 2010, pp. 1180-1185.

[17] M. Ma, M. Gupta, Z. Li, L. Zhai, K.K. Gleason, R.E. Cohen, M.F. Rubner, and G.C. Rutledge, "Decorated Electrospun Fibers Exhibiting Superhydrophobicity," *Advanced Materials*, vol. 19, 2007, pp. 255-259.

[18] M. KANG, R. JUNG, H. KIM, and H. JIN, “Preparation of superhydrophobic polystyrene membranes by electrospinning,” *Colloids and Surfaces A: Physicochemical and Engineering Aspects*, vol. 313-314, 2008, pp. 411-414.

4. Drug Release using patterned polymers

4.1 Introduction

The continuous development of new drug is leading to several improvements in the field of pharmaceutics and health care. However, one of the most challenging topics in this field deals with the possibilities of control the release of drugs in terms of extending the release over a predetermined period of time and of targeting a specific location. This would limit the concentration of drugs in the body between determined upper and lower levels, reduce the necessity of frequent and regular doses uptake and reduce adverse effects on non-targeted tissues, resulting in a more effective therapy and in a better quality of life for patients. For this purpose, many drug delivery devices (DDDs) have been developed: MEMS (micro-electro-mechanical systems) [1], magnetic controlled devices [2], 3D printing [3], micro-fabricated devices [4] and matrix reservoir system [5]. The possibility of topically specific release of a number of different types of drugs as been demonstrated [6-10]: proteins, hydrophilic or hydrophobic molecules, natural-derived molecules, cancer therapy drugs. The development of drug release is an interesting topic also in tissue engineering [11-15]. The delivery of growth factors, proteins and biomolecules is exploited to guide cells proliferation, development and activity in order to regenerate damaged tissues. Scaffolds are used in combination with cells and with growth factors, thus the control over the concentration and disposition of biomolecules is a fundamental topic to obtain specific cells behaviors.

Among the above mentioned DDDs, those composed of biodegradable polymers have assumed an increasing importance. Synthetic biodegradable polymers, especially thermo-plastic aliphatic polyesters like PCL, PLA and PLGA, have been studied intensively due to their excellent biocompatibility, processability and the possibility to control their in vivo life-time. Drugs have been incorporated in micro- and nano-carriers composed of these materials. Micro- and nano-fibers [14,16-23] or particles [13,24-28], rods [14,29], and films [6,30] were studied as biodegradable delivery devices .

Among the above mentioned DDDs, electrospun mats have been recognized as very promising. The production of very small polymeric fibers (from 50nm to 15um) is of great interest in different industrial and research areas, from the production of filters, textiles, composite materials, to many applications in the field of tissue engineering [16,18,31-36]. Electrospinning of biodegradable polymers leads to the production of structures that can mimic the natural ECM (extra-cellular matrix), providing an optimized environment for cells growth. This allows creating scaffold for cells growth that can also release active biomolecules to enhance and guide cells activity. A further advantage of this technique is that a variety of fibers morphology can be obtained [33,37-46]: fibers with patterned or wrinkled surfaces, coaxial, hollow, ribbon-like, porous fibers have been produced with this technique. In particular, electrospun fibers with surface decorated with pores were observed when produced in a humid environment [39,42,47-49].

In this work, we studied the process of pores array formation by self-assembling as a method to produce polymeric porous structures for drug delivery. In

particular, we studied the release of proteins from porous films produced with the Breath Figures templating method and from coaxial electrospun fibers with porous surface. Experiments with BFs patterned films studies the release of fibrinogen (FNG), a protein with a M_w of 340kDa, chosen as a model for big proteins. The protein released by the electrospun samples was bovine serum albumin (BSA), a 66 kDa protein extensively used as a model protein in release studies and important because various vaccines and protein pharmaceuticals contain BSA or human albumin as a stabilizing agent or excipient [50,51].

4.2 Materials & Methods

4.*2.1 Protein encapsulation in BFs films*

Porous films patterned with the Breath Figures templating method were produced and fibrinogen (FNG) was trapped on pores surface with the methods explained in chapter 3.

4.2.2 Encapsulation efficiency and binding force

To assess the initial concentration of fibrinogen in samples, a Micro-BCA assay kit was used, purchased from Pierce, Thermo Scientific, following the protocol provided by the producer. To increase the quality of measurement samples immersed in working reagent were incubated overnight at 37°C.

The force of bounds between fibrinogen and pores surface was also tested. Samples were washed with sequential immersions in solvents with increasing capacity of inducing debonding: the first three washes were performed in water, than in a solution of water and isopropyl alcohol at a concentration of 10%, 30%, 50% and 70%. Immersion was performed for 20 minutes each, in static conditions at room temperature. After each step, the immersion solution was collected and freeze-dried. The powder was resuspended in Lithium Dodecyl Sulfate (LDS) and analyzed with sodium dodecyl sulfate polyacrylamide gel electrophoresis (SDS-PAGE), using 3-8% tris-acetate gels. After electrophoresis, Silver Stain was used to color proteins and the total amount of fibrinogen was calculated.

4.2.3 Release test from BFs films

Films, after fibrinogen encapsulation, were cut in squares of 1cm^2 and put in eppendorf tubes. 1ml per sample of PBS containing 0.02% sodium azide (NaN_3) was added to each tube. A polyethylene ring kept the samples fully immersed, avoiding buoyancy. Samples were stored at 37°C, to mimic the human body conditions. At regular time points 500µl of each solution was collected and 500µl of fresh PBS was added in each tube. Since the collected solutions were too diluted for the detection technique, they were freeze-dried and resuspended in PBS, to obtain a higher concentration. Solutions were then analyzed with a Micro-BCA assay kit, following the protocol provided by the producer.

4.2.4 Residual protein in films

The amount and distribution of fibrinogen in films were assessed by means of a confocal microscope (Nikon eclipse, TI-E). Samples containing fibrinogen were immersed in a solution of FITC-conjugated concanavalin A (FITC-conA), 100µg/ml in PBS, for 18 hours at 4°C; then they were washed 3 times in PBS. Fluorescent signal detection was performed at 488nm. Confocal microscopy was used to localize the fibrinogen in pores arrays, to assess its presence on pores walls and bottoms.

4.2.5 Citotoxicity test

The citotoxicity of films containing Jeffamine was tested using LDH-based in vitro toxicology assay (kit TOX7 Sigma Aldrich). Samples composed of PDLLA and PCL with different Jeffamine concentrations and Jeffamine itself were used in the test. Toxicity was evaluated using both films and extracts. The latter were obtained immersing the samples in PBS at 37°C for 72 hours. The solution was then extracted in a concentration of 7mg/ml.

MRC5 cells (fibroblast cell line derived from normal lung tissue) were seeded in Tissue Culture Plates in a concentration of 10^4 cells/ml and cultured for 24 hours in a culture medium composed of: RPMI-1640 without phenol red, 10 % of FBS, 1% of L-Glutamine, 1% of Sodium Piruvate, 1% of non essential Aminoacids and 1% of antibiotic/antimicotic. After 24 hours of culture, the medium was withdrawn, wells with cells washed in PBS and samples of

films (7mg) or 0.25ml of extracts where added. Then, culture wells were filled with medium, for a total volume of 1 ml. Films tested was previously sterilized by immersion in ethanol for 18 hours at 4°C, while bulk Jeffamine was sterilized for 20 minutes in ethanol at room temperature, in order to avoid its dissolution. Cells in contact with extracts were cultured for 24 additional hours, while cells in contact with materials were cultured for 7 days. At the end of the culture, surnatants were withdrawn and centrifuge at 250g for 4 minutes, to pellet debris. An aliquot of 0.5 ml of each sample was transferred in a clean well. 1 ml of assay mixture was added to each well and incubated in a dark environment for 30 minutes, to allow the reaction between the assay mixture and the LDH eventually present in the aliquots. Reactions was terminated adding 150 µl of hydrochloric acid 1M to each well. 100 µl of each sample was put in a 96-well plate and the absorbance at 490 nm was detected. The background absorbance was measured at 690 and subtracted from the previous measurement. Wells cultured with cells but without the addition of films or extracts were used as controls.

4.2.6 Electrospun mats production

The electrospun fibers are composed of an ester-terminated Poly(ε-caprolactone), (PCL) with inherent viscosity of 1.0-1.3 dL/g (Mw is approximately 120-150 kDa) The polymer was purchased from Lactel. The polymer used for the core of fibers is

polyethylene glycol (PEG) with a Mw of 8 kDa, provided by Sigma-Aldrich. Albumin, from Bovine Serum, (BSA) was obtained from Sigma-Aldrich. Dichloromethane and Chloroform (containing 1% of ethanol) were both purchased from EMD Chemicals. To dissolve BSA and PEG Milli-Q water was used. Weight measurements were performed using a Mettler Toledo AX105 scales. SEM images were obtained using a FEI Quanta 400 ESEM FEG, after gold sputtering. Image analysis to assess fibers diameter were performed with the software ImageJ. MS Excel was used to elaborate data obtained by the release study while the fitting of the curve was performed using the software OriginPro 7.0.

The solutions used for the production of scaffolds were prepared dissolving PCL in chloroform in a concentration of 11% in weight, under stirring conditions until the complete dissolution of the polymer. A concentration of 7% has been tested in a pre-study, too, but 11% leads to better fiber stability during the coaxial electrospinning process. Due to the volatility of the solvent fresh solutions were used in different experimental sessions and conserved in closed vials for short periods of time. PEG and BSA were co-dissolved in water under mild stirring. The concentrations were 400mg of PEG and 200mg of BSA per ml of water.

The electrospinning apparatus is composed of a PE syringe connected to a syringe-pump which flow was regulated from 0.6 to 10 ml/h. The target is composed of a copper plate (10X10 cm) covered with a plate glass of the same dimension. The distance between the needle tip and the target was varied in the range of 15-35 cm. An electric potential of 10-30 kV was applied between the needle (18 or 22 gauge) and the target. To focus the electric field a copper ring

(positively charged as the needle is) of 10cm of diameter was disposed around the needle. The apparatus is enclosed in a closed chamber where the humidity is controlled fluxing 100% RH air or nitrogen and measuring the humidity and the temperature with a thermo-hygrometer.

The coaxial electrospinning apparatus is composed of two syringes placed on to two syringe-pumps (figure 4.1). The syringes are connected by means of silicone tubes to a coaxial needle, composed of a 22 gauge needle coaxially disposed into a 16 gauge one. The solution of PEG and BSA is pumped through the inner needle (flow rate of 0.1- 0.2 ml/h), while the PCL solution (flow rate of 10-15ml/h) pass through the outer one. The target is a copper plate with a plate glass on it. The applied voltage between the needle and the plate is in the range of 20-30 kV while the distance is 20-40 cm.

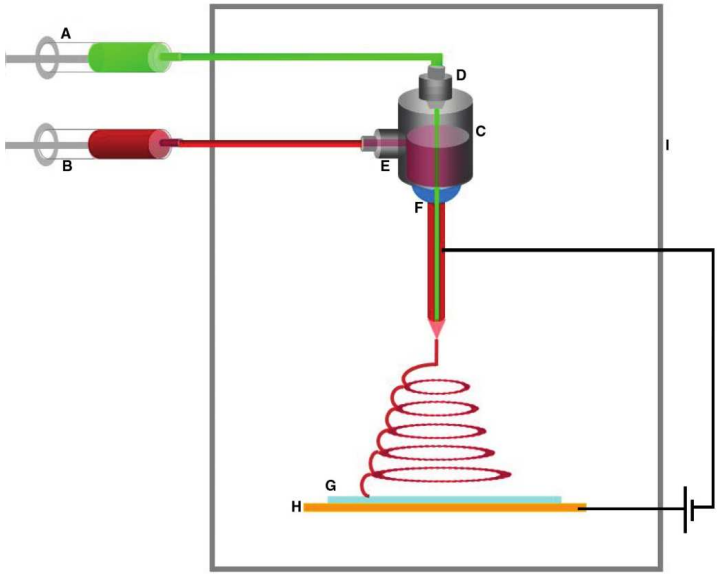

Fig.4.1: Scheme of the coaxial electrospinning apparatus [32]

Due the large number of variables, not all the possible combinations of different settings have been tried, but only some of them. The settings resulting in higher stability of the fibers were chosen to produce the scaffolds (table with the selected parameters). Scaffolds were cut in disks of 8mm diameters and approximately 1 mm thick. These dimensions were chosen as they are the dimension of a critical size defect in rats. After the production, samples were weighted and their thickness measured.

Scaffolds produced with the traditional electrospinning were loaded with BSA through a physical adsorbance on their fibers surface. 0.5 ml of solution of BSA in water (100mg/ml) was forced to pass through each scaffold; then the scaffold

were immersed in the solution for 1 hour and, after this, rinsed in pure water to remove excess of solution. The loaded scaffolds were then lyophilized to remove water.

4.2.7 Protein release from fibers

The quantity of protein loaded in each scaffold was determined dissolving them in 1 ml of DCM; 10 ml of PBS was added to the solution, to promote the dissolution of the BSA and the precipitation of PCL. The solution was strongly stirred for 2 hours, to let the DCM evaporate completely. 1 ml of the remaining PBS solution was then analyzed with the micro-BCA kit, provided by Thermo Scientific, using a Power Wave X340 multiwell plates reader, produced by BioTek Instruments,Inc.

The release test was performed immersing each scaffold in 1ml of PBS at 37°C. At regular time points samples of 0.5 ml were taken and analyzed with the micro-BCA kit. 0.5 ml of fresh PBS was added to replace the withdrawn solution.

After the release study, scaffolds were observed with the SEM and compared to scaffolds obtained from the same mats but which didn't undergo the release process, to understand how the immersion in PBS affects fibers morphology.

4.3 Results and Discussion

4.*3.1 Protein encapsulation*

Films patterned with the Breath Figures method was produced with poly-d,l-lactic acid (PDLLA) and polycaprolactone (PCL). This templating process allows the formation of porous structures on the surface of films. The addition of Jeffamine, an amphiphilic polymer with two amino groups at its ends, leads to the functionalization of the surface of pores, which is enriched with amino groups. This chemical pattern was used to bind fibrinogen in the pores, as described in chapter 3. Three sets of samples were analyzed, depending on the mechanism used to bind the fibrinogen: physical adsorption of the protein on the polymeric film without chemical functionalization; chemical binding to amino groups; enhanced chemical binding to amino groups by means of EDAC, a zero-length crosslinker. As discussed in the previous chapter, homogeneity and efficiency of encapsulation were observed to increase with the addition of Jeffamine and with the use of EDAC.

4.3.2 Encapsulation efficiency and binding force

To better understand the efficacy of protein encapsulation, an in-situ measurement of the quantity of fibrinogen trapped in the pores was performed, using a micro-BCA test on samples. Furthermore, the strength of bonds linking fibrinogen to the films was tested through a sequence of successive washes and analyzing, by means of electrophoresis, the quantity of protein removed.

The encapsulation efficiency of PDLLA films, measured as the quantity of fibrinogen trapped in the films, is shown in figure 4.2.

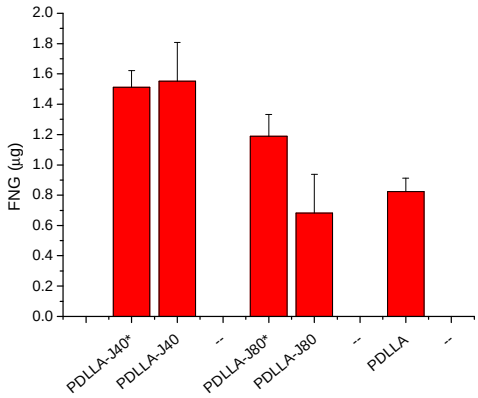

*Fig.4.2: quantity of fibrinogen entrapped in PDLLA films.*indicates the use of EDAC*

Fibrinogen solution penetrates the pores and interacts with their surface; the graph show an increase in the quantity of protein encapsulated when Jeffamine is used. Interestingly, this value is higher in films with 4% of Jeffamine than in those with 8%. This trend can be attributed to the difference in pores size, resulting in a different total surface. However, data show that the presence of amino groups strongly increase fibrinogen encapsulation. The films with 12% were not tested due to their particular structure, which don't allow an efficient encapsulation. Data relative to films with 8% of Jeffamine evidence an increase when chemical binding is enhanced by the presence of EDAC.

Films composed of PCL don't show an increase in the quantity of fibrinogen entrapped when EDAC is used (figure 4.3). Jeffamine, also in this case, has a significant effect on the results, improving the efficacy of protein binding. Passing from 8% to 12% of its concentration, however, decrease the total amount of fibrinogen in films, suggesting that pores size has an important role in the process.

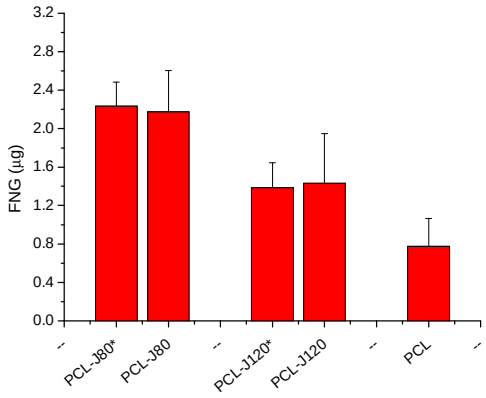

*Fig.4.3: quantity of fibrinogen entrapped in PCL films.*indicates the use of EDAC*

From both tests (on PDLLA and PCL), it is evident that the chemical functionalization of pores leads to better results in term of quantity of fibrinogen in films. Pure polymers always lead to lower values of protein detected. On the other hands, high percentage of Jeffamine modifies the structures of surface pattern, increasing the mean pore size and, thus, decreasing the total surface. In films composed of PCL, in addition, pores structure includes also a population on nanopores and the formation of big pores below the film surface (see chapter 3).

The latter can constitute a reservoir for the fibrinogen, explaining its higher quantity in PCL than in PDLLA films.

Binding force of fibrinogen was tested measuring the quantity released after a series of washes in water and isopropyl alcohol. Detection of the amount of protein measured is shown in figure 4.4. When EDAC is used to enhance the formation of peptide bonds between fibrinogen and Jeffamine, the release value is very small and occurs mainly when isopropyl alcohol is used at high concentrations. On the contrary, when EDAC is not used, washes with water remove a large part of the protein.

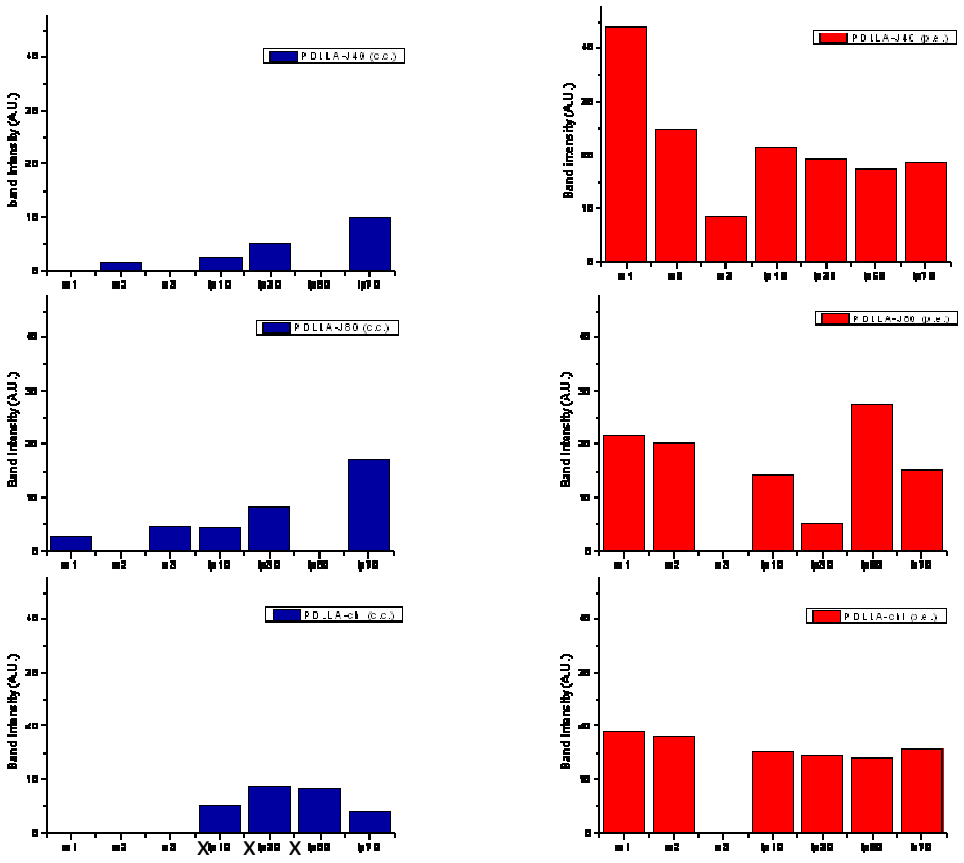

Fig.4.4: Results of binding force tests on PDLLA films, for encapsulation with (left column) or without (right column) EDAC, at different Jeffamine concentration: 4%(first row),8%(second row),0%(third row)

In this test, wettability of the samples is an important parameter, which influences the values obtained. In samples of PDLLA, for instance, poor wettability doesn't allow a correct testing. However, binding strength is evidenced to be

stronger when EDAC is used. Jeffamine addition seems to have little influence on binding strength in PDLLA films. A different results is obtained with PCL films, in which both Jeffamine presence and EDAC use influence the release of protein (figure 4.5), shifting the break of bonds to the last washes.

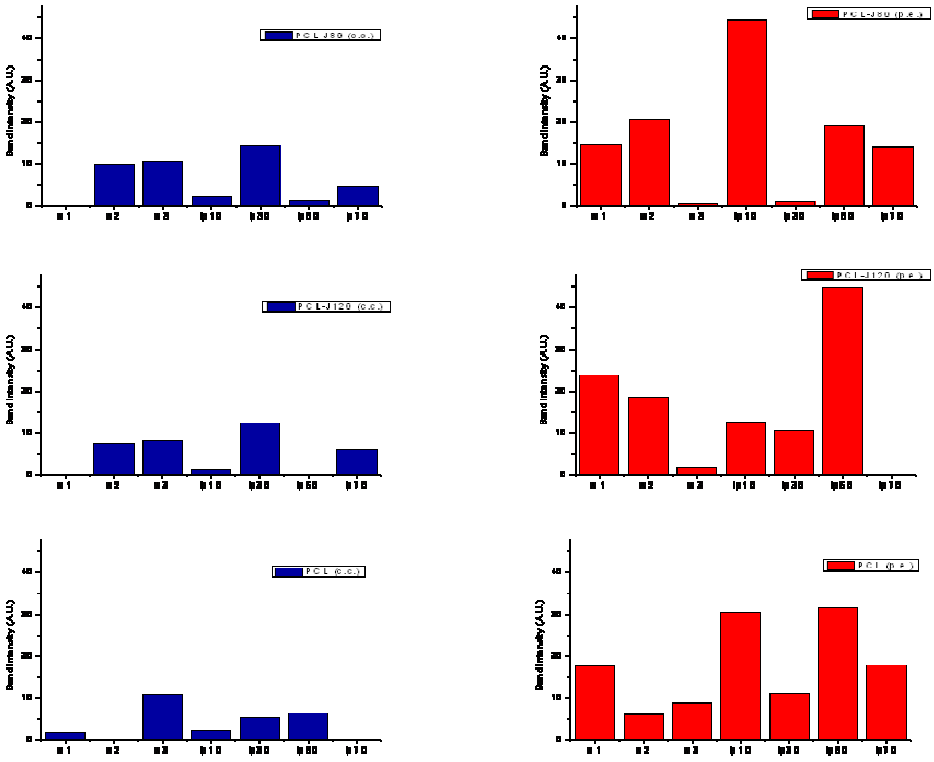

Fig.4.5: Results of binding force tests on PCL films, for encapsulation with (left column) or without (right column) EDAC, at different Jeffamine concentration: 4%(first row),8%(second row),0%(third row)

4.3.3 Release test

Data obtained measuring the release of fibrinogen from PDLLA films are shown in figure 4.6. A general consideration is that the release is not constant over all the test period. Graph shows a multi-step release, composed of periods where the protein is released faster and periods where the release rate is lower. Probably, this behavior is due to the complex geometry of these systems, in which pores structure plays a major role. Dimension, interconnectivity and structures of pores determine sample interaction with the liquid in which it is immersed, thus influencing protein desorption. The possibility of modulating this multi-step behavior can be used when a non-constant release of drugs is needed. Modification of the pores features leads to different behavior, leading to the possibility of tuning the release in multiple ways.

The graph obtained with PDLLA films (without EDAC) shows that addition of Jeffamine determines a more regular release, compared to the pure PDLLA films. Release is generally higher in the first week, and then it becomes lower. Considering that films with Jeffamine have a higher initial concentration of fibrinogen, due to better encapsulation efficiency, it seems that the chemical bounding delays the release. This can explain also the difference observed in films with 4% and 8% of Jeffamine. The latter encapsulate less protein, as shown above, but also present a lower release rate. A similar result is obtained with PCL films, as shown in figure 4.7; release rate decreases when Jeffamine concentration is increased, even though the initial concentration is lower.

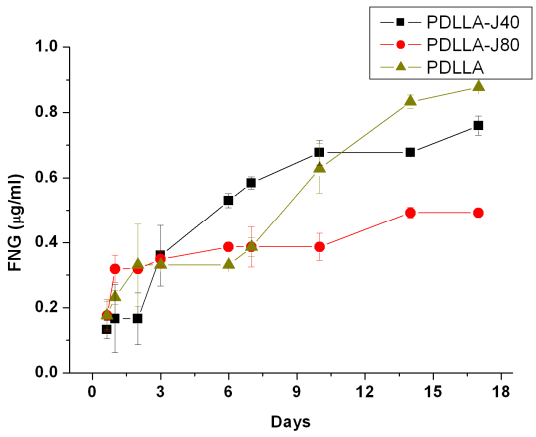

Fig.4.6: cumulative release of fibrinogen in PDLLA films with different Jeffamine concentration

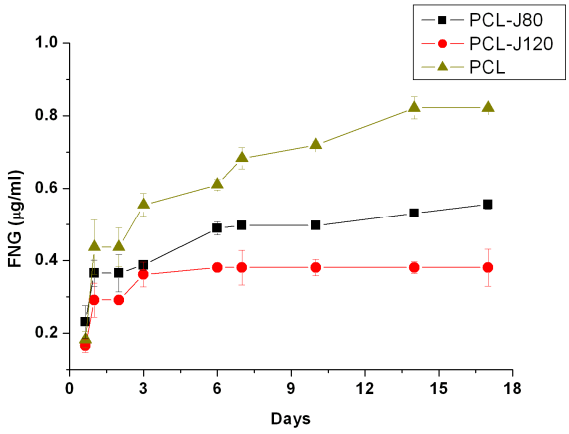

Fig.4.7: cumulative release of fibrinogen in PCL films with different Jeffamine concentration

The delaying effect of Jeffamine was observed also when EDAC was used to enhance binding of fibrinogen to pores in PDLLA films (figure 4.8). Even though the 8% films present a high initial burst release, the release rate is lower compared to pure PDLLA films. Also in PCL films (figure 4.9) a high burst release was observed with a concentration of Jeffamine of 8%. Chemical bounding was expected to eliminate initial burst effects, but some samples show high quantity of protein released in the first stage of the experiment. On the other hand, the PCL-12%Jeffamine films don't present any burst effect, suggesting that this phenomenon is not due to Jeffamine addition. Interestingly, all the other samples don't have a fast burst release, which is a diffuse problem in other drug release devices.

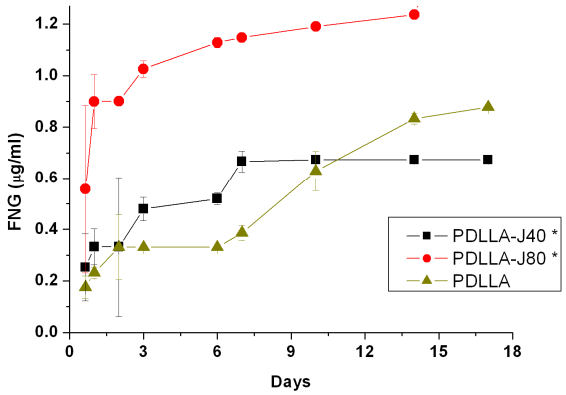

*Fig.4.8: cumulative release of fibrinogen in PDLLA films with different Jeffamine concentration. * indicates that EDAC was used in protein encapsulation process*

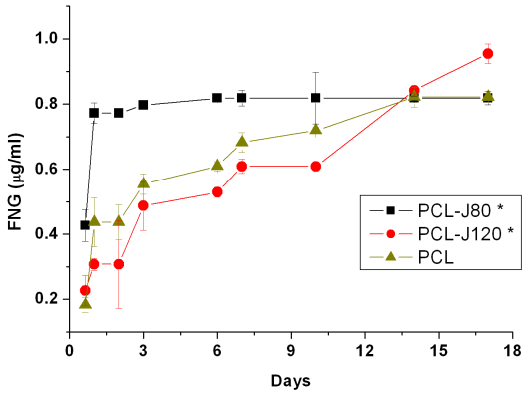

*Fig.4.9: cumulative release of fibrinogen in PCL films with different Jeffamine concentration. * indicates that EDAC was used in protein encapsulation process*

4.3.4 Residual protein in films

To monitor the release mechanism from BFs patterned films, the residual fibrinogen still trapped in pores was detected at regular time points, corresponding to 7 and 14 days. Confocal microscopy allows to qualitative measure the distribution and amount of fibrinogen that remains in pores after the sample was immersed in PBS for a certain amount of time.

Films composed of pure PDLLA release fibrinogen almost completely in two weeks. Figure 4.10 shows the residual fibrinogen at the two time points. At the seventh day the surface of films and pores walls present a very low fluorescent signal, evidencing that the protein have been released. Nevertheless, fibrinogen is still present in pores bottom. After 14 days, also this signal disappears. The

release mechanism, thus, is faster for areas closer to the film surface, while proteins trapped deeper in the pores need longer time to be removed. This can explain the two-step behavior observed in the release study.

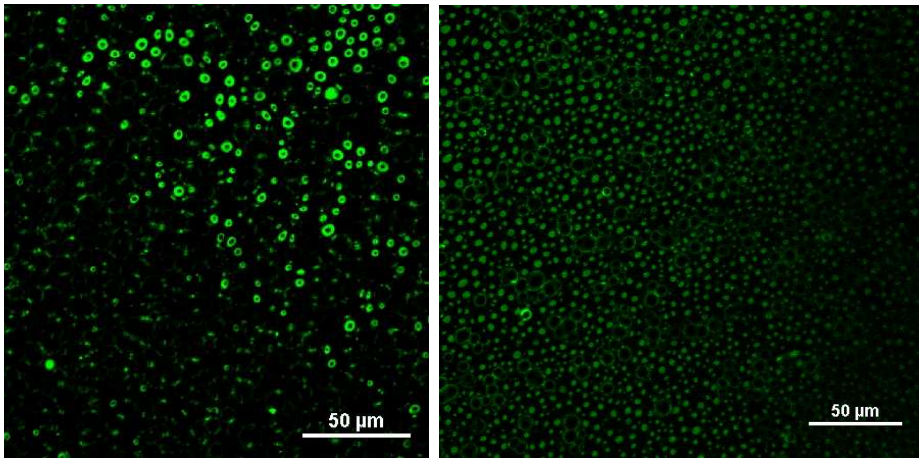

Fig4.10: Residual fibrinogen in PDLLA films after 7(left) and 14(right) days. Image of 7days is diveded in two different focal planes: film surface (bottom left corner) and pores bottom (top right corner). Image of 14 days is focused on pores bottom.

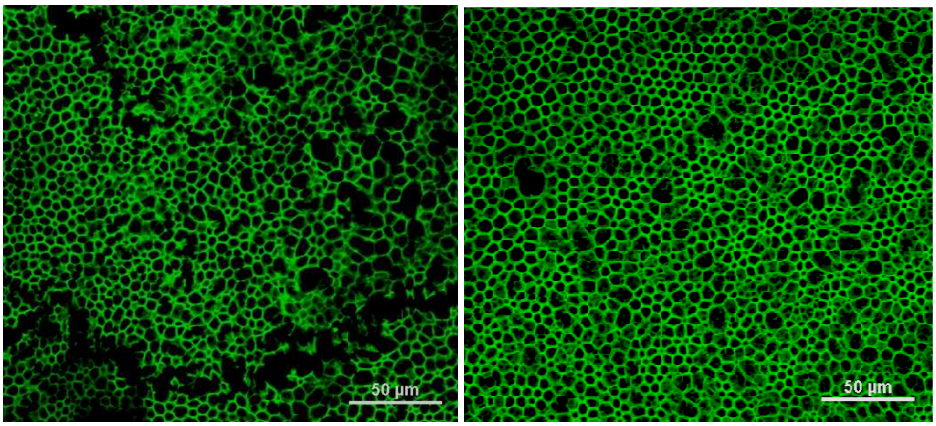

Fig4.11: Residual fibrinogen in PDLLA films with 4% of Jeffamine, after 7(left) and 14(right) days. Both pictures are focused on film surface.

When Jeffamine is added, the release is slower, so the fluorescent signal due to the presence of fibrinogen is higher for both time points, as visible in figure 4.11. The protein is still present also on pores walls after 14 days. Release studies evidenced that the encapsulation efficiency in this films is very high and the release rate is low. The presence of a high quantity of fibrinogen still trapped in pores is a confirmation of the previous data.

Figure 4.12 shows the data obtained with films with the same composition but with the use of EDAC to bind fibrinogen. The test on this samples shows a very high fluorescent signal. The initial concentration was similar to the one of films obtained without the crosslinker, but the release rate was lower. These data shows that the time needed for the complete release of the fibrinogen entrapped in the patterned films containing Jeffamine is higher than two weeks.

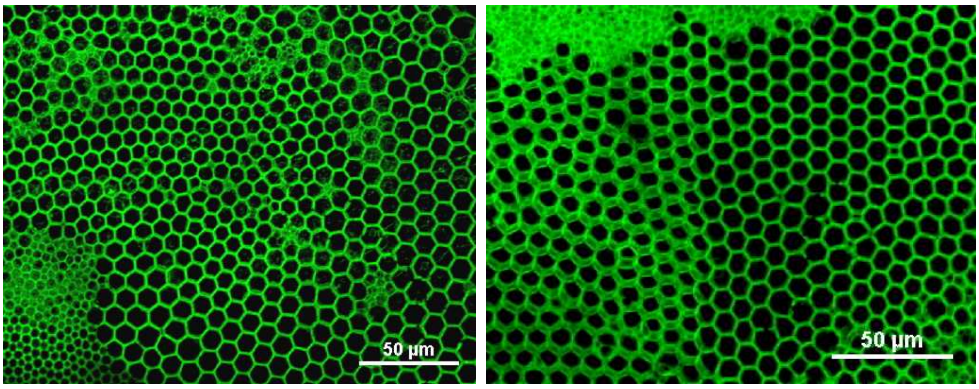

Fig4.12: Residual fibrinogen in PDLLA films with 4% of Jeffamine, after 7(left) and 14(right) days. Both pictures are focused on film surface. EDAC was used in protein encapsulation process

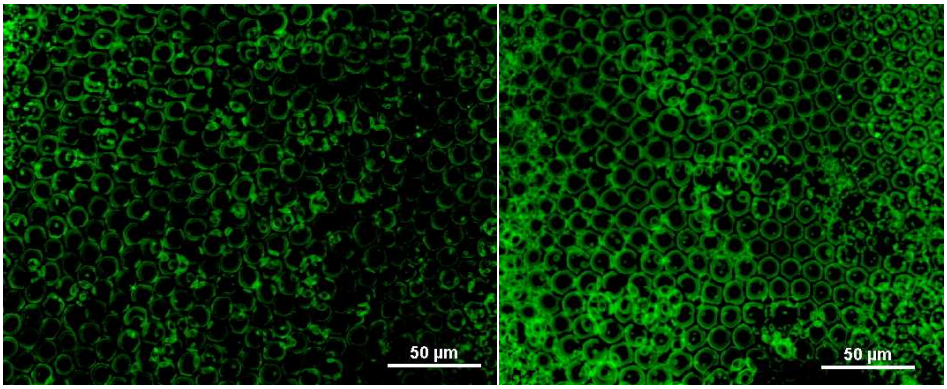

Fig4.13: Residual fibrinogen in PDLLA films with 8% of Jeffamine, after 7(left) and 14(right) days. Both pictures are focused on film surface.

When the concentration of Jeffamine was doubled, no significant difference was observed (figure 4.13 and 4.14). Fibrinogen is still present after two weeks of release, and is distributed also on pores walls (figure 4.15).

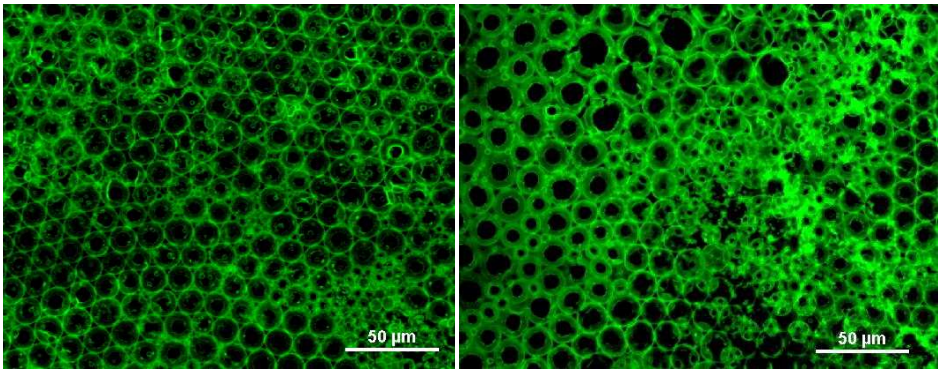

Fig4.14: Residual fibrinogen in PDLLA films with 8% of Jeffamine, after 7(left) and 14(right) days. Both pictures are focused on film surface. EDAC was used

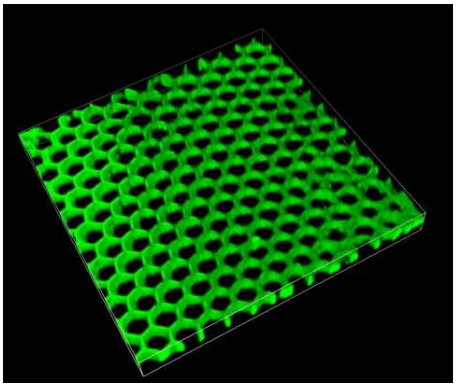

Fig4.15: 3D image of esidual fibrinogen in PDLLA film with 8% of Jeffamine, after 7 days. EDAC was used in protein encapsulation process

The experiment was performed also on films composed of PCL (see figure 4.16). These films show an higher protein encapsulation efficiency and the quantity of fibrinogen which remains in pores seems to be higher compared to the PDLLA films. Desorption of fibrinogen, again, is faster near the surface, while pores bottom releases the protein slower.

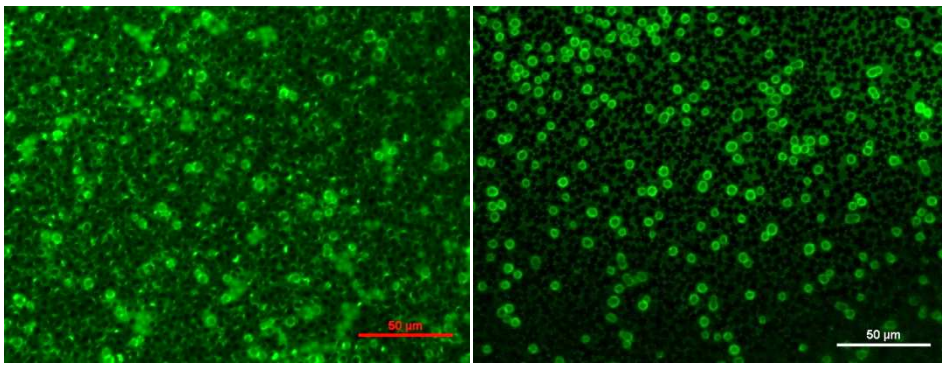

Fig4.16: Residual fibrinogen in PCL films, after 7(left) and 14(right) days. Both pictures are focused on pores bottom.

The images obtained testing samples of PCL and 8% of Jeffamine display a weak signal related to the protein near the surface, as shown in figure 4.17. The distribution of fibrinogen looks still homogeneous, but the total amount of protein is low. The same consideration holds for the 2-weeks samples. Interestingly, below the surface some spots appear, which present a high fluorescent signal. The spots corrispond to pores situated below the surface, at the interconnections among superficial pores. SEM observation evidenced the presence of pores situated below the surface, interconnecting more superficial

pores, which probably act as reservoir for fibrinogen. When binding was enhanced with EDAC, the fluorescent signal is more intense in both time points, as shown in figure 4.18.

Similar results were obtained with samples containing 12% of Jeffamine (figure 4.19). Fibrinogen is still homogeneously distributed in pores, but the total amount seems to be lower compared to PDLLA films. In this case, furthermore, a strong influence of enhanced conjugation with EDAC on the residual fibrinogen quantity was observed, as shown in figure 4.20.

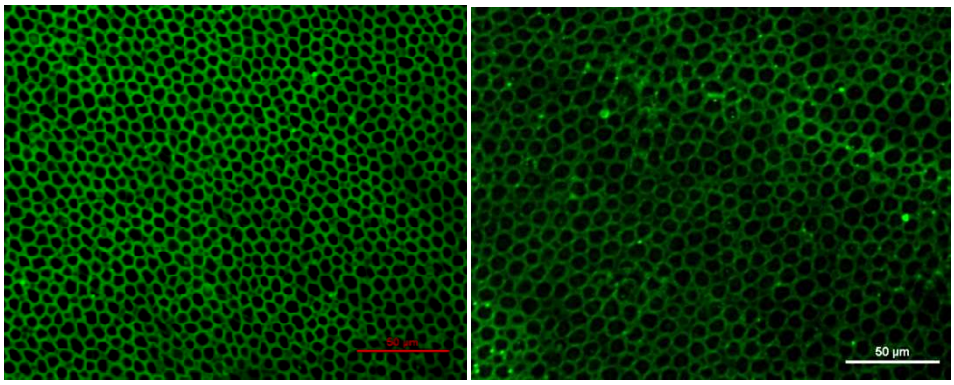

Fig4.17: Residual fibrinogen in PCL-8%Jeffamine films, after 7(left) and 14(right) days. Both pictures are focused below film surface.

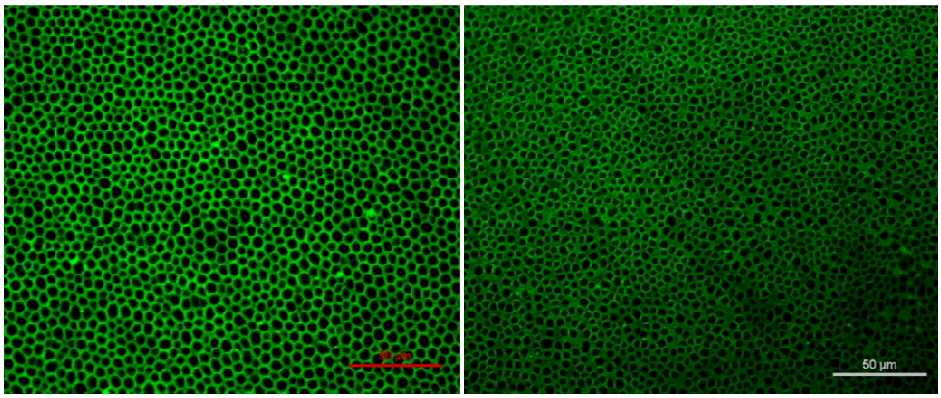

Fig4.18: Residual fibrinogen in PCL-8%Jeffamine films, after 7(left) and 14(right) days. Both pictures are focused below film surface. EDAC was used in protein encapsulation process

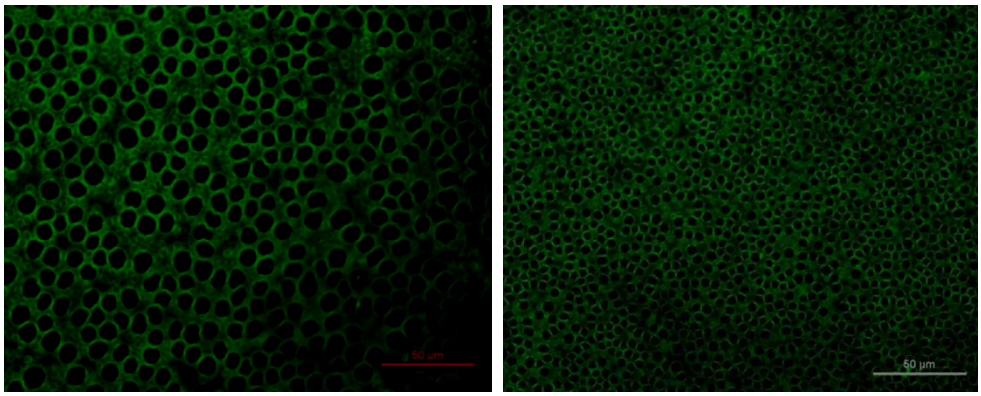

Fig4.19: Residual fibrinogen in PCL-12%Jeffamine films, after 7(left) and 14(right) days. Both pictures are focused below film surface.

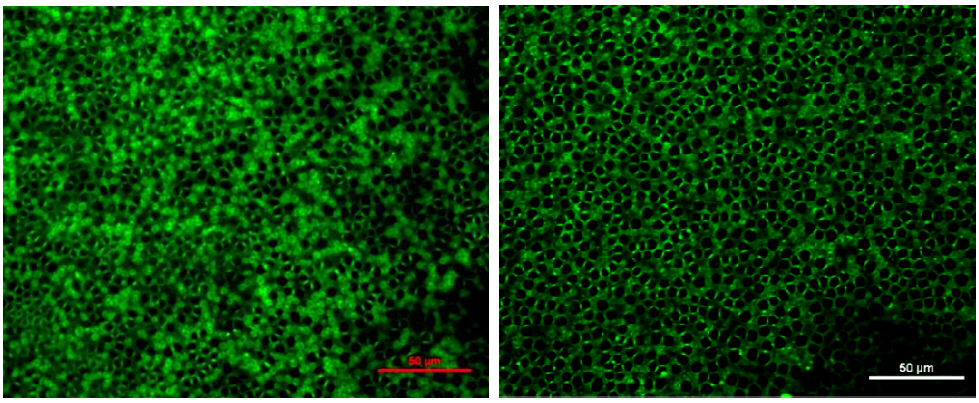

Fig4.20: Residual fibrinogen in PCL-12%Jeffamine films, after 7(left) and 14(right) days. Both pictures are focused below film surface. EDAC was used in protein encapsulation process

4.3.5 Citotoxicity test

Films of PDLLA or PCL were studied in our experiments as drug delivery devices. The idea is to use them as internal patches which can release drugs in a controlled way. For this purpose, the materials used should not damage cells, which they would be in intimate contact with in human body. For this reason, their citotoxicity was evaluated. Lactate Dehydrogenase (LDH) is a cytoplasmic enzyme released by cells when the cellular membrane is damaged. The amount of LDH in the culture medium is proportional to the number of dead cells during culture. Therefore, the concentration of this enzyme can be a measure of the cytotoxicity of a substance. The results of the test are shown in figure 4.21. The measurements, proportional to the number of dead cells, are lower and less variable for experiments performed with extracts, probably due to the shorter

culture period (1 day vs 7 days). Significant differences exist, both for samples in contacts with films and with extracts. However, these differences are probably due to the variability intrinsic in cell cultures and do not depend on samples citotoxicity, as evidenced by a comparison with the control sample. The culture of cells without the addition of materials or extracts leads to the higher number of dead cells, meaning that Jeffamine and its combination with PDLLA or PCL are not citotoxic.

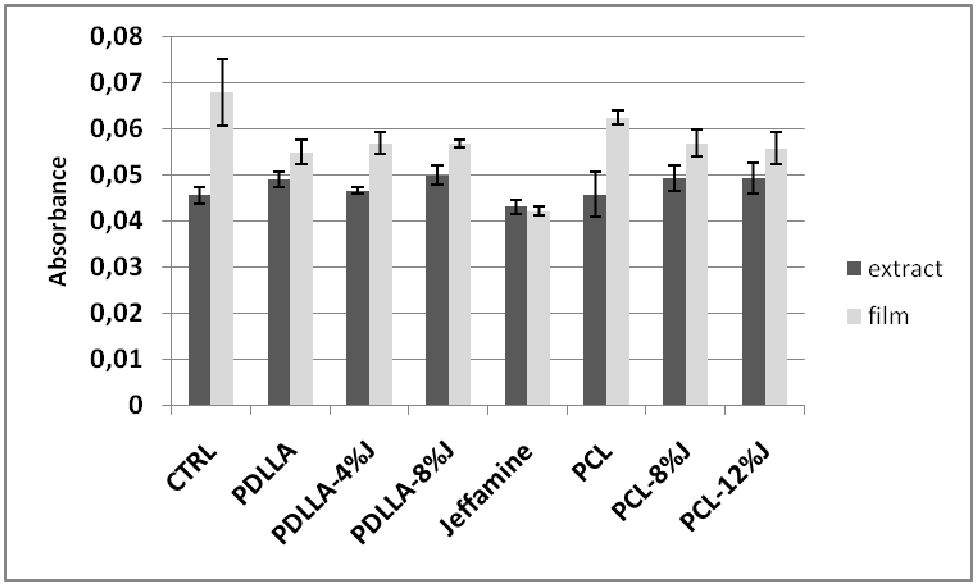

Fig4.21: result of citotoxicity test on Jeffamine, PDLLA and PCL samples

4.3.6 Electrospun mats production

Micrometric fibers were produced with two different electrospinning processes. Traditional electrospinning leads to pure PCL fibers, while coaxial electrospinning allowed the production of fibers composed of an outer sheath of PCL which cover an inner core made of PEG. In both the techniques, control of the environmental humidity leads to the formation on the fiber surface of a pattern of self-assembled pores. An example of the capacity of controlling the surface pattern of fibers is shown in figure 4.22. Fibers produced in a dry environment presented a smooth surface; the increase in humidity during the process, on the other hand, leads to the formation of sub-micrometric pores on fiber surface. The reason for the appearance of pores is related to water droplets condensation on polymer surface from the humid environment. Droplets nucleation and growth are guided by the cooling of polymer solution due to solvent evaporation, with the same mechanism already observed in Breath Figures templating method for polymeric films (see chapter 1). In electrospinning, however, fibers solidify in a very short time and undergo a dramatic stretching during their movement towards the target; for this reason, droplets organization in an ordered array is hindered.

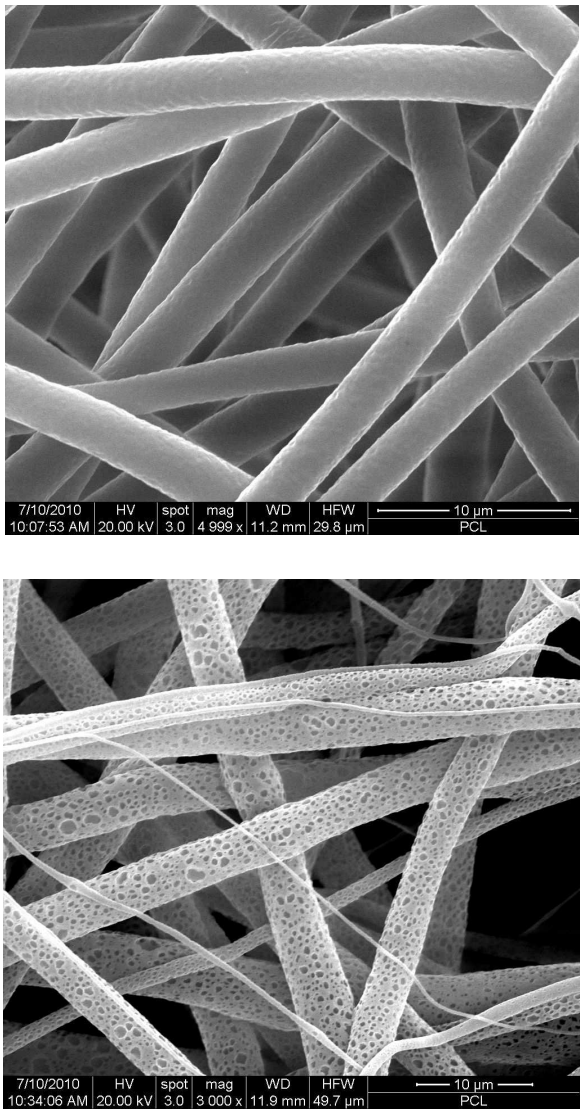

Fig4.22: SEM images of fibers produced starting form a PCL-Chloroform solution 11%. Process parameters are the same. RH is 40% (top) or 70% (bottom). Scale bar is 10µm

Interestingly, in the samples observed, small fibers present smoother surface, while pores forms preferentially on fibers with bigger diameter. This is connected to the kinetic of the process. Solvent evaporates and the polymer harden faster from small fibers, hindering the process which leads to pores formation. Complete solvent evaporation in electrospinning occurs in a very short time and the physical process leading to surface pattern has a similar characteristic time. Figure 4.23 shows a set of fibers with irregular diameter. The formation of pores on a fiber appears to be related to its diameter. A fiber with an irregular section presents pores only in regions where the diameter is bigger, while regions with a smaller diameter have a smooth surface. The presence of surface pores is, thus, related not only to the relative humidity during the electrospinning process, but also to fiber diameter and to process parameters. An interesting observation is the presence of a population of very small nanofibers, due to the splitting of the polymer jet into multiple jets.

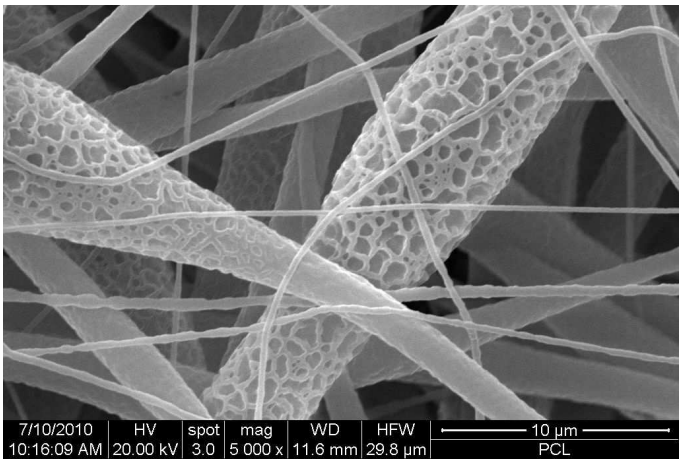

Fig4.23: SEM images of fibers produced starting form a PCL-Chloroform solution 11%. RH is 70%. Scale bar is 10µm

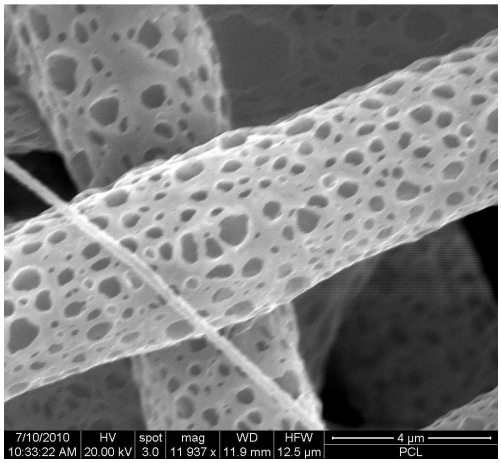

Fig4.24: SEM images of fibers produced starting form a PCL-Chloroform solution 11%. RH is 70%. Scale bar is 4µm

The pores which decorate the fibers surface are irregular in shape and dimension. Their diameter is generally included in a wide range of dimension, from 1 µm to 50 nm, as shown in figure 4.24.

Electrospun mats conformation seems to be little affected by environmental humidity, as evidenced by figure 4.25. However, a less compact mat seems to be obtained at high RH.

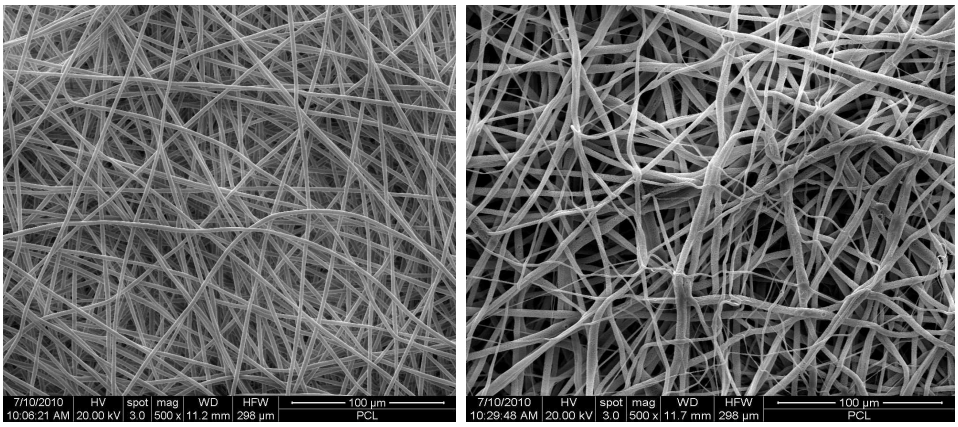

Fig4.25: SEM images of mats produced starting form a PCL-Chloroform solution 11%. Process parameters are the same. RH is 40% (left) or 70% (right)

4.2.7 Protein release from fibers

The possibility of tuning the fiber surface patterns was exploited to produce fibers with different porous surfaces and the influence of this features on drug release was evaluated.

With the traditional electrospinning apparatus, four samples of PCL electrospun mats were produced, varying two parameters: humidity during the electrospinning process (30% or 70%) and the mean diameter of fibers ("small" =about 3µm or "large"=about 4.5µm). BSA was adsorbed on the surface of fibers, so the influence of surface pores and of fiber diameter was evaluated during release test. The surface topography of fibers is shown in figure 4.26. The mean diameter of fibers in samples produced with 30% RH was d= (2.8±0.5) µm and d= (4.3±0.9).

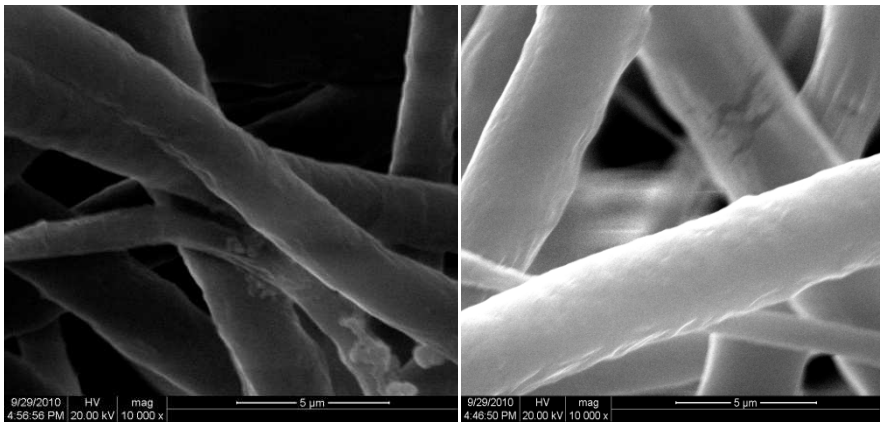

Fig4.26: SEM images of PCL fibers, produced with RH =30%. Scale bar is 5µm

Figure 4.27 shows the patterned surface of fibers produced in a humid environment (RH=70%). The mean diameter of the two samples was d= (3±0.4) and d= (4.8±1).

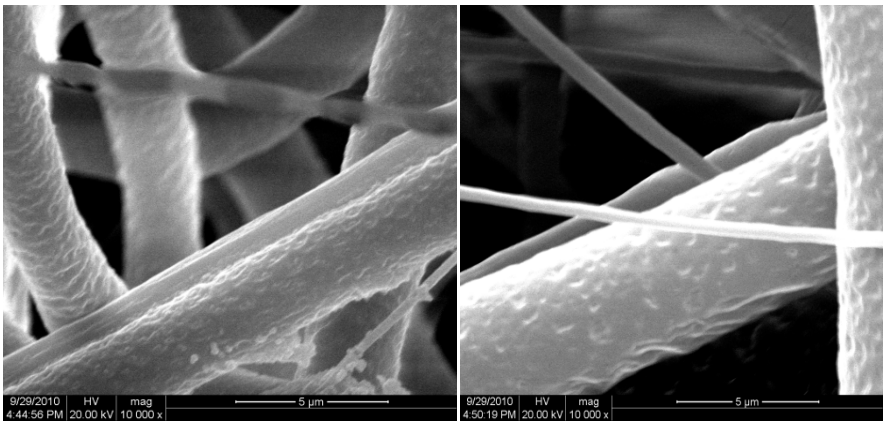

Fig4.27: SEM images of PCL fibers, produced with RH =70%. Scale bar is 5µm

The surface of fibers produced with RH = 70% presented an array of pores with small depth.

The cumulative release of albumin is presented in figure 4.28.

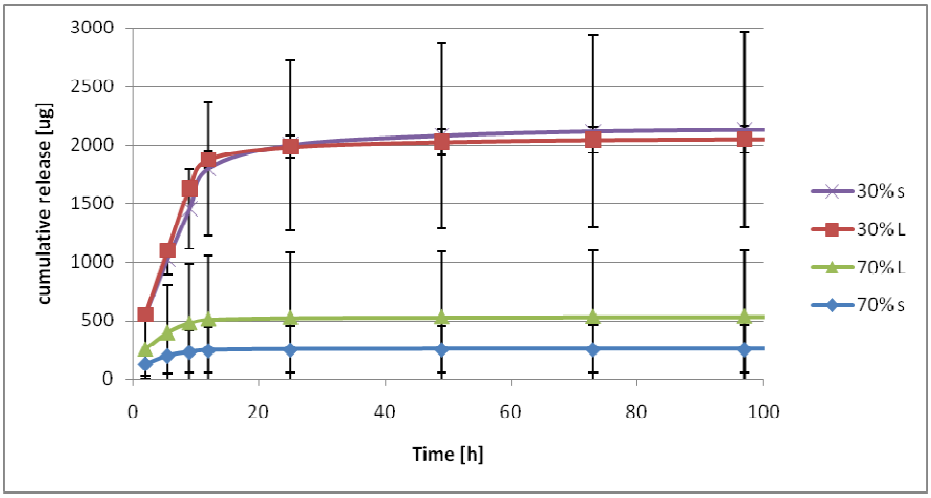

Fig4.28: Cumulative release of albumin adsorbed on surface of electrospun fibers produced with different RH. "s" indicates fibers with a mean diameter of about 3µm, "l" indicates a diameter of about 4.5µm

Albumin is released very fast, due to its hydrophilicity, and almost completely in 12 hours, indipendently of the samples considered. Surprisingly, samples with a smooth fiber surface released a higher total amount of albumin compared to samples produced at high relative humidity. Fiber diameter, on the other hand, don't influence the release, at least in the range of diameter considered in this experiment. The difference observed in samples probably does not depend on the surface properties, but instead, relays on the structure of the whole mat. Electrospinning at high RH led to mats which appeared to have a higher porosity among fibers. Such a structure can not release gradually albumin and, probably,

loses the protein adsorbed during the whases after the adsorption process. This could account for the lower amount of albumin released during the test.

Coaxial electrospinning was used to produce mats with different surface pattern. Albumin was entrapped in the core of fibers, blended with PEG. In this exeperiment, four samples were produced with different value of RH: 40%, 50%, 60% and 65%. The surface of fibers and the measure of their diameter is highlighted in figure 4.29. The increase in environmental humidity level leads to the formation of pores patterns on fibres surface. Moreover, pores seems to cover the entire surface of fibers, while pore depth increases with increasing humidity. As discussed above, pores formed preferentially on big fibers.

The release test showed interesting results (figure 4.30). Fibers with a porous surface, produced at high RH value, released an higher amount of albumin compared to smooth fibers.

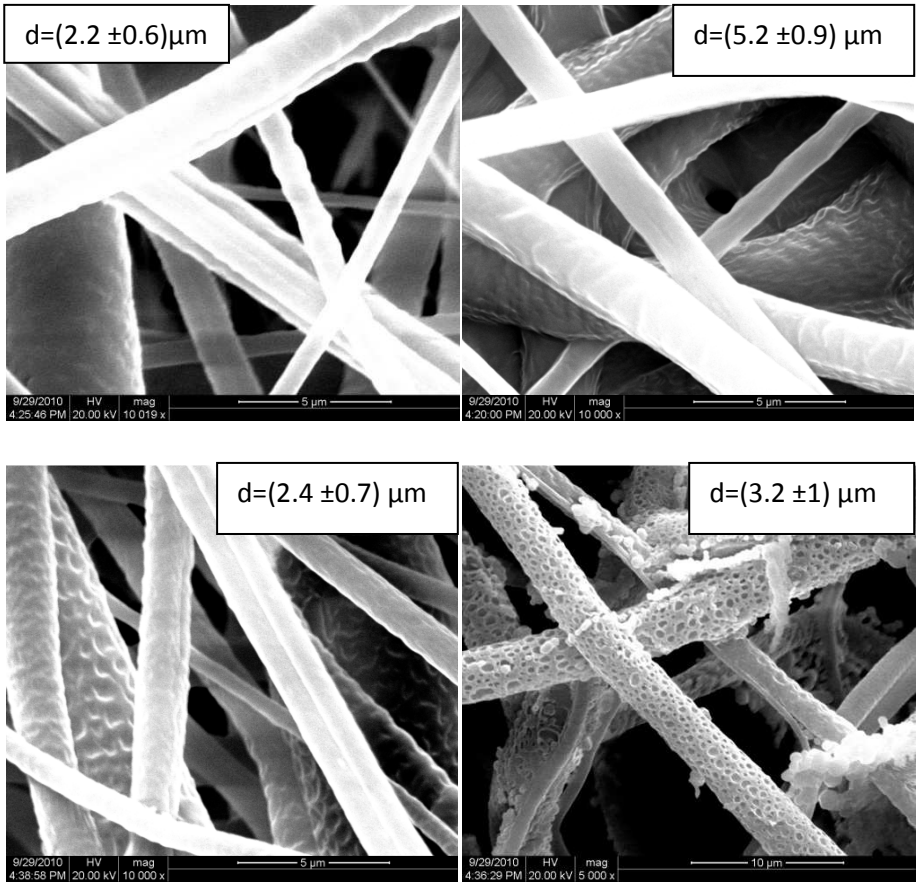

Fig4.29: SEM images of PCL fibers. RH is 40%(top right), 50%(top left),60%(bottom left)and 65%(bottom right). Scale bar is 10µm for the bottom right picture, 5 µm for other pictures. Diameter dimension is indicated on pictures

Release data plot is normalized on the initial albumin concentration, so differences in release are not related to the encapsulated amount of protein. Two

regimes of release can be observed in this experiment. The first one is a very fast release, occuring in the first 12 hours of immersion in PBS. The second stage of release is slower and took place up to the end of the experiment.

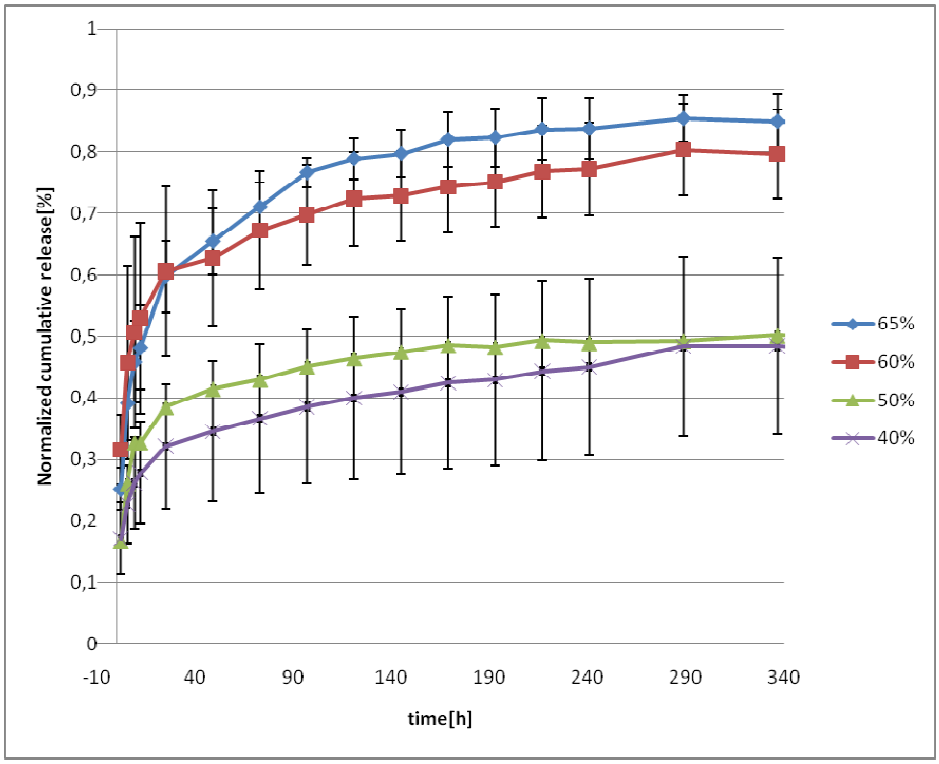

Fig4.30: Cumulative release of albumin adsorbed on surface of coaxial electrospun fibers produced with different RH.

In order to account for this two stages of release, a mathematical equation was used to fit the data and to better understand the different behavior of samples. Equation 4.1 is the linear combination of two exponantial curves, each one

describing the release in one of the two stages observed in the release. The equation proved to fit properly the data, resulting in a R^2 higher than 0.99.

$$\%R = \alpha_1\left(1 - exp\left(-\frac{t}{\tau_1}\right)\right) + \alpha_2\left(1 - exp\left(-\frac{t}{\tau_2}\right)\right) \quad [4.1]$$

where, %R is the percentage of drug released, t is the time, α is a scaling factor and τ is a characteristic time. Considering each addendum of the equation, he parameter α is related to the maximum release, being the value of release at infinite time, while τ is a parameter which influences the curvature of the graph. The values obtained analyzing the four samples are reported in table 4.1.

	40%	50%	60%	65%
α_1	0.24 ± 0.09	0.21 ±0.001	0.48 ±0.08	0.45 ±0.01
τ_1	0.16 ±0.12	0.15 ±0.03	0.16 ±0.04	0.32 ±0.02
α_2	0.21 ±0.01	0.21 ±0.001	0.61 ±0.08	0.41 ±0.01
τ_2	0.01 ±0.001	0.01 ±0.001	0.012 ±0.001	0.01 ±0.001
R^2	0.997	0.998	0.990	0.998

Table 4.1: parameters of equation 4.1 calculated for the fitting of release data

Data fitting approximates the release plots with two exponential curves. The first one describes the fast release in the first day, while the second addendum accounts for the slow and prolonged release of albumin. Indeed, parameter α_1 is the percentage of protein released in the first 12 hours, while the sum $\alpha 1+\alpha 2$ corresponds to the total amount of albumin released during the experiment. The main difference among samples is the value of the scaling parameters α; for samples produced at high humidity (RH > 60%), this value is doubled respect to other samples. This accounts for the high difference observed in the total amount of protein released. Sample with a patterned fiber surface, indeed, released up to the 85% of albumin, while smooth fibers released about 50% of the protein encapsulated in their core. The characteristic times, on the other hand, do not change significantly, except for $\tau_1$of the sample produced at RH=65%.

The equation used is based on a very good model for desorption of drugs from polymer nanofibers, described by Srikar and coworkers [52]. In this model, release is not controlled by solid-state diffusion of the drug inside the polymer. The rate-limiting step, instead, is the desorption of drug from the nanopores present in PCL. Nanopores forms in this polymer during solidification, depending on polymer solution concentration and polymer molecular weight, and affects the value of the parameter α. The value of the characteristic time, affecting the total duration of the release process, depends on the enthalpy of desorption, which in turns depends on the interactions between the drug and the polymer.

The experiments performed confirm this model. The calculated characteristic times do not show significant differences, since the polymer and the drug used

are the same for all the samples. On the other hand, it was demonstrated that the nanoporosity parameter α depends not only on polymer concentration and molecular weight, but also on the preesnce of pores on the surface of fibers. Experiments evidence that an increase in the humidity during electrospinning leads to the formation of pores on fiber surface, which alters the total amount of drug released. The possibility of releasing in a pre-determined time almost all the biomolecules entrapped in coaxial fibers is important when powerful drugs are used and allows eliminating a further release due to degradation of fibers at long time. Fibers were observed with SEM after the release to demonstrate that no fibers dissolution occurs during the release (see as example figure 4.31). PCL degrades in a very long period (up to 2 years) and the images shows that the release was due only to desorption of drug.

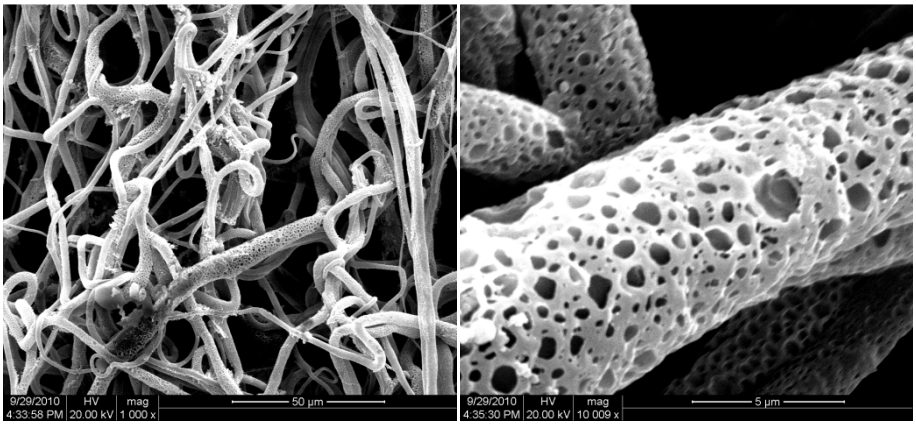

Fig4.31: SEM images of PCL fibers, produced with RH =65%, after the release test in PBS for 340 hours. Scale bar is 5µm

Mats were more disordered, due to the effect of immersion in PBS, but no significant variations on fibers were observed. SEM images, however, shows a decrease in the number of small nanofibers present. Probably, some of them were composed only of PEG (with BSA in it), without the outer sheath of PCL. The immersion in PBS dissolves them very quickly, accounting for the fast release observed in the first 12 hours, which was not explainable with the desorption model.

4.4 Conclusion

Experiments performed show that the use of self-assembling mechanism to generate a porous pattern on polymeric surfaces can be a powerful tool in drug release.

BFs templating method was used to produce an array of monodisperse pores on the surface of polymeric films. An additional self-assembling process was exploited to functionalize the surface of pores with amino groups, through the addition of an amino-terminated macromolecule (Jeffamine) to the solution. Chemical functionalization allows binding a protein (fibrinogen) to the pores surface. The encapsulation efficiency and binding force was evidenced to depend on the amount of Jeffamine added and to the binding method used. The same parameters influence also the release of fibrinogen from porous films.

Functionalization of pores was observed to increase encapsulation efficiency and to delay the process of desorption, leading to longer time of release. The analysis of the patterned films after a partial release demonstrated that pores constitute a reservoir for fibrinogen and that their conformation leads to a multi-step drug release.

Pores were generated also on the surface of electrospun fibers, increasing the humidity during the production process. Coaxial fibers composed of a sheath of PCL enveloping a core of PEG containing BSA were produced and their surface was decorated with pores with this simple technique. Albumin release from these fibers was studied, evidencing a correspondence between the fibers surface topography and the mechanism of release. The presence of a porous pattern on fibers was demonstrated to control the total amount of drug that can be released in a determined time, completing a model for drug release from nanofibers.

4.5 Bibliography

[1] Y. Li, R.S. Shawgo, B. Tyler, P.T. Henderson, J.S. Vogel, A. Rosenberg, P.B. Storm, R. Langer, H. Brem, and M.J. Cima, "In vivo release from a drug delivery MEMS device.," *Journal of controlled release : official journal of the Controlled Release Society*, vol. 100, Nov. 2004, pp. 211-9.

[2] W.-C. Huang, S.-H. Hu, K.-H. Liu, S.-Y. Chen, and D.-M. Liu, "A flexible drug delivery chip for the magnetically-controlled release of anti-epileptic drugs.," *Journal of controlled release : official journal of the Controlled Release Society*, vol. 139, Nov. 2009, pp. 221-8.

[3] D.-G. Yu, C. Branford-White, Z.-H. Ma, L.-M. Zhu, X.-Y. Li, and X.-L. Yang, "Novel drug delivery devices for providing linear release profiles fabricated by 3DP.," *International journal of pharmaceutics*, vol. 370, Mar. 2009, pp. 160-6.

[4] S. Tao, "Microfabricated drug delivery systems: from particles to pores," *Advanced Drug Delivery Reviews*, vol. 55, 2003, pp. 315-328.

[5] C. Li, L. Cheng, Y. Zhang, S. Guo, and W. Wu, "Effects of implant diameter, drug loading and end-capping on praziquantel release from PCL implants.," *International journal of pharmaceutics*, vol. 386, Feb. 2010, pp. 23-9.

[6] L.L. Lao, S.S. Venkatraman, and N. a Peppas, "A novel model and experimental analysis of hydrophilic and hydrophobic agent release from biodegradable polymers.," *Journal of biomedical materials research. Part A*, vol. 90, 2009, pp. 1054-65.

[7] D. a LaVan, T. McGuire, and R. Langer, “Small-scale systems for in vivo drug delivery.,” *Nature biotechnology*, vol. 21, 2003, pp. 1184-91.

[8] K. Lee and S. Yuk, “Polymeric protein delivery systems,” *Progress in Polymer Science*, vol. 32, 2007, pp. 669-697.

[9] J. Cleland, “Emerging protein delivery methods,” *Current Opinion in Biotechnology*, vol. 12, Apr. 2001, pp. 212-219.

[10] S.D. Putney and P.A. Burke, “Improving protein therapeutics with sustained-release formulations.,” *Nature biotechnology*, vol. 16, 1998, pp. 153-7.

[11] S.P. Baldwin, “Materials for protein delivery in tissue engineering,” *Advanced Drug Delivery Reviews*, vol. 33, Aug. 1998, pp. 71-86.

[12] J.D. Kretlow, L. Klouda, and A.G. Mikos, “Injectable matrices and scaffolds for drug delivery in tissue engineering.,” *Advanced drug delivery reviews*, vol. 59, 2007, pp. 263-73.

[13] F. Quaglia, “Bioinspired tissue engineering: the great promise of protein delivery technologies.,” *International journal of pharmaceutics*, vol. 364, Dec. 2008, pp. 281-97.

[14] M. Biondi, F. Ungaro, F. Quaglia, and P.A. Netti, “Controlled drug delivery in tissue engineering.,” *Advanced drug delivery reviews*, vol. 60, 2008, pp. 229-42.

[15] J.E. Babensee, L.V. McIntire, and A.G. Mikos, “Growth factor delivery for tissue engineering,” *Pharmaceutical research*, vol. 17, 2000, p. 497–504.

[16] N. Ashammakhi, I. Wimpenny, L. Nikkola, and Y. Yang, “Electrospinning: Methods and Development of Biodegradable Nanofibres for Drug Release,” *Journal of Biomedical Nanotechnology*, vol. 5, Feb. 2009, pp. 1-19.

[17] Y. Lu, H. Jiang, K. Tu, and L. Wang, “Mild immobilization of diverse macromolecular bioactive agents onto multifunctional fibrous membranes prepared by coaxial electrospinning.,” *Acta biomaterialia*, vol. 5, Jun. 2009, pp. 1562-74.

[18] S. Agarwal, J. Wendorff, and a Greiner, “Use of electrospinning technique for biomedical applications,” *Polymer*, vol. 49, Dec. 2008, pp. 5603-5621.

[19] J. Zeng, “Biodegradable electrospun fibers for drug delivery,” *Journal of Controlled Release*, vol. 92, 2003, pp. 227-231.

[20] Y.Z. Zhang, B. Su, J. Venugopal, S. Ramakrishna, and C.T. Lim, “Biomimetic and bioactive nanofibrous scaffolds from electrospun composite nanofibers.,” *International journal of nanomedicine*, vol. 2, Jan. 2007, pp. 623-38.

[21] R. a Thakur, C.A. Florek, J. Kohn, and B.B. Michniak, “Electrospun nanofibrous polymeric scaffold with targeted drug release profiles for potential application as wound dressing.,” *International journal of pharmaceutics*, vol. 364, 2008, pp. 87-93.

[22] R. Langer and D. a Tirrell, “Designing materials for biology and medicine.,” *Nature*, vol. 428, Apr. 2004, pp. 487-92.

[23] S. Cartmell, “Controlled release scaffolds for bone tissue engineering.,” *Journal of pharmaceutical sciences*, vol. 98, 2009, pp. 430-41.

[24] V.R. Sinha and A. Trehan, “Biodegradable microspheres for protein delivery.,” *Journal of controlled release : official journal of the Controlled Release Society*, vol. 90, Jul. 2003, pp. 261-80.

[25] H. Sah, “A new strategy to determine the actual protein content of poly(lactide-co-glycolide) microspheres.,” *Journal of pharmaceutical sciences*, vol. 86, Nov. 1997, pp. 1315-8.

[26] Y. Pan, Y.-jian Li, H.-ying Zhao, J.-min Zheng, H. Xu, G. Wei, J.-song Hao, and F.-de Cui, “Bioadhesive polysaccharide in protein delivery system: chitosan nanoparticles improve the intestinal absorption of insulin in vivo.,” *International journal of pharmaceutics*, vol. 249, Dec. 2002, pp. 139-47.

[27] S. Cohen, T. Yoshioka, M. Lucarelli, L.H. Hwang, and R. Langer, “Controlled delivery systems for proteins based on poly (lactic/glycolic acid) microspheres,” *Pharmaceutical Research*, vol. 8, 1991, p. 713–720.

[28] S. Huang, Y. Wang, T. Liang, F. Jin, S. Liu, and Y. Jin, “Fabrication and characterization of a novel microparticle with gyrus-patterned surface and growth factor delivery for cartilage tissue engineering,” *Materials Science and Engineering: C*, vol. 29, May. 2009, pp. 1351-1356.

[29] M.C. Hacker, a Haesslein, H. Ueda, W.J. Foster, C. a Garcia, D.M. Ammon, R.N. Borazjani, J.F. Kunzler, J.C. Salamone, and a G. Mikos, “Biodegradable fumarate-based drug-delivery systems for ophthalmic applications.,” *Journal of biomedical materials research. Part A*, vol. 88, 2009, pp. 976-89.

[30] L.Y. Shieh, “Erosion and release from biodegradable polyanhydrides,” Massachusetts Institute of Technology, 1995.

[31] Z.-ming Huang, “A review on polymer nanofibers by electrospinning and their applications in nanocomposites,” *Composites Science and Technology*, vol. 63, 2003, pp. 2223-2253.

[32] A. Saraf, G. Lozier, A. Haesslein, F.K. Kasper, R.M. Raphael, L.S. Baggett, and A.G. Mikos, “Fabrication of nonwoven coaxial fiber meshes by electrospinning.,” *Tissue engineering. Part C, Methods*, vol. 15, Sep. 2009, pp. 333-344.

[33] M. Bognitzki, W. Czado, T. Frese, A. Schaper, M. Hellwig, M. Steinhart, A. Greiner, and J.H. Wendorff, “Nanostructured Fibers via Electrospinning,” *Advanced Materials*, vol. 13, 2001, pp. 70-72.

[34] Y.M. Shin, M.M. Hohman, M.P. Brenner, and G.C. Rutledge, “Electrospinning: A whipping fluid jet generates submicron polymer fibers,” *Applied Physics Letters*, vol. 78, 2001, p. 1149.

[35] S. Chakraborty, I.-C. Liao, A. Adler, and K.W. Leong, “Electrohydrodynamics: A facile technique to fabricate drug delivery systems.,” *Advanced drug delivery reviews*, vol. 61, Oct. 2009, pp. 1043-54.

[36] L. Moroni, J.R. de Wijn, and C.A. van Blitterswijk, “Integrating novel technologies to fabricate smart scaffolds.,” *Journal of biomaterials science. Polymer edition*, vol. 19, Jan. 2008, pp. 543-72.

[37] M. KANG, R. JUNG, H. KIM, and H. JIN, “Preparation of superhydrophobic polystyrene membranes by electrospinning,” *Colloids and Surfaces A: Physicochemical and Engineering Aspects*, vol. 313-314, 2008, pp. 411-414.

[38] J.T. McCann, M. Marquez, and Y. Xia, “Highly porous fibers by electrospinning into a cryogenic liquid.,” *Journal of the American Chemical Society*, vol. 128, Feb. 2006, pp. 1436-7.

[39] C.L. Casper, J.S. Stephens, N.G. Tassi, D.B. Chase, and J.F. Rabolt, "Controlling Surface Morphology of Electrospun Polystyrene Fibers: Effect of Humidity and Molecular Weight in the Electrospinning Process," *Macromolecules*, vol. 37, Jan. 2004, pp. 573-578.

[40] M. Bognitzki, T. Frese, M. Steinhart, A. Greiner, J.H. Wendorff, A. Schaper, and M. Hellwig, "Preparation of fibers with nanoscaled morphologies: Electrospinning of polymer blends," *Polymer Engineering & Science*, vol. 41, Jun. 2001, pp. 982-989.

[41] M. Galvin, K. Kiick, D. Pochan, J. Sun, and N. Wagner, "Enhancing the Properties of Nanoscale Electrospun Polymer Fibers Through Chemical Architecture, Surface Texturing and Optimization of Processing Protocols," *Macromolecules*, 2003, pp. 16-18.

[42] S. Megelski, J.S. Stephens, D.B. Chase, and J.F. Rabolt, "Micro- and Nanostructured Surface Morphology on Electrospun Polymer Fibers," *Macromolecules*, vol. 35, Oct. 2002, pp. 8456-8466.

[43] K. Kim, M. Kang, I.-joo Chin, and H.-joon Jin, "Unique Surface Morphology of Electrospun Polystyrene Fibers from a N,N-Dimethylformamide Solution," *Macromol. Res.*, vol. 13, 2005, pp. 533-537.

[44] P. Gibson, H. Schreuder-Gibson, and A.N.S.C. MA, "Patterned electrospray fiber structures," *Nanomanufacturing handbook*, 2006, p. 351.

[45] M. Ma, M. Gupta, Z. Li, L. Zhai, K.K. Gleason, R.E. Cohen, M.F. Rubner, and G.C. Rutledge, "Decorated Electrospun Fibers Exhibiting Superhydrophobicity," *Advanced Materials*, vol. 19, 2007, pp. 255-259.

[46] L. Wang, C.-L. Pai, M.C. Boyce, and G.C. Rutledge, “Wrinkled surface topographies of electrospun polymer fibers,” *Applied Physics Letters*, vol. 94, 2009, p. 151916.

[47] M.F. Leong, K.S. Chian, P.S. Mhaisalkar, W.F. Ong, and B.D. Ratner, “Effect of electrospun poly(D,L-lactide) fibrous scaffold with nanoporous surface on attachment of porcine esophageal epithelial cells and protein adsorption.,” *Journal of biomedical materials research. Part A*, vol. 89, 2009, pp. 1040-8.

[48] C.J. Luo, M. Nangrejo, and M. Edirisinghe, “A novel method of selecting solvents for polymer electrospinning,” *Polymer*, vol. 51, 2010, pp. 1654-1662.

[49] J. Zheng, a He, J. Li, J. Xu, and C. Han, “Studies on the controlled morphology and wettability of polystyrene surfaces by electrospinning or electrospraying,” *Polymer*, vol. 47, 2006, pp. 7095-7102.

[50] M. Gandhi, S. Raman, A. Yarin, C. Megaridis, and R. Gemeinhart, “Mechanistic Examination of Protein Release from Polymer Nanofibers.,” *Molecular pharmaceutics*, Jan. 2009.

[51] P. Saha and J.H. Kou, “Effect of bovine serum albumin on drug permeability estimation across Caco-2 monolayers.,” *European journal of pharmaceutics and biopharmaceutics : official journal of Arbeitsgemeinschaft für Pharmazeutische Verfahrenstechnik e.V*, vol. 54, Nov. 2002, pp. 319-24.

[52] R. Srikar, A.L. Yarin, C.M. Megaridis, A.V. Bazilevsky, and E. Kelley, “Desorption-limited mechanism of release from polymer nanofibers.,” *Langmuir : the ACS journal of surfaces and colloids*, vol. 24, Feb. 2008, pp. 965-74.

5. Final Remarks

This thesis investigated the production of controlled topographic and chemical features on polymers through a self-assembling process involving water droplets condensing from a humid environment. We studied the formation of pores via the Breath Figures method on polymeric films, analyzing dimension, distribution of size, morphology and order of pores. The fundamental role of interfacial and kinetic effects was demonstrated, and a phenomenological model is proposed to describe Breath Figures formation.

Polymeric films with a topographic and chemical pattern were obtained. We demonstrated that the addition of hydrophilic groups in the polymeric solution during BFs formation leads to the functionalization of the pores surface. We found that this addiction determines also a variation in pores size and order, depending on the concentration. PDLLA and PCL films decorated with an array of pores with amino groups in the inner surface were produced. Moreover, we exploited this chemical pattern to bind proteins, obtaining an array of pores with the protein on the surface. We analyzed the influence of amino groups concentration and of the binding process on the encapsulation efficiency.

Finally, we tested the possibility of using the Breath Figures method to pattern the surface of polymeric films and fibers to produce Drug Delivery Devices. We observed that the functionalization and morphology of pores influenced the release of fibrinogen from patterned films. In the same way, the release of

proteins from coaxial electrospun fibers was demonstrated to depend on the presence of pores on their surface, which especially influences the total amount of protein released.

Concluding, this work demonstrated that self-assembling of water droplets on polymeric solution surface is a simple, cheap and flexible system which allows producing a variety of interesting porous structures. We explored the application of porous films and fibers in drug release and in protein controlled disposition in 3-D arrays. We demonstrated, finally, that this process can generate powerful polymeric system for biomedical application.